# Structural design and characterisation of FRC precast segments

DOCTORAL THESIS

Doctoral thesis written by:
Lin Liao

Directed by:
Antonio Aguado de Cea
Albert de la Fuente Antequera
Sergio Henrique Pialarissi Cavalaro

Barcelona, September 2015

Universitat Politècnica de Catalunya
Departament d´Enginyeria de la Construcció

UNIVERSITAT POLITÈCNICA DE CATALUNYA
BARCELONATECH
Escola de Doctorat

# Acta de calificación de tesis doctoral

**Curso académico:**

Nombre y apellidos: Lin Liao

Programa de doctorado: Construction Engineering

Unidad estructural responsable del programa: Department of Construction Engineering

## Resolución del Tribunal

Reunido el Tribunal designado a tal efecto, el doctorando / la doctoranda expone el tema de la su tesis doctoral titulada: Structural design and characterisation of FRC precast segments.

.

Acabada la lectura y después de dar respuesta a las cuestiones formuladas por los miembros titulares del tribunal, éste otorga la calificación:

☐ NO APTO ☐ APROBADO ☐ NOTABLE ☐ SOBRESALIENTE

| | | |
|---|---|---|
| (Nombre, apellidos y firma)<br>Presidente/a | | (Nombre, apellidos y firma)<br>Secretario/a |
| (Nombre, apellidos y firma)<br>Vocal | (Nombre, apellidos y firma)<br>Vocal | (Nombre, apellidos y firma)<br>Vocal |

_____, _____ de _____ de _____

El resultado del escrutinio de los votos emitidos por los miembros titulares del tribunal, efectuado por la Escuela de Doctorado, a instancia de la Comisión de Doctorado de la UPC, otorga la MENCIÓN CUM LAUDE:

☐ SÍ ☐ NO

| | |
|---|---|
| (Nombre, apellidos y firma)<br>Presidente de la Comisión Permanente de la Escuela de Doctorado | (Nombre, apellidos y firma)<br>Secretario de la Comisión Permanente de la Escuela de Doctorado |

Barcelona a _____ de _____ de _____

*Three passions, simple but overwhelmingly strong, have governed my life: the longing for love, the search for knowledge, and unbearable pity for the suffering of mankind.*

*（Bertrand Russell，1872—1970）*

# ACKNOWLEDGEMENTS

Time is like a fleeting show, looking back through the three years of Ph.D. life, tones of memories come into my mind. Three years have passed, there have been frustration of failure as well as the joy of success. There are too many people and things worth remembering; thanks to the encouragement and care from professors and friends, I could manage to make progress continuously in this most important journey of my life.

I would like to acknowledge Professor Antonio Aguado de cea, for giving me the opportunity to work at the Department of Construction Engineering, Polytechnic University of Catalonia (UPC). Without this opportunity, I probably have become a construction worker working in a hostile environment more than 10 hours every day.

I would like to acknowledge my supervisor Professor Albert de la Fuente Antequera, for guiding my research work and correcting those scientific papers patiently. I am sincerely grateful that he treats me as a brother, cares my daily life and shares with me his wonderful life experience. Thank him for inviting me to eat pizza when we work overtime during the weekend, I wish we would have chance to sit together again in the future to recall the golden memories.

I would like to acknowledge my supervisor Professor Sergio Henrique Pialarissi Cavalaro for guiding my research work and help me to understand the philosophy of doing the Ph.D. research. Thank him for helping me to overcome the fear in my heart at the most difficult period of my study. He is one of the most intelligent and professional person I have ever met; he helped me broaden my horizon and restructure my knowledge and this would benefit me through my life.

I would like to acknowledge Professor Changsuo Zhang in Taiyuan University of Technology for giving me opportunities to work with him since 2009, even though I was just a sophomore that time. He helped me overcome my inferiority and encouraged me to explore the world by myself. I am convinced that without his guidance, I cannot have the chance to experience such a wonderful life.

I would like to acknowledge the China Scholarship Council for providing me the scholarship, without this funding support, it would be impossible for me to dedicate myself to the research work. Special thanks to the Ministry of Science and Innovation for the economic support received through Research Project BIA2010-17478: Construction processes by means of fibre reinforced concrete.

Special thanks to Doctor Pablo Pujadas Álvarez and Doctor Ana Blanco Álvarez, for their encouragement when I encountered difficulties. All their kindness and sincerity made me feel the beauty of the world. I give my special thanks to Doctor Pablo Pujadas Álvarez for calling at my office every day to kill the boring time during the break.

I am also very grateful for the help of the technician staffs of the laboratory, Tomàs García, Carlos Hurtado and Jordi la Fuente, especially Robert Mc-Aloon, Jordi Cabrerizo and Camilo Bernad for all fun and hard moments we experienced during the experimental campaign; thank them for starting working with me even at 8:00 AM sometimes.

I thank Carme, Carmeta, Mercè and Montse Santos, who have always been very attentive, gracious and kind whenever I needed anything.

I thank my Chinese friends in Barcelona who experienced and shared the most precious three years' time with me. They are: Yikun Hu, Zhitong Zhao, Furong Liu, Xin Zhang, Haoran Zhang, Jing Ye, Jing Yang, Chaoren Liu and Ying Guo. Hope we would have chance to meet each other in China.

I furthermore thank all the people of the research group who helped me in making this Ph.D. They are: Julia, Jordi, Yohei, Edu, Ricardo, Renan, Tai, Carlos, Tina, Fran, Razmik, Marta, Amin, Ruben, Melyne, Andresa, Sandra, Issac, Luis and Nacho. All of them would be a part of my life forever; I will miss those days we spent together after I go back to China.

Finally, I would like to acknowledge my family who sacrificed a lot in order to provide me such opportunities that led me towards success. My parents are over sixty, they have never been away from the farmland they cultivate day and night; they do not know anything about my major and profession because they are illiterate. But they give me the most selfless and greatest love, no matter where I am and whatever difficulties I endure; their smile and encouragement are always my biggest motivation to move on. My two older brothers began to provide free financial assistance to me since they graduated from college, whenever I encountered any difficulties; they always give me the greatest support. My wife Huang Ting, spends her most beautiful age accompanying me through my most anxious and difficult period without any complaints, thanks for her support and patience in these three years, especially during the writing of this thesis.

# SUMMARY

Concrete technology has changed greatly in the past decades. Steel fibre reinforced concrete (SFRC) is an example of the development in this field. It is obtained by adding fibres that act as a reinforcement of the cement matrix, improving the tenacity, cracking control and durability of the concrete members. In certain applications, SFRC has become an alternative material to concrete reinforced with conventional steel rebar. Despite of numerous advantages of SFRC, problems and uncertainties still exist regarding the design, the characterization and the performance of this material. Furthermore, the structural design and the properties of SFRC in real-scale elements as well as the fibre distribution are not properly clarified. All these issues need to be addressed in order to promote the safe and efficient use of the material.

The objective of this doctoral thesis is to develop a systematic and innovative approach for the design optimization and characterisation of FRC precast segment. In total, 4 subjects are covered: a critical study related to the design of FRC precast segment considering the ductility requirements of the Model Code 2010; the experimental and analytical study of concrete blocks subjected to concentrated loads; the design procedure and experimental research on FRC precast segment for shafts and the anisotropy of the FRC precast segment.

The first subject presents an analysis of the technical requirements demanded by the Model Code 2010 when steel fibres are the only reinforcement for concrete elements. According to this revision, an alternative approach according to the Model Code 2010 which is more compatible with the requirements of the application in tunnels is proposed. This approach may lead to the reduction of the fibre content required to guarantee a minimum ductility of the element. In order to evaluate the repercussion of the ductility criteria in terms of fibre consumption, a case study of Metro L9 of Barcelona is presented.

The second subject contributes to the understanding about the behaviour of concrete blocks subjected to concentrated load. An experimental programme is performed to evaluate the influence of the height-to-length ratios in the mechanical response of the blocks. Based on the observations derived, a strut-and-tie model is adopted to assess the value of the loads $F_{cr}$ and $F_{max}$ for short blocks and long blocks. A case study of Metro Line 9 in Barcelona is conducted, and the results of the study indicates that with an appropriate safety factors for the SLS and the ULS, no traditional reinforcement is required to resist the tensile stresses due to the concentrated loads applied by the jacks of the tunnel boring machine.

The third subject is to verify that it is viable to replace the traditional reinforcement with steel fibres in the segmental lining ring of shaft constructed with vertical shaft machine. An analytical formulation based on MC 2010 is proposed to evaluate the minimum requirements the FRC must fulfil to carry out this replacement. Likewise, an experimental campaign was performed to characterize the mechanical behaviour of both conventional and self-compacting concrete reinforced with fibre content ($C_f$) between 30 and 60 kg/m$^3$. Posteriorly, another full-scale experimental campaign of bending test on segments is performed to verify the ductile behaviour of two types of segments under failure scenario. These results are used to validate the proposed formula.

The last subject focuses on the study of the anisotropy in terms of fibre distribution and local mechanical response of segments with conventional and self-compacting SFRC. For that, a large number of cores extracted from real-scale segments are tested for the fibre distribution with the inductive method and, then, for the mechanical response with the Barcelona test. A conceptual model for the fibre orientation is proposed based on the average values obtained from the tests.

# RESUMEN

La tecnología del hormigón ha avanzado notablemente en las últimas décadas. En este sentido, el hormigón reforzado con fibras (HRF) es un ejemplo del desarrollo en este campo. Este se obtiene mediante la adición de fibras que actúan como un refuerzo de la matriz de cemento, mejorando la tenacidad y el control de la figuración y, por ende, la durabilidad. En ciertas aplicaciones, HRF se ha convertido en un material alternativo para hormigón armado convencional. A pesar de las numerosas ventajas asociadas al uso del HRF, todavía existen incertidumbres en cuanto al diseño, la caracterización y el desempeño mecánico de este material. En particular, es necesario desarrollar adecuadamente el concepto y requerimiento de ductilidad de las estructuras de HRF así como integrar de forma fidedigna aspectos de orientación y de distribución de fibras en el diseño. Todas estas cuestiones deben abordarse con el fin de promover el uso seguro y eficiente del material.

El objetivo de esta tesis doctoral es el desarrollo de un enfoque sistemático e innovador para el diseño y caracterización de dovelas de HRF para la ejecución de revestimiento de túneles. En total, esta tesis se cubren 4 aspectos: un estudio crítico en relación con el diseño del dovelas de HRF teniendo en cuenta los requisitos de ductilidad del Código Modelo 2010; un estudio experimental y analítico de bloques de hormigón sometidas a cargas concentradas; el pre – diseño de dovelas para la ejecución de pozos verticales y el análisis de anisotropía en la distribución y orientación de fibras.

En el primer tema se aborda un análisis de los requisitos técnicos exigidos por el Código Modelo de 2010 en estructuras de HRF en las que las fibras son los únicos elementos de refuerzo del hormigón. De acuerdo con esta revisión, se propone un enfoque alternativo y compatible con el MC 2010 más alineado con lo requerimiento estructurales y necesidades resistentes de las dovelas de HRF. Este enfoque conduce a la optimización del contenido de fibra necesaria para garantizar la ductilidad adecuada para estos elementos estructurales. Con el fin de evaluar la repercusión de los criterios de ductilidad en términos de consumo de fibra, se presenta un estudio de caso de Metro L9 de Barcelona.

El segundo campo de investigación tratado contribuye al conocimiento en relación al comportamiento de elementos de hormigón sometidos a cargas concentradas. En este sentido, se ha llevado a cabo una campaña experimental para evaluar la influencia del ratio altura – ancho en el mecanismo de rotura de los bloques ensayados. En base a las observaciones, se ha planteado un modelo de bielas y tirantes para evaluar las cargas de figuración y de rotura de los bloques. La formulación propuesta se ha empleado para

evaluar dichas cargas en el caso de empuje de los gatos de las dovelas diseñadas para los túneles de la Línea 9 del Metro de Barcelona. Los resultados ponen de manifiesto que, empleando los coeficientes de seguridad adecuados, no se requiere armadura pasiva adicional para resistir los esfuerzos de tracción que se generan en la fase de empuje de los gatos, en el caso particular estudiado.

En la tercera fase se ha extendido el estudio en relación al diseño de dovelas de túnel a dovelas de HRF para la ejecución de revestimientos de túneles verticales. En esta línea, se ha propuesto una formulación analítica y cerrada, basada también en MC 2010, para evaluar los requerimientos resistentes del HRF y que permiten eliminar parte o la totalidad de la armadura en forma de barras mediante el uso de fibras estructurales. En este contexto, se ha llevado a cabo una campaña experimental de caracterización de hormigones convencionales y autocompactantes, reforzados con cuantías de fibras de entre 30 y 60 kg/m$^3$. En base a los resultados obtenidos y a la formulación propuesta, se estableció una cuantía de 50 kg/m$^3$ para la ejecución de 4 dovelas a escala real con los dos tipos de hormigones. Dos de estas dovelas se ensayaron a flexión en el laboratorio de Tecnología de Estructuras Lluís Agulló de la UPC y se verificó que el tipo y cuantía de fibras establecidos eran los adecuados para garantizar la ductilidad necesaria de las dovelas y eliminar la totalidad de la armadura pasiva. Estos ensayos sirvieron también para validar la formulación propuesta.

Por último, en la cuarta línea de investigación se estudia en profundidad a nivel experimental la anisotropía de la distribución, cuantía y orientación de las fibras en dovelas de hormigón convencional y de hormigón autocompactante reforzadas con fibras. Para ello, se extrajeron un número elevado y representativo de testigos de las dovelas a escala real fabricadas. Se emplearon métodos no destructivos tipo inductivo para evaluar la cuantía y orientación de las fibras. Asimismo, se empleó el ensayo Barcelona (ensayo destructivo) para evaluar también ambas variables así como la resistencia a tracción residual de los hormigones. En base a los resultados se propone un modelo conceptual para estimar la orientación de las fibras en estos elementos estructurales.

# TABLE OF CONTENTS

# LIST OF FIGURES

# LIST OF TABLES

# LIST OF EQUATIONS

# LIST OF SYMBOLS

| | |
|---|---|
| a | Length of concrete blocks |
| A | Area |
| $a_1$ | Length of support plate |
| $a_2$ | Half width of the STM active zone at the bottom of concrete blocks |
| $A_c$ | Area of concrete |
| $A_s$ | Area of steel |
| $A_{s,min}$ | The minimum area of steel |
| b | Cross sectional width of the segment; Width of concrete blocks |
| $b_1$ | Width of support plate |
| C.V | Coefficient of variation |
| $C_f$ | Fibre content |
| $C_{f,min}$ | The minimum value of fibre content |
| $C_{fm}$ | The average value of fibre content |
| CMOD | Crack mouth opening displacement of concrete |
| $d_f$ | Cross section fibre diameter |
| E | Modulus of elasticity |
| $E_c$ | Modulus of elasticity of concrete |
| $E_{cm}$ | Average modulus of elasticity of concrete |
| $e_e$ | External eccentricity |
| $e_i$ | Internal eccentricity |
| $e_{tot}$ | Total eccentricity |
| F | Applied force |
| $F_{0.2}$ | Force corresponding to a crack width of 0.2 mm |
| $f_c$ | Uniaxial compressive strength of the concrete |
| $F_{cc}$ | Compressive force on the concrete resulting from an applied M |
| $f_{cd}$ | Design compressive strength |

| | |
|---|---|
| $f_{ck}$ | Characteristic value of $f_c$ |
| $f_{cm}$ | Average compressive strength of concrete |
| $F_{cr}$ | First crack load of concrete blocks |
| $f_{ct}$ | Tensile strength of concrete |
| $F_{ct}$ | Tensile force on the concrete resulting from an applied M |
| $f_{ct,fl}$ | Flexural tensile strength of the concrete |
| $f_{ctm,fl}$ | Average flexural tensile strength |
| $f_{ctm1}$ | Average tensile strengths of concrete obtained from the Barcelona test |
| $f_{ctm2}$ | Average tensile strengths of concrete obtained from the Brazilian test |
| $f_f$ | Yielding strength of fibre |
| $f_{Ftu}$ | Ultimate residual tensile strength of the FRC; $f_{Ftu} = f_{R3}/3$ |
| $f_{LOP}$ | Limit of proportionality strength of the FRC |
| $f_{LOPk}$ | Characteristic values of $f_{LOP}$ |
| $f_{LOPm}$ | Average value of $f_{LOP}$ |
| $F_{max}$ | Maximum load |
| $f_{R1}$ | Residual flexural tensile strength CMOD=0.5 mm |
| $f_{R1d}$ | Design strength of $f_{R1}$ required |
| $f_{R1k}$ | Characteristic values of $f_{R1}$ |
| $f_{R1m}$ | Average value of $f_{R1}$ |
| $f_{R1m, min}$ | Minimum average value of $f_{R1}$ |
| $f_{R3}$ | Residual flexural tensile strength CMOD=2.5 mm |
| $f_{R3d}$ | Design strength of $f_{R3}$ required |
| $f_{R3k}$ | Characteristic values of $f_{R3}$ |
| $f_{R3m}$ | Average value of $f_{R3}$ |
| $f_{R3m, alt}$ | Required $f_{R3m, min}$ according to the alternative approach |
| $f_{R3m, min}$ | Minimum average value of $f_{R3}$ |
| $f_{R4}$ | Residual flexural tensile strength CMOD=3.5 mm |
| $f_{Ri}$ | Residual flexural tensile strength of the FRC corresponding to $CMOD_i$ |
| fy | Tensile strength of steel |
| h | Height of the segment |
| $h_1$ | Height of support plate |
| $h_{sp}$ | Distance between the notch tip and the top of the specimen |
| $h_T$ | Height of concrete blocks |

| | |
|---|---|
| $k_1$ | Coefficient of depth in confined zone in concrete blocks |
| $k_2$ | Eccentricity factor of concrete blocks |
| L | Length |
| LVDT | Linear variable differential transformer |
| $l_f$ | Fibre length |
| $l_o$ | Span between supports of the 1st stacked segment |
| M | Bending moment |
| $M_{cr}$ | Cracking bending moment |
| $M_{crd}$ | Design cracking bending moment |
| $M_d$ | Design bending moment |
| $M_k$ | Characteristic value of axial forces |
| $M_{SLS}$ | Bending moment at service load |
| $M_u$ | Ultimate bending moment |
| N | Axial forces |
| $N_k$ | Characteristic value of axial forces |
| $P_{cr}$ | Cracking load |
| $P_{max}$ | The maximum load |
| $P_{SLS}$ | Service load |
| $P_u$ | Ultimate load |
| $q_1$ | Maximum pressure in concrete blocks |
| $q_2$ | Pressure at the edge of active concrete blocks |
| $q_a$ | Uniform pressure at the bottom of concrete blocks |
| $SF_{cr}$ | Cracking safety factor |
| STM | Strut and tie model |
| T | Age of the concrete |
| V | Shear force |
| $V_k$ | Characteristic value of shear force |
| $w$ | Crack width |
| $w_{tot}$ | Total crack width |
| $x_n$ | Neutral axis depth |
| $\alpha$ | Angle of the conical wedge |
| $\beta$ | Angle of the secondary crack in concrete blocks |
| $\gamma_c$ | Partial safety factor for the compressive concrete strength |

| | |
|---|---|
| $\gamma_f$ | Partial safety factor for the residual flexural tensile strength of the FRC |
| $\gamma_{G*}$ | Partial safety factor for action of the ground |
| $\gamma_{SW}$ | Partial safety factor for the self-weight of segments |
| $\delta$ | Vertical displacement |
| $\delta_{peak}$ | Peak vertical displacement |
| $\delta_{SLS}$ | Vertical displacement at service limit state load |
| $\delta_u$ | Ultimate vertical displacement |
| $\Delta\delta$ | Increment of vertical displacement |
| $\eta$ | Fibre orientation number |
| $\eta_{Max}$ | Maximum fibre orientation number |
| $\eta_{Min}$ | Minimum fibre orientation number |
| $\theta$ | Angle |
| $\theta_{Max}$ | Maximum angle correspond to the maximum fibre orientation number |
| $\theta_{Min}$ | Minimum angle correspond to the minimum fibre orientation number |
| $\lambda$ | Slenderness ratio of the tunnel ring |
| $\lambda_f$ | Aspect ratio of the fibre |
| $\rho_s$ | The proportion of reinforcement |
| $\rho_{s,min}$ | The minimum proportion of reinforcement |
| $\sigma$ | Stress; Standard deviation |
| $\sigma c$ | Stress of concrete |
| $\sigma_{c,max}$ | Maximum compressive stress of concrete |
| $\sigma_{ct,max}$ | Maximum tensile stress of concrete |
| $\phi$ | Diameter of steel fibre |
| $\phi_i$ | Diameter of tunnels |
| $\chi$ | Section curvature |
| $\Omega$ | Isotropy factor of concrete |
| $\Psi$: | Coefficient for transforming characteristic values of the tensile strength in average values |

# 1. INTRODUCTION

## 1.1 BACKGROUND AND CONTEXT

Concrete technology has changed greatly in the past decades. The mixtures as well as the applications of concrete have evolved in conjunction with a greater understanding of the material. In the process, new types of concrete appeared in response to the requirements of special applications. An example is Fibre reinforced concrete (FRC), obtained by the inclusion of small amounts of fibres. The fibres work as rigid inclusions that improve the mechanical behaviour of the concrete by means of bridging the cracks (Di Prisco et al. 2009 & Minelli et al. 2011 & Tiberti et al. 2013). The resulting material presents an enhanced post-cracking performance in terms of tenacity, cracking control and durability, being an alternative to traditional reinforced concrete with conventional rebar in certain cases.

The research on steel fibre reinforced concrete (SFRC) started by the 1960s. Since then, exhaustive studies have been performed to reach deeper understanding of this material. Steel fibres is in the form of short discrete fibres randomly distributed in the concrete matrix, and work as a rigid inclusions like aggregates, thus to improve the mechanical behaviour of the concrete. Parallel to the achievements made in the research, SFRC has been used in different situations with structural responsibility. In these applications the use of SFRC in could not only save material and labour force, but also could save time and manufacturing cost. Probably, one of the most relevant use of SFRC with structural responsibility is found in the construction of tunnels and shafts.

Precast concrete segments gradually developed as a predominant tunnel lining approach in Tunnel Boring Machines TBM constructed tunnels in the past decades. The construction of linings formed by precast concrete segments installed by a TBM is a well-established approach, especially in long tunnels excavated in weak fractured rock or soft ground. Generally, these precast concrete segments are reinforced with rebars to resist the tensile strength at SLS and ULS.

Except in the case of asymmetric loading, tunnels tend to be subjected mainly to compression throughout the service life. In this context, the reinforcement is intended to comply with minimum ductility requirements in order to resist the stresses that might arise during transient stages (demoulding, stocking, transportation and installation). However, the use of only conventional reinforcement might not be enough to avoid the formation of visible cracks or of spalling of the concrete cover. In addition that, it implies intensive labour work and increases the time needed for preparation of the formwork prior to casting the segments.

The inclusion of fibres may be an interesting approach to mitigate some of the problems above mentioned. On one hand, fibres are dispersed in the concrete mass, reaching even the concrete cover layer. The presence of fibres close to the concrete cover would contribute to resist the bursting and spalling stresses induced by the thrust of jack during the assembly of segments and advance of the TBM. Several studies suggest that SFRC helped to reduce the incidence of bursting in segments of tunnel that required high excavation forces (de Waal et al. 1999 & Schnütgen et al. 2003)). On the other hand, the addition of fibres also increases the fatigue and impact resistance of concrete, which is of great importance to stand the unintentional impact loads during production and construction phases.

Since 1980s FRC has been included in projects worldwide as a material for the construction of tunnel segments. Nowadays, a combination of conventional reinforcement and fibre reinforcement in the production of precast segments is an extended approach, especially in linings with large diameter (Plizzari et al. 2006 & Plizzari et al. 2007 & De la Fuente et al. 2012). Nevertheless, in tunnels mainly subjected to compression in service stage, it would be even possible to adopt fibres as the sole reinforcement to resist the tensile stresses during the transient stages and avoid brittle failure. For that, however, the FRC would have to provide enough ductility to comply with the minimum requirements established in codes and recommendations.

Some of the tunnels constructed with FRC are presented *in Table 1.1.* It is evident that FRC precast segments have been used in tunnels with different functions, i.e. water supply (WS), waste water (WW), gas pipeline (GP), power cable (PC), subway (SW), railway (RW), and road tunnels (RT). Steel fibre is the main type of fibre used in the cases reported in *Table 1.1*, with a content that ranges from 25 kg/m$^3$ to 60 kg/m$^3$. Notice that a total substitution of the traditional reinforcement by fibres is observed in many applications.

*Table 1.1 Tunnels lined by FRC precast segments (ACI 544, 2014)*

| Tunnel Name | Year | Country | Function | $D_i$ (m) | h,(m) | $D_i/h$ | Cf | Bars |
|---|---|---|---|---|---|---|---|---|
| Metrosud | 1982 | Italy | SW | 5.8 | 0.30 | 19.3 | - | No |
| Fanaco | 1989 | Italy | WS | 3.0 | 0.20 | 15.0 | - | No |
| Heathrow Baggage Handling | 1993 | England | SV | 4.5 | 0.15 | 30.0 | 30 | No |
| Heathrow Express | 1994 | England | RW | 5.7 | 0.22 | 25.9 | 30 | No |
| Napoli metro | 1995 | Italy | SW | 5.8 | 0.30 | 19.3 | 40 | No |
| Lesotho Highlands | 1995 | South Africa | WS | 4.5 | 0.30 | 15.0 | 50 | No |
| Hachinger | 1998 | Germany | WS | 2.2 | 0.18 | 12.2 | - | No |
| 2nd Heinenoord | 1999 | Netherlands | RT | 7.6 | 0.35 | 21.7 | - | No |
| Jubilee Line | 1999 | England | SW | 4.5 | 0.20 | 22.3 | 30 | No |
| Trasvases Manabi (La Esperanza) | 2001 | Ecuador | WS | 3.5 | 0.20 | 17.5 | 30 | No |
| Essen | 2001 | Germany | SW | 7.3 | 0.35 | 20.9 | - | No |
| Sorenberg | 2002 | Switzerland | GP | 3.8 | 0.25 | 15.2 | 40 | No |
| Canal de Navarra | 2003 | Spain | WS | 5.4 | 0.25 | 21.6 | - | No |
| Oënzberg-TBM | 2003 | Switzerland | RW | 11.4 | 0.40 | 28.5 | 30 | Yes |
| Oënzberg-Shield | 2003 | Switzerland | RW | 11.4 | 0.40 | 28.5 | 60 | No |
| Barcelona Metro Lin 9 - Can Zam Stretch | 2003 | Spain | SW | 10.9 | 0.35 | 31.1 | 60 | Yes |
| Channel Tunnel Rail Link (CTRL) | 2004 | England | RW | 7.2 | 0.35 | 20.4 | 30 | No |
| Hofoldinger Stollen | 2004 | Germany | WS | 2.9 | 0.18 | 16.1 | 40 | No |
| Heathrow Express Extension HexEx) | 2005 | England | RW | 5.7 | 0.22 | 25.9 | 30 | No |
| San Vicente | 2006 | USA | WS | 3.2 | 0.18 | 17.8 | 30 | No |
| Heathrow– SWOT | 2006 | England | WS | 2.9 | 0.20 | 14.5 | 30 | No |
| Barcelona Metro Line 9 - Stretch I | 2006 | Spain | SW | 8.4 | 0.32 | 26.3 | 30 | Yes |
| Lötschberg | 2007 | Switzerland | PL | 4.5 | 0.22 | 20.5 | - | No |
| Valencia Metro Line 1 | 2007 | Venezuela | SW | 8.4 | 0.40 | 21.0 | 40 | Yes |
| Gold Coast Desalination Plant | 2008 | Australia | WS | 3.4 | 0.20 | 17.0 | 35 | No |
| Big Walnut Sewer | 2008 | USA | WW | 3.7 | 0.23 | 16.1 | 35 | Yes |
| Heathrow – PiccEx | 2008 | England | SW | 4.5 | 0.15 | 30.0 | 30 | No |
| Hobson Bay | 2009 | New Zeeland | WW | 3.7 | 0.25 | 14.8 | 40 | No |
| Copenhagen District Heating Tunnel | 2009 | Denmark | WS | 4.2 | 0.30 | 14.0 | 35 | No |
| Docklands Light Railway (DLR) Extension | 2009 | England | RW | 5.3 | 0.25 | 21.2 | - | No |
| Fontsanta–Trinitat Interconnection | 2010 | Spain | WS | 5.2 | 0.20 | 26.0 | 25 | Yes |
| Clem Jones - Clem 7 | 2010 | Australia | RT | 11.2 | 0.40 | 28.0 | 37 | Yes |
| Ems-Dollard Crossing | 2010 | Germany-Netherlands | GP | 3.0 | 0.25 | 12.0 | - | No |
| City West Cable Tunnel (CWCT) | 2010 | Australia | PC | 2.5 | 0.20 | 12.5 | - | No |
| Adelaide Desalination Plant | 2010 | Australia | WS | 2.8 | 0.20 | 14.0 | 35 | No |
| FGC Terrassa | 2010 | Spain | RW | 6.0 | 0.30 | 20.0 | 25 | Yes |
| Brightwater East | 2011 | USA | WW | 5.1 | 0.26 | 19.6 | 35 | No |
| Brightwater Central | 2011 | USA | WW | 4.7 | 0.33 | 14.2 | 40 | No |
| Brightwater West | 2011 | USA | WW | 3.7 | 0.26 | 14.2 | 35 | No |
| East side CSO | 2011 | USA | WW | 6.7 | 0.36 | 18.6 | - | No |
| Victorian Desalination Plant | 2011 | Australia | WS | 4.0 | 0.23 | 17.4 | - | No |
| Monte Lirio | 2012 | Panama | WS | 3.2 | 0.25 | 12.8 | 40 | No |
| Pando | 2012 | Panama | WS | 3.0 | 0.25 | 12.0 | 40 | No |
| El Alto | 2013 | Panama | WS | 5.8 | 0.35 | 16.6 | 40 | No |
| Wehrhahn | 2014 | Germany | SW | 8.3 | 0.30 | 27.7 | 40 | No |
| STEP Abu Dhabi Lot T-02 | 2014 | UAE | WW | 6.3 | 0.28 | 22.5 | 40 | Yes |

## 1.2 MOTIVATIONS

Thanks to the inclusion of guidelines for the design of FRC elements in codes and recommendations (DBV 1992 & CNR 2006 & CPH 2008 & Model Code 2010), it is now possible to consider the structural contribution of this material. In spite of advantages, it is still necessary to perform a critical analysis of the implications related with the direct use of these guidelines for the design of segments reinforced with fibres. This may lead to an over conservative or uneconomical design, inhibiting the use of FRC. An update or adaptation the philosophy taking into account the particularities and the conditions found in tunnels and shafts might be necessary.

Several numerical and experimental studies were performed in order to improve the design of FRC precast segments against cracking and spalling when subjected to concentrated loads during installation in the tunnel. Most studies focus on elements with similar height-to-length ratios. To contemplate the wide variety of dimensions and loading patterns found in practice, additional experimental assessments are yet required. These studies could support the calibration of analytical formulations to assess the cracking and the failure load depending on the dimensions of the elements, promoting an optimization of the design.

Moreover, a recent trend introduced in the Model Code 2010 is to consider the existence of favourable or unfavourable fibre orientation in the design since this parameter is directly related with the mechanical performance. For the case of tunnelling segments, few studies focus on the fibre distribution induced by the flow of concrete and the wall-effect from the formwork. Therefore, it is necessary to understand in detail the fibre distribution within the precast segments depending on the flowability of the concrete used.

The motivations of this thesis are trying to improve the design philosophy of steel fibre reinforce precast concrete segments (SFRPCSs) considering the ductility requirements according to the popular guideline MC 2010. In addition that, in order to overcome the lack of FEM numerical simulation and to understand different characteristics of SFRPCSs, different experimental programmes were performed. These motivations would be discussed in different chapters of the thesis.

## 1.3 OBJECTIVES

### 1.3.1 General objectives

The general objective this doctoral thesis is to develop a systematic and innovative approach for the design optimization and characterisation of SFRC precast segment. This general objective may be divided in the four parts presented below.

A. Study the most recent design procedure for FRC structures and propose an alternative approach more compatible with the conditions found in tunnels and shafts.

B. Extend the study of elements subjected to concentrated loads by considering different height-to-length ratios with and without fibre reinforcement, thus to validate simplified analytical formulations that may be applied for the verification of concrete segments in SLS and ULS.

C. Propose an analytical formulation based on MC 2010 for the re-design of FRC precast segment and validate it with different tests.

D. Evaluate the fibre distribution in segments and propose a conceptual model to predict its distribution pattern.

### 1.3.2 Specific objectives

In response to the various objectives mentioned above, several specific objectives are set. The main specific objectives pursued in order to achieve the overall objectives are presented in the *Table 1.2*.

*Table 1.2 Specific objectives of the thesis*

| Subject | Specific objectives |
|---|---|
| General Objective A:<br><br>Critical analysis of the design of FRC precast segments based on the MC 2010 | • Identify the most restrictive condition in transient situations regarding the ultimate load and determine the minimum reinforcement according to the MC 2010.<br>• Propose an alternative definition of the minimum ductility for the segmental linings in order to avoid overestimations.<br>• Perform a case study of Metro L9 of Barcelona to evaluate the repercussion of the ductility criteria proposed and defined by MC 2010 in terms of fibre consumption. |
| General Objective B:<br><br>Concrete blocks subjected to concentrated load | • Conduct an experimental programme to assess the mechanical response of small-scale concrete specimens with different dimensions subjected to concentrated loads.<br>• Identify the mechanical behaviour of concrete blocks and determine their crack pattern when subjected to the concentrated loads.<br>• Propose strut and tie models to assess $F_{cr}$ and $F_{max}$ based on the experimental tests.<br>• Perform a case study of Metro L9 of Barcelona to evaluate the repercussion of the models proposed. |
| General Objective C:<br><br>Re-design of FRC precast segments | • Propose an analytical formulation based on MC 2010 evaluate the minimum requirements the FRC must fulfil to carry out the conventional replacement.<br>• Perform an experimental campaign to characterize the mechanical behaviour of both conventional and self-compacting concrete reinforced with fibre content ($C_f$) between 30 and 60 kg/m$^3$.<br>• Perform full-scale experimental campaign of bending test on segments is performed to verify the ductile behaviour of two types of segments under failure scenario.<br>• Validate the proposed formulation using the test results. |
| General Objective D:<br><br>Anisotropy property of the FRC precast segments | • Assess the fibre distribution depending on the types of samples.<br>• Analyse the global and local anisotropy of segments with conventional and self-compacting concrete reinforced with fibres.<br>• Analyse the fibre distribution depending on the position inside the segment.<br>• Propose a conceptual model to predict the fibre distribution for both types of segments. |

## 1.4 STRUCTURE OF THE THESIS

The thesis is subdivided into six parts as shown in *Figure 1.1*. Chapter 1 introduces the motivations and objectives of the research. The objectives are achieved from Chapter 2 – Chapter 5. It is necessary to point out that the research work of Chapter 2 and Chapter 3 are based on the project *Metro Line 9 of Barcelona (section Bon Pastor–Can Zam)* and Chapter 4 and Chapter 5 are based on the project *Montcada shaft (section Sants—Sagrera)*, located in high speed railway line Madrid-Zaragoza-Barcelona-French frontier.

Chapter 2 covers the General Objective A. The detail design procedure in the MC 2010 for the FRC elements considering the influence of thickness on the residual tensile strength is analysed. Based on this, an alternative approach is proposed for the design of FRC segments to assure a ductility compatible with the load actually applied in the transient stages. In order to verify the feasibility of the alternative approach, a case study of Metro L9 of Barcelona was conducted, numerical simulation as well as sectional analysis of segments stocking were performed.

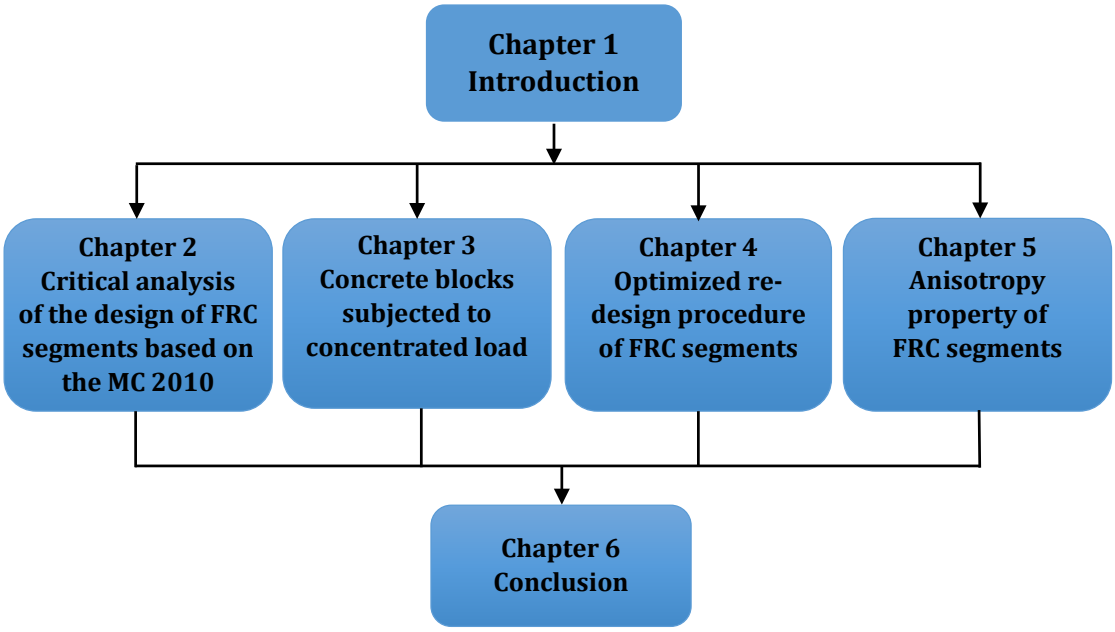


*Figure 1.1 Structure of the Thesis*

Chapter 3 focuses on the General Objective B. An experimental investigation is performed for the study of concrete blocks subjected to concentrated loads by considering different height-to-length ratios with and without fibre reinforcement. Based on the test results, three simplified analytical formulations based on strut and tie model were proposed for the verification of concrete segments in SLS and ULS. Finally, in order to understand the repercussion of the model proposed, a case study of Metro L9 of Barcelona is conducted.

Given the lack of information on the design of FRC segments, a complete design process of FRC segments for the Montcada shaft is presented in Chapter 4 in response to the General Objective C. After that, both small-scale and full-scale experimental programmes were performed in order to determine the content of fibres for the production of segments. A

comparison of the mechanical performance between segments with conventional and self-compacting concrete is presented. Moreover, the re-design method developed is validated.

Chapter 5 addresses the General Objective D. Inductive tests and Barcelona tests are performed in cores drilled form full-scale segments with the purpose of assessing the fibre distribution. Through the analysis of the results, a clear view about the fibre distribution depending on the zones of segments and the type of concrete was obtained. Based on the observations derived from the study, a conceptual model for the fibre distribution within segments is proposed.

Finally, Chapter 6 presents the conclusions of each of subjects addressed in this thesis and provides recommendations for future studies

# 2. DESIGN OF FRC TUNNEL SEGMENTS CONSIDERING THE DUCTILITY REQUIREMENTS OF THE MODEL CODE 2010

## 2.1 INTRODUCTION

As a composite material, it is beneficial to use FRC to improve the mechanical response of precast segments for tunnels (di Prisco et al. 2009 & Walraven 2009 & Burguers et al. 2007 & Hilar et al.2012), enhancing their ductility and fire resistance as well as their mechanical performance during transient load stages. Due to these advantages, the use of structural fibres contributes to the replacement of traditional passive reinforcement, accelerating the production process and increasing the competitiveness of the FRC. Proof of this are the numerous experiences in which precast FRC segments have been used in highway, railway, metro, water supply, gas transport and service tunnels, as shown in the *Table 1.1.*

The structural use of fibres has been regulated by the national codes in Germany in 1992 (DBV1992), Italy in 2006 (CNR 2006), and Spain in 2008 (CPH 2008), for instance. More recently, recommendations about the design of FRC structures were also included in the Model Code (2010), with constitutive equations (Blanco et al. 2010 & Blanco et al. 2013) and models for the Service Limit State and Ultimate Limit State (SLS and ULS, respectively). An increase in the use of FRC in tunnels segments has been observed as a result of that (Caratelli et al. 2012). In this regard, it is necessary to update the philosophy applied to the design of tunnel segments in compliance with the particular requirements proposed in the MC 2010, evaluating its applicability and repercussions.

## 2.2 OBJECTIVES

The objective of this chapter is to present a critical analysis of the design of FRC segments according to the ductility requirements from the MC 2010 and to propose an alternative approach more compatible with the conditions found in practice. First, the design procedure from the MC 2010 is analysed and adapted to FRC segmented linings. Then, the alternative approach is presented. The applicability and repercussion of both approaches in terms of fibre consumption are evaluated in the specific case of the Metro Line 9 from Barcelona, using sectional analysis and results obtained in an experimental programme with full-scale segments. This study shows the possible consequences of applying the design philosophy of the MC 2010 for FRC segments and it indicates alternative design considerations that could be implemented if certain conditions are fulfilled and it provides an example on how it may be used to optimize the fibre content required.

## 2.3 DESIGN PROCEDURE BASED ON THE MC 2010

In tunnels with large internal diameter, segments are usually subjected to high bending moments during the transient and the service stages - the latter being generally the most unfavourable design condition. The replacement of traditional reinforcement by fibres is limited, generally leading to expensive solutions since high amounts of fibre are needed to achieve an equivalent mechanical response. In these cases, mixed reinforcement configurations consisting of a minimum amount of steel bars (that provide resistant capacity in ULS) and a moderate dosage of fibres (that control the crack width in SLS) are attractive solutions.

On the other hand, tunnels with smaller internal diameter tend to be predominantly compressed during service, these being less sensible to either asymmetric loads derived from the soil or other discontinuities. As a result, the main reinforcement usually consists of a minimum amount of rebars established in codes to avoid brittle failure of the segments that might occur during the transient load situations. In such cases, the complete substitution of the traditional reinforcement by fibres may be a suitable alternative from the technical and the economic points of view.

The most relevant transient situations correspond to the demoulding, stocking, transport, manipulation, and the placement of the segments inside the tunnel and the application of the thrust forces by the jacks (Caratelli et al. 2012 & de Waal et al. 1999 & Kooiman 2000 & Blom 2002 & Cavalaro et al. 2011), as shown in *Figure 2.1.* The SLS and ULS limit conditions considered in the structural verification in each one of these transient situations vary depending on the load pattern applied. For instance, the demoulding, the stocking, the transport and the manipulation are characterized by load patterns that induce bending moments and might generate bending cracks or failure. Conversely, the placement of the segments, and the application of the thrust forces are characterized by a concentrated load in a reduced area that might generate localized cracking.

Although verifications should be performed for both types of load patterns, the first is directly related with the design guidelines provided by the MC 2010 for FRC, whereas the

bursting and the splitting require special considerations (Haring et al. 2002 & Sorelli et al. 2005 & Groeneweg 2007 & Burgers et al. 2007 & Tiberti et al. 2014), Therefore, considering the main objective of the paper, only the transient load situations that lead to bending are analysed here.


*Figure 2.1 Temporary load stages of a segment: a) demoulding b) stocking, c) transport and d) thrust of jack*

If fibres are applied as the only reinforcement, the MC 2010 imposes three mechanical criteria based on the load – displacement curve shown in *Figure 2.2a* that any FRC structure should fulfil. First, the ultimate load ($P_u$) resisted shall be higher than both the cracking ($P_{cr}$) and the service ($P_{SLS}$) loads. Second, the ultimate vertical displacement ($\delta_u$) should be larger than the observed in the service limit state ($\delta_{SLS}$) calculated performing a linear elastic analysis with the assumptions of uncracked concrete and initial elastic Young's modulus. Third, the $\delta_{SLS}$ should be at least 5 times lower than the vertical displacement $\delta_{peak}$ estimated for the maximum load ($P_{max}$).

The first requirement about the ultimate load is a condition established in most reinforced concrete codes that intend to avoid the brittle failure in case of cracking ($P_u \geq P_{cr}$). This requirement may be translated in terms of the bending moment through the equivalent relation $M_u \geq M_{cr}$ (de la Fuente et al. 2011 & de la Fuente et al. 2012 & Levi et al. 1985 & Chiaia et al. 2009 & Chiaia et al. 2009), in which $M_u$ and $M_{cr}$ are the ultimate and the cracking bending moments, respectively. The restriction $P_u \geq P_{SLS}$ ($M_u \geq M_{SLS}$) is rarely limiting the design of precast segments for tunnels since bending moments are usually small and $P_{cr} \geq P_{SLS}$ ($M_{cr} > M_{SLS}$) during transient situations. In this sense, cracking is rather

caused by accidental loads or even to inadequate support or handling of the segment and should be treated differently (Sugimoto et al. 2006 & Cavalaro et al. 2012 & Cavalaro et al. 2012). Hence, the condition $M_u \geq M_{cr}$ tend to be the most restrictive condition regarding the ultimate load.

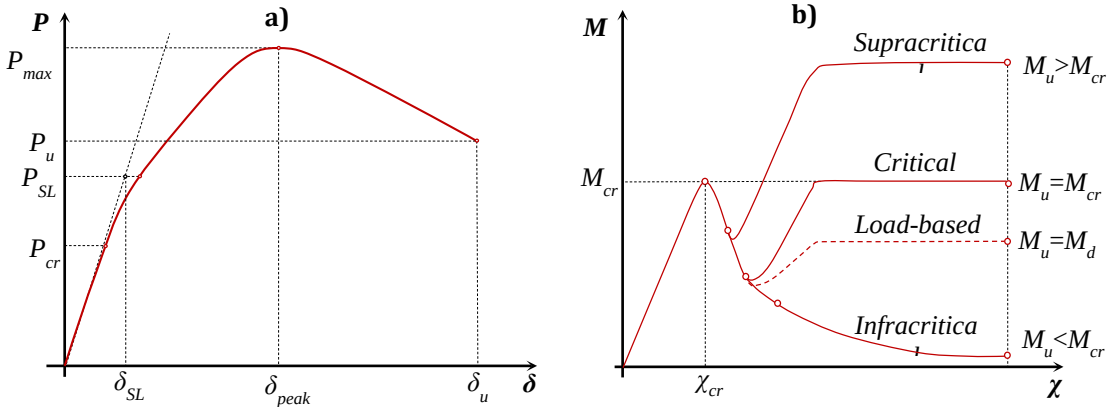


*Figure 2.2 a) P-δ curve for a FRC structure and b) M-χ diagram for different sectional responses*

The two displacement requirements ($\delta_u \geq \delta_{SLS}$; $\delta_{peak} \geq 5\delta_{SLS}$) intend to guarantee a minimum deformability of the most unfavourable sections in order to activate the redistribution capacity of statically indeterminate structures. It is important to remark that precast segments tend to assume a statically determinate configuration during the transient stages. Therefore, in this case the deformability requirements would not be necessary since the condition $M_u \geq M_{cr}$ is sufficient to guarantee the ductility in case of a hypothetical flexural rupture (Hilar et al.2012 & de la Fuente et al. 2011 & de la Fuente et al. 2012 & Levi et al. 1985 & Chiaia et al. 2009 & Chiaia et al. 2009 ). Consequently, the minimum reinforcement according with the MC 2010 is determined by the ductility requirement expressed through $M_u \geq M_{cr}$.

The moment-curvature diagram ($M - \chi$) presented in *Figure 2.2b* includes different reinforcement configurations (infracritical, critical and supracritical) (Levi et al. 1985). Notice that by imposing $M_u \geq M_{cr}$, only critical and supracritical reinforcement configurations are allowed according to the design philosophy from the MC 2010. Needless to say that if the design bending moment $M_d$ is higher than $M_{cr}$, the requirement to be imposed shall be $M_u \geq M_d$ (Bakhshi et al. 2014 & Bakhshi et al. 2014 & Bakhshi et al. 2014 & Bakhshi et al. 2013). This means that a supracritical reinforcement arrangement should be used (*Figure 2.2b*), thus making the total replacement of the rebars by fibres less competitive.

To determine the minimum amount of fibre reinforcement required, the condition $M_u \geq M_{cr}$ must be solved by using nonlinear sectional analysis (*Figure 2.3*) and by imposing the constitutive equations suggested in the MC 2010. In this sense, a rigid-plastic response may be assumed to simulate both the compressive and post-cracking tensile responses of the FRC. By doing so, the residual flexural tensile strength related to a crack mouth opening displacement of 2.5 mm ($f_{R3}$) can be derived and established as a control parameter for the tests to be performed during production. This criteria related to the

deformation is also adopted in the MC 2010 as a reference for the verification of the ULS of FRC structures.

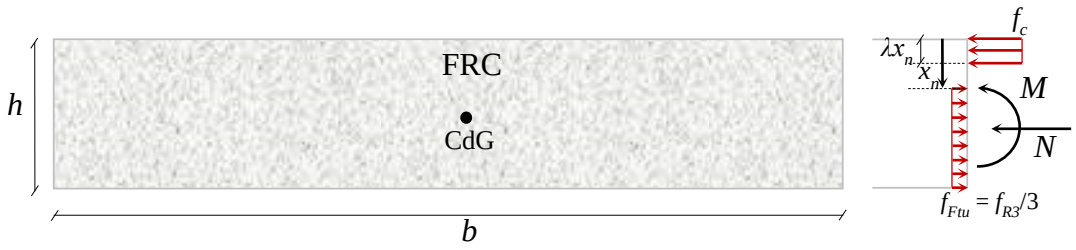


*Figure 2.3 FRC cross – section of a precast segment subjected to axial stresses*

In typical transient load situations observed in practice, a simple bending condition may be expected. *Equation 2.1* and *Equation* 2.2 are derived by imposing the equilibrium conditions and by assuming external axial forces are $N \approx 0$ (these forces are usually small and their exclusion leads to results on the safe side as they tend to produce compressed in the cross – sections).

$$N = f_c b \lambda x_n - f_{Ftu} b (h - x_n) = 0 \qquad \text{Equation 2.1}$$

$$N = f_c b \lambda x_n \frac{5h - x_n}{10} = M_u \qquad \text{Equation 2.2}$$

In *Equation 2.1* and *Equation* 2.2, $f_c$ is the uniaxial compressive strength of the concrete, $f_{Ftu}$ is the residual tensile strength of the FRC, $b$ is the width of the segment, $h$ is the height of the segment, and $x_n$ is neutral axis depth. The value adopted here for the parameter $\lambda$ is 0.8 (4/5), according to the recommendation of the MC 2010.

*Equation 2.1* and *Equation* 2.2 may be combined to obtain *Equation 2.3* that provides the required value of $f_{R3}$. It should be emphasized that depending on the limit state analysed, the partial safety factors for both the material and loads might differ. Moreover, the time dependency of $f_{R3}$ and $f_c$ should be taken into account as well.

$$f_{R3} \geq \frac{12 f_c}{\frac{1}{\left(-1 + \sqrt{1 + 2\frac{M}{f_c b h^2}}\right)} - 5} \qquad \text{Equation 2.3}$$

According to the MC 2010, the minimum average value of $f_{R3}$ ($f_{R3m,\,min}$) is derived imposing in *Equation 2.3* the condition $M_u = M_{cr} = b \cdot h^2 \cdot f_{ctm,fl}/6$, with the average compressive strength ($f_{cm}$) and the average flexural tensile strength ($f_{ctm,fl}$) of concrete. As a result, *Equation 2.4* is obtained. Notice that the calculation is performed with average values of loads and material properties. Moreover, the $f_{R3m,\,min}$ required depends solely on the mechanical properties of concrete. Thus, should the mechanical properties of the material increase with time, $f_{R3m,\,min}$ would also increase.

$$f_{R3m,min} = \frac{12 f_{cm}}{\frac{1}{\left(-1 + \sqrt{1 + \frac{f_{ctm,fl}}{3 f_{cm}}}\right)} - 5} \qquad \text{Equation 2.4}$$

As an example of application, the curves $f_{R3m,\,min}$ versus time calculated for concrete strength classes C30, C50 and C70 are shown in *Figure 2.4a, 2.4b* and *2.4c,* respectively. Furthermore, these curves are particularized for a representative range of $h$; 0.2 – 0.5 m being representative heights for precast concrete segments. The time dependency of the mechanical parameters involved in the formulation was considered by means of the expressions suggested in the MC 2010. *Figure 2.4d* summarizes the influence of the thickness $h$ on $f_{R3m,\,min}$ for the same concrete classes.

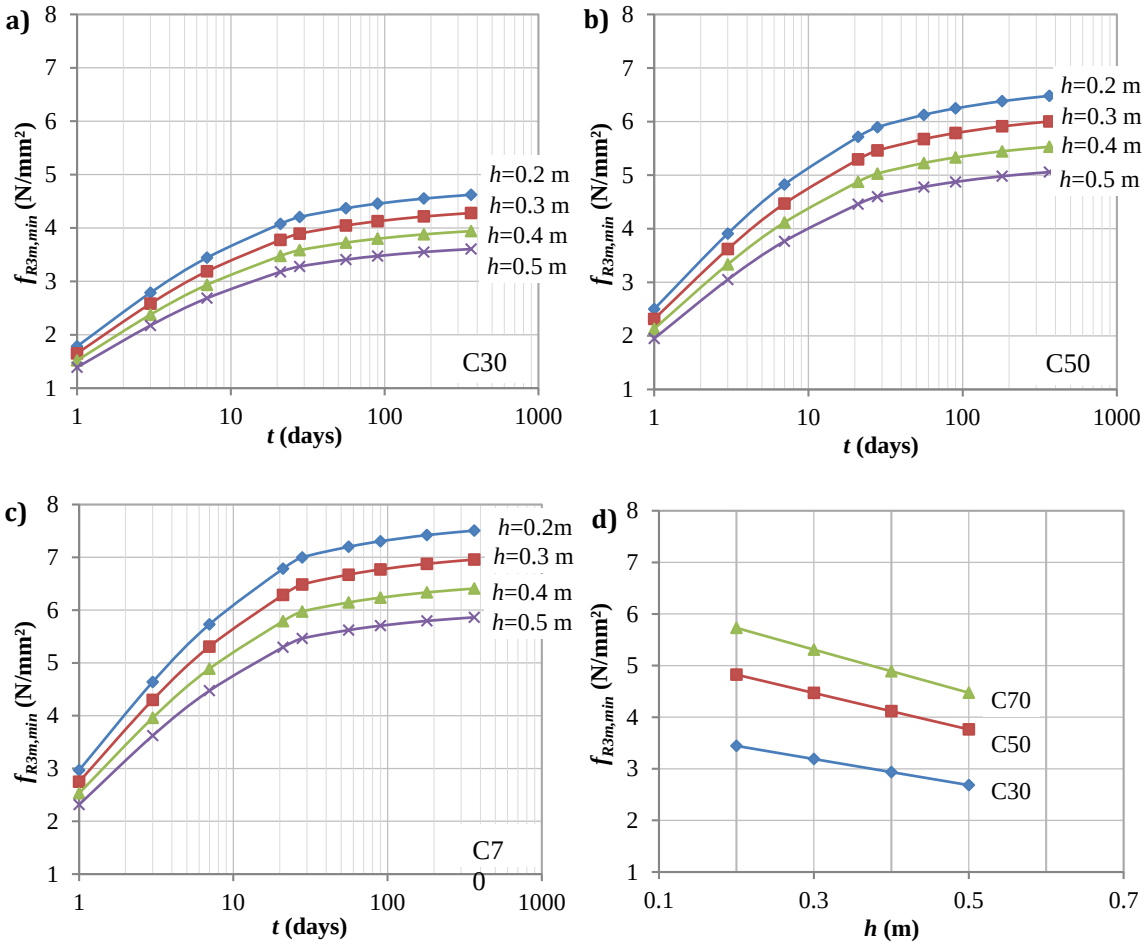


Figure 2.4 *Age – dependency of the required $f_{R3m,}$ min for concrete classes a) C30, b) C50, c) C70 and d) dependency of h on $f_{R3m,min}$ at 7 days*

The results presented in *Figure 2.4* highlight that the $f_{R3m,\,min}$ required decreases as $h$ increases. Moreover, it is observed that $f_{R3m,\,min}$ increases with time due to the time dependency of $f_{ctm,fl}$ and of $f_{cm}$. Such an observation might lead to the erroneous conclusion that higher fibre contents would be required if the segment is subjected to the transient loads at later ages. Nevertheless, it is important to consider that, for the same fibre content, the $f_{R3}$ also increases with the concrete age. Therefore, even though the value of $f_{R3m,\,min}$ required increases with time, the fibre content $C_f$ probably will not increase since the pull – out mechanism also improves with time.

Despite that, apparent contradictions may arise from the data in *Figure 2.4.* Suppose the hypothetical case of a segment designed to be transported 7 days after of production that

had its transport delayed by additional 7 days. The magnitude and the variability of the transient loads are often well established during the project phase (far better than the soil loads, for instance) due to the systematic and controlled production processes (Camós et al. 2014). In fact, these actions should not vary considerably unless changes in the production process are introduced. Hence, the cracking safety factor should increase with time since $f_{ctm,fl}$ also increases. In other words, even though it would be safer to transport the segment at later ages, a higher $f_{R3m,\,min}$ would be required according to the results presented in *Figure 2.4.* A similar situation would be observed, for example, if the concrete used present a higher compressive strength than the originally defined in the project. In this case, a higher $f_{ctm,fl}$ would be obtained and higher values of $f_{R3m,min}$ are necessary to guarantee a ductile response of the segment despite having in reality a higher cracking safety factor.

The paradox would be even more evident if this philosophy was applied for a tunnel in which the thickness of the segment is governed by limitations of the TBM jacks (minimum height of the segment to fit the jack, for instance). In this case, $M_{cr} \geq M_d$ and, consequently, when the ductility limitation is applied, the $f_{R3m,\,min}$ derived from this requirement would correspond to a load that is higher that used for the ULS, whose probability of being surpassed is not relevant. In this context, one might question if it is reasonable to provide ductility for a load that is higher than that considered in the ULS for a transient stage.

This issue concerns the considerations included in the new design philosophy of the MC-2010 when applied to segmented linings. It is evident that for safety reasons a minimum ductility must be maintained to avoid brittle failure. The main issue is how such ductility should be defined in the case of segmented linings. To provide a reasonable alternative, it is important to consider the special context in which these elements are designed and used.

As mentioned before, in certain tunnels, segments are designed not to crack in transient stages and in service, presenting enough safety margins to account for the safety coefficients proposed in codes. For this reason, the likelihood of cracking is already contemplated in the design of the segments. Moreover, in tunnels subjected to mainly compressive loads in service (except in particular stretches), the transient load cases tend to be the critical ones. These are observed for a short period, before the elements have to fulfil their service life under controlled conditions. Consequently, if cracking due to imperfections or other damages occur, they may be detected and corrected before construction of the tunnels with small or even no repercussion to the performance of the structure and to the safety of workers. Another relevant aspect is that, in transient stages, the segments are normally subjected to statically determinate support configurations (Bakhshi et al. 2014 & Bakhshi et al. 2014 & Bakhshi et al. 2014 & Bakhshi et al. 2013). Therefore, no stress redistribution should be expected, thus reducing the justification for a critical or supercritical ductility.

In this context, the use of a residual strength that leads to a critical or supercritical ductility does not seem compatible with the stress produced due to the transient loads. If

segments are designed not to crack, this criterion is excessively severe and could provide a structural response above the required for safety reasons, resulting in an overestimation of the minimum residual strength needed. To avoid overestimations, an alternative definition of the minimum ductility is proposed in the present study for the segmented lining.

Notice that the load applied in transient stages is mainly the result of the self-weight of the segments, which does not vary excessively due to the quality control of the precast producer. If by any chance cracking occurs, it should be the result of thermo-hygrometric stresses (induced, for instance, by shrinkage) or due to impacts that are limited in time. In both cases, the load that generates the crack tends to dissipate in a short time; as soon as the cracks are formed the stresses are released. To provoke the failure in such situation, the remaining load or that applied in later stages must be high enough to increase the crack opening. Taking into consideration that thermo-hygrometric induced stresses or impacts dissipate soon after the crack is formed, the only remaining load that could increase the crack opening up to failure would be expected during the posterior transient stages. As long as the remaining resistant capacity of the cracked cross – section is enough to resist theses loads, in addition to a safety margin introduced by the partial safety factor of the material and the load, the ductile failure would be assured.

Therefore, instead of estimating the minimum residual strength from the average cracking bending moment, a load-based criterion is suggested to assure ductility compatible with the load actually applied in the transient stages. This strength is calculated with the design values of the forces that act on the segment taking into account the corresponding safety factors for the materials and the actions (those suggested in the MC 2010, for instance). Such load-based criterion could yield the structural response indicated in the dotted curve from *Figure 2.2b.* This way, if cracking occurs for the reasons mentioned previously, the segment would still present enough ductility to safely carry the loads applied. It is important to remark that the alternative approach proposed here should be applied only if the segments are designed not to crack, the tunnel is subjected mainly to compression in the service stage and the critical load occurs in the transient stages under controlled conditions.

Taking the example of an element subjected to a bending moment (included in this section), the required $f_{R3m,\,min}$ according to the alternative approach proposed ($f_{R3m,\,alt}$) may be obtained through *Equation 2.5*. This equation includes the concrete safety factor ($\gamma_c$) that is multiplied by the design strength $f_{R3}$ required ($f_{R3d}$) to obtain the characteristic value of $f_{R3}$ ($f_{R3k}$). The letter is divided by the coefficient $\psi$, intended to transform characteristic values of the tensile strength in average values. The $f_{R3d}$ may be substituted by *Equation 2.3* if the design compressive strength ($f_{cd}$) and the design bending moment ($M_d$) calculated with the partial safety factors are used.

$$f_{R3m,alt} \geq \frac{\gamma_c}{\psi} f_{R3d} = \frac{\gamma_c}{\psi} \frac{12 f_{cd}}{\frac{1}{\left(-1 + \sqrt{1 + 2\frac{M_d}{f_{cd} b h^2}}\right)} - 5} \qquad \text{Equation 2.5}$$

*Equation 2.5* implies that the service loads do not affect the minimum $f_{R3}$ value estimated, regardless of the nature of the load applied. For example, in case of a tunnel subjected to asymmetric seismic loads, the alternative approach should be valid as long as the design loads are not high enough to produce cracks in the segments and the transient stages still represent the critical condition. Otherwise, a specific analysis should be performed.

To evaluate the repercussion of the ductility criteria proposed here and defined by MC 2010 in terms of fibre consumption, their application to the Metro L9 of Barcelona is presented in the next section.

## 2.4 METRO L9 OF BARCELONA

The Metro L9 of Barcelona counts 46 stations and 15 interchanges with a total length of 44 km and connects the airport (El Prat), the justice district (Ciutat de la Justicia) and the high speed railway station (Barcelona Sants Station). The construction is performed with a TBM with approximately 12.0 m of diameter. So far, this is probably one of the most studied TBM-bored tunnels and this is still under construction. In this sense, experimental and numerical analysis related with the FRC were extensively performed (Gettu et al. 2003 & Gettu et al. 2004 & Molins et al. 2011 & Arnau et al. 2011). Likewise, particular numerical studies concerning the concentrated load induced by the jacks were also developed to explain some of the cracks observed during the construction of the tunnel (Burguers 2006).

The Bon Pastor – Can Zam stretch is analysed in the present study. It consists of a ring with $D_i$ = 10.90 m and this is divided in 7 segments and 1 key with $h$ = 0.35 mm and $b$ = 1.8 mm. The segments were initially designed with a C50/60 concrete reinforced with traditional rebars and 30 kg/m$^3$ of steel fibres. The structural contribution of the fibres was originally not considered in the design. These were only intended to reduce the incidence of damages due to impact during manipulation and placing of the segments. *Figure 2.5* shows the layout of the ring and the reinforcement used.

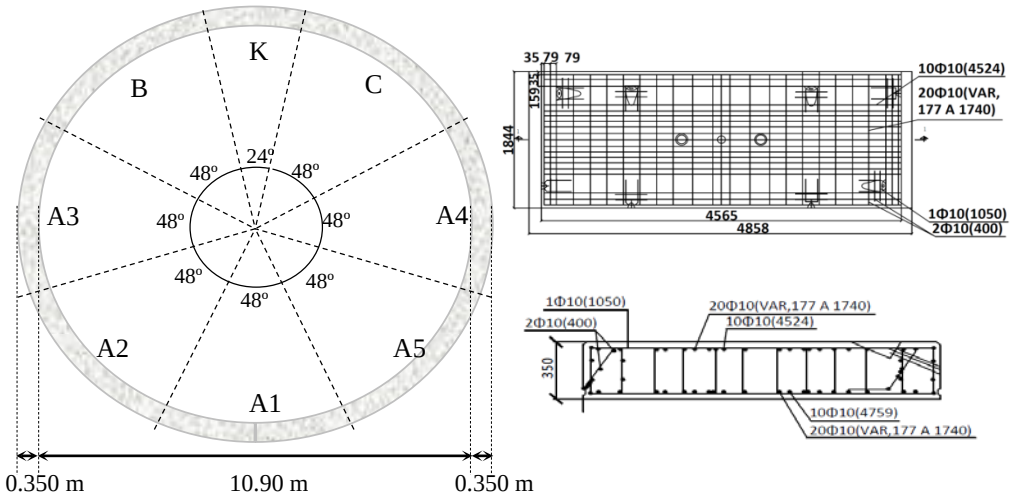


*Figure 2.5 Ring dimensions of the Can Zam – Bon Pastor Stretch of Barcelona's Metro L9*

## 2.5 NUMERICAL SIMULATIONS

In this context, the total substitution of the rebars by steel fibres was analysed. First, a numerical study considering the possible load cases was developed in order to verify the suitability of this reinforcement strategy. The results of this analysis were reported in (Gettu et al. 2003). The main conclusions derived were the following:

- The worst load condition is expected during the stocking. After demoulding, only three segments can be stacked to avoid concrete cracking. The remaining segments of the ring can be stacked seven days after casting. This load situation was analysed in detail since this is critical in terms of design and productivity.

- The advance of the TBM during construction is accomplished by means of 15 jacks that have a contact area of 1.374 x 0.350 m2 and introduce a total force of 90 MN in the segmented lining. This load situation was simulated considering 35 mm of eccentricity of the thrust jacks (see *Figure 2.6*). The numerical results indicated the presence of bursting stresses in the disturbed zone generated by this local force. The tensile stresses reach values above the tensile strength of concrete (fct). Therefore, cracking of the concrete is highly probable during the construction of the tunnel due to the application of the thrust loads of the jacks. Fortunately, fibres contribute, bridging cracks and controlling their width. Besides, this is a transient load phase, and once the tunnel is in service, the cracks tend to close due to the compression introduced by the soil.

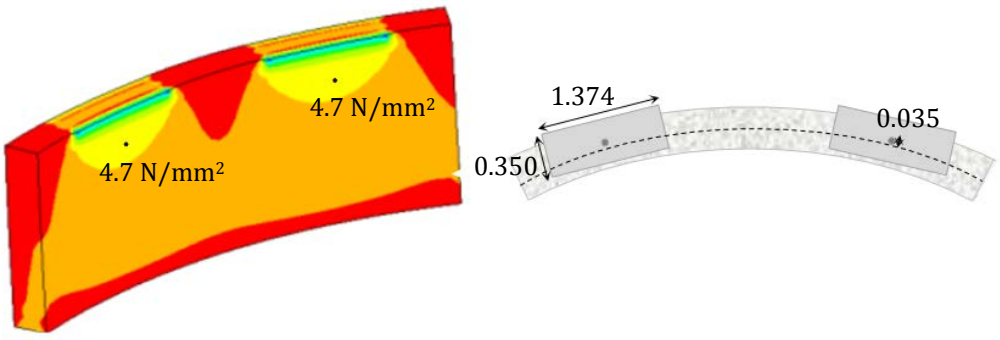


Figure 2.6 *Dimensions of the jacks and eccentricity considered for the numerical analysis*

- The behaviour of the supports and their interaction with both the soil and water was also analysed numerically. Fourteen load cases were studied considering the existence of plastic hinges in the radial joints. The tensile stresses obtained with the model were below 0.785 N/mm$^2$ for the worst – case scenario, meaning that the cross – section of the segments conserve its integrity during the service life unless cracks appear during the stocking or other transient load situations. In any case, this stress level is low and the concrete cracking due to bending combined with axial loading is unlikely to occur. Therefore, it was concluded that the ring is subjected to compression during its service life and the reinforcement is mainly needed to control the crack widths during the transient load situations.

## 2.6 EXPERIMENTAL PROGRAMME

### 2.6.1 Materials

Once identified with numerical analysis that the critical load occurs in the transient stage during stocking, an experimental programme was conducted with real-scale segments in order to verify the substitution of the steel rebars by fibres. The composition of the concrete is presented in *Table 2.1.* Mixes were produced with different steel fibre contents ($C_f$) of 20, 30, 40, 50 and 60 kg/m$^3$ in order to assess the mechanical performance of the FRC with different amounts of fibres (Gettu et al. 2003). With this regard, hooked-end steel fibres with a length ($l_f$) of 50 mm, a cross – section diameter ($d_f$) of 1.00 mm and a yielding strength ($f_f$) of 1100 N/mm$^2$ were used. The amount of superplasticizer added to the concrete increased with the fibre content to assure similar workability (4 cm of slump in the cone test) and equivalent behaviour in terms of fibre distribution inside the segment (Pujadas et al. 2014 & Pujadas et al. 2015 & Blanco et al. 2015), which is essential for the comparison of the structural responses.

*Table 2.1 Composition of concrete*

| Material | Dosage (kg/m$^3$) |
|---|---|
| Cement type I 52.5R | 400 |
| Granitic sand 0-4 mm | 846 |
| Granitic aggregate 5-12 mm | 443 |
| Granitic aggregate 12-20 mm | 550 |
| Water | 153 |
| Superplasticizer | From 5.6 to 6.4 |
| Fibres | 20, 30, 40, 50 and 60 |

From each composition, four prismatic specimens with 150mm x 150mm x 600mm were cast and cured under conditions that emulate those experienced of the segments. They were cured during 6 hours at 40 °C and 80% of relative humidity. After that, they were stored at 20 °C and 50% of relative humidity during 7 days. Finally, they were kept under the conditions of the production hall and tested at 28 days according with the standard UNE-EN 14651(2005) to characterize the limit of proportionality $f_{LOP}$ and the residual flexural strengths $f_{R1}$ and $f_{R3}$. The average values of $f_{LOP}$, $f_{R1}$ and $f_{R3}$ ($f_{LOPm}$, $f_{R1m}$ and $f_{R3m}$, respectively) are included in Figure 2.7, along with the corresponding coefficient of variation.

The results summarized in *Figure 2.7* highlight that the mechanical properties measured tend to increase with $C_f$, which is consistent with the results from (Barros et al. 2005). It is important to remark that the FRC showed a softening behaviour in all cases. A linear regression of the data included in *Figure 2.7* leads to *Equation 2.6* and *Equation 2.7* for the assessment of the $f_{R1m}$ and $f_{R3m}$ depending on $C_f$ (in kg/m$^3$). In the present study, these equations are considered as a reference to estimate the $C_f$ needed in the design of the segments.

$$f_{R1m} = 0.063C_f + 1.64 \qquad \text{Equation 2.6}$$

$$f_{R3m} = 0.089C_f$$ Equation 2.7

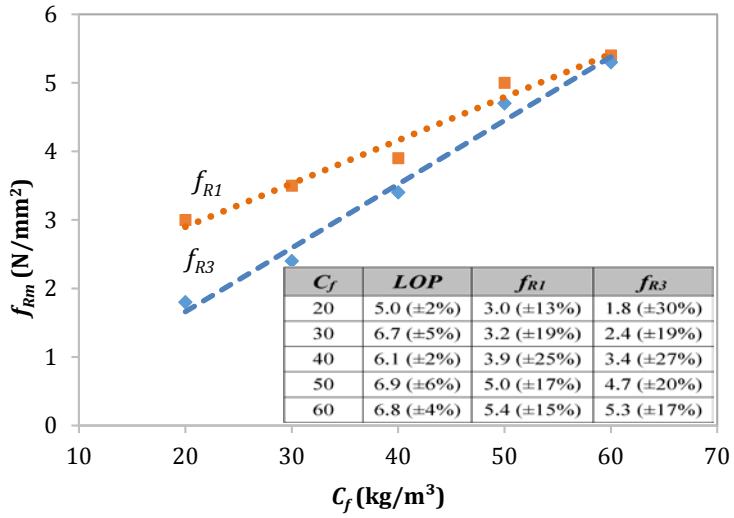


*Figure 2.7 Average residual flexural tensile strength depending on fibre content*

### 2.6.2 Real scale tests related with the stocking procedure

The numerical approach proposed to estimate $f_{R3}$ was compared with the results derived from the experimental programme on full-scale tests reproducing the stacking process. Even though FRC with a wide range of fibre contents were tested to evaluate the repercussion of the ductility criteria proposed by the MC 2010 in terms of design, segments reinforced with traditional rebars and 30 kg/m$^3$ of fibre and segments reinforced with 60 kg/m$^3$ of fibres were produced for real-scale tests.

During the storage (see *Figure 2.8*), the supports placed at the bottom of the pile are fixed, whereas the supports placed between adjacent segments should be aligned vertically without inducing eccentricities. In practice, however, slight deviations from the perfect alignment may occur in the support between segments. This generates bending moments and, ultimately, damages if $M_{cr}$ is exceeded. Although the first segment from the pile has the highest loading, the critical load case in terms of bending moment is likely to occur in the second segment since it may be subjected to a larger eccentricity.

Tests were performed to evaluate the performance of segments if eccentricities are present. For that, they were stored in piles. The first segment was placed over the fixed support. Then, the second segment was positioned over the supports that had an eccentricity equal to $e_e$ with the axis of the fixed support at the base of the pile. Next, the third segment was placed with an eccentricity $e_i$ with respect to the axis of the fixed support at the base (see *Figure 2.8*). Since a symmetric configuration is assumed to generate the highest bending moment, the theoretical free span that should exist in an ideal situation ($l_o$=2.8 m) for the second segment was increased by a distance of $2e_e$. Moreover, the total eccentricity $e_{tot}$ applied for the third segment to the second one at each loading point was equal to $e_e + e_i$. Finally, the other segments that compose a ring were placed over the existing pile, achieving the configuration of 8 segments (7 + the key segment) depicted in *Figure 2.8.*

During the stacking process, the number and the width of cracks were measured. For that, two transducers were $_{placed}$ at both sides of the second segment (see*Figure 2.8*), close to the bottom of the lateral face that form the circumferential joint (indicated by T1). An additional transducer was installed along the imaginary line that connects the support and the point of application of load to capture possible shear strains (indicated by T2).

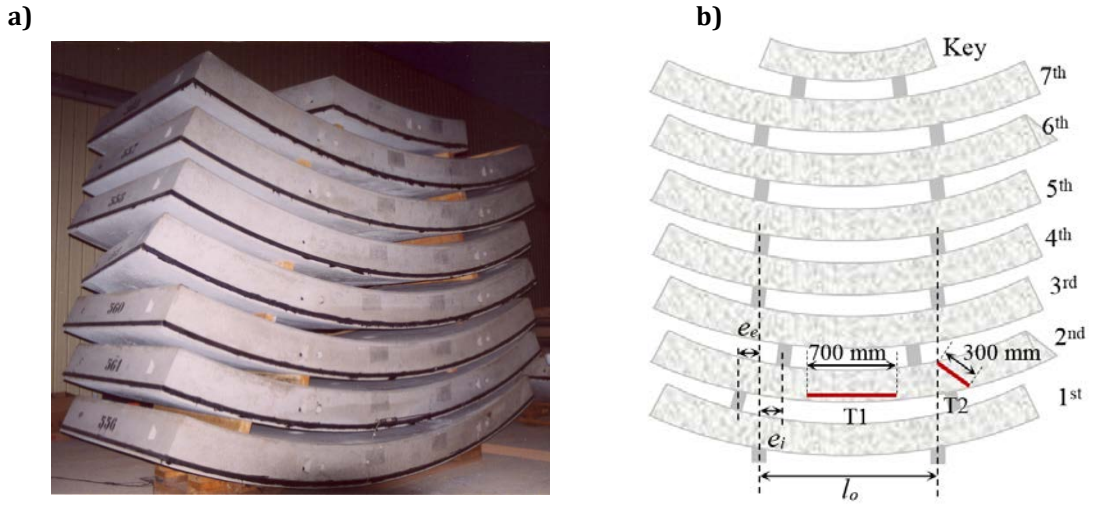


*Figure 2.8 Test simulating the effects of the eccentricity in a pile of a) 3 segments and b) 7 segments plus a key*

The accidental values for $e_e$ and $e_i$ expected during construction are close to 0.10 m (Gettu et al. 2003). Since the aim of the experimental programme was to evaluate the mechanical response of the segments with two different reinforcement strategies, values of $e_e = e_i = e$ were set to 0.25 m and to 0.50 m. Notice that the latter represents an exaggeration intended to force that $M_d > M_{cr}$ , in order to favour concrete cracking and the activation of the reinforcement.

*Figure 2.9a* presents the results obtained in terms of total crack width (average value measured by the transducers T1 placed at both lateral faces) versus the number of segments in the pile ($n_s$). It is evident that the segment with mixed reinforcement (rebars + 30 kg/m$^3$ of fibres) shows a ductile behaviour. The crack occurred when the 6$^{th}$ segment was placed (4 segments stacked over the 2$^{nd}$ segment). Nevertheless, additional segments could be staked since the bars and the fibres became active after cracking, hence limiting the total crack opening to a value of 0.4 mm. In this sense, a variation of curve may be observed for values of $n_s$ between 5 and 6, confirming a change of stiffness due to cracking.

The segment with 60 kg/m$^3$ of fibres and an eccentricity $e$ of 0.50 m also cracked when the 6$^{th}$ segment was placed. The results highlight that the amount of 60 kg/m$^3$ of fibres was insufficient to guarantee a ductile behaviour in this case since a wide crack appeared and a brittle failure took place (*Figure 2.9b*). On the other hand, the results indicate that the segment with 60 kg/m$^3$ of fibres and eccentricity $e$ of 0.25 m presents a linear elastic behaviour during the complete test, showing no visible crack. In the next section, this phenomenon is studied through a numerical analysis.

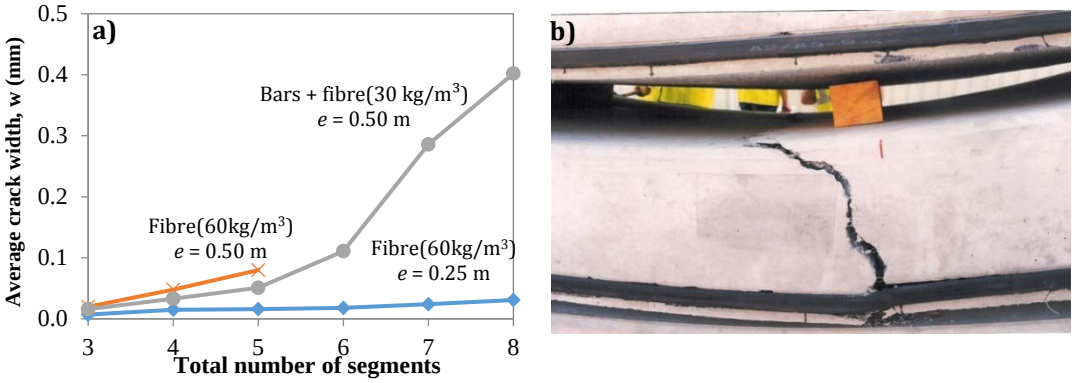


*Figure 2.9 Detail of a) average crack width measured and b) expected brittle failure of segment reinforced only with 60 kg/m³ of fibres and subjected to eccentricities of 0.50 m*

## 2.7 ANALYSIS OF SECTIONAL RESPONSE

The structural analysis based on the design approaches presented in Section 2 is used to assess the minimum flexural residual strength that guarantees ductility. The second segment is subjected to its self-weight *(Figure 2.10a*) and the total load transmitted by the upper segments (*Figure 2.10b*). The self-weight of the segment is represented by means of a uniformly distributed load $p$ = 16.2 kN/m and the force applied by the upper segments by $F = n_s \cdot P_s$, $P_s$ being the self–weight of each individual segment (75.2 kN). The maximum bending moments are $M_{p,max}$ and $M_{F,max}$, depicted in *Figure 2.10*.

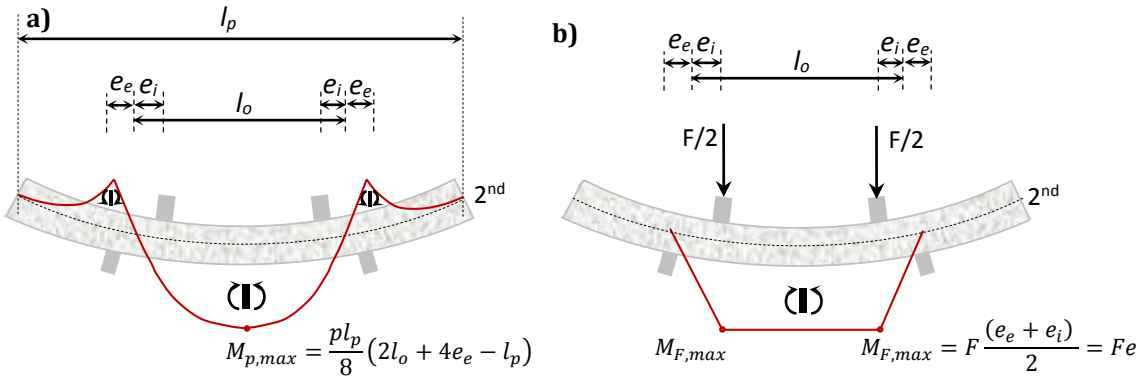


*Figure 2.10 Bending moment diagrams for a) self-weight and b) segments stocked*

The cracking safety factor $SF_{cr}$, understood as a deterministic parameter, is defined as the ratio of the cracking bending moment of the cross – section ($M_{cr}$) and the total bending moment produced by the loads applied ($M_{tot} = M_{p,max} + M_{F,max}$). *Figure 2.11a* shows the curves that relate $SF_{cr}$ and the eccentricity $e$ for different numbers of segments in the pile. It is important to remark that the average flexural tensile strength of the concrete ($f_{ctm,fl}$) involved in the assessment of $M_{cr}$ was calculated using the results of the bending tests shown in *Figure 2.7* and imposing that $f_{ctm,fl} = f_{LOPm}$. Given the fact that the concrete age at the date of testing the segments was 4 days only and these had undergone vapour curing, the strength at 28 days was reduced by 15%.

The curves from *Figure 2.11a* confirm the results from the tests. They show that for an eccentricity of 0.25 m, the probability of cracking is low since $SF_{cr}$ reaches values close to

1.5 for the maximum load (7 segments + key). On the contrary, for eccentricities close to 0.50 m, cracking occurs ($SF_{cr}$ < 1.0) when the number of segments piled is higher than 5. Bearing in mind that $e_e$ and $e_i$ should not be over 0.10 m in practice, the likelihood of cracking is small since for this eccentricity $SF_{cr}$ is 3.2. In this context, only a minimum reinforcement should be placed in order to guarantee a ductile response in the unlike case of cracking.

*Figure 2.11b* shows the curves that relate $f_{R3m,\,min}$ and $e$ for different values of $n_s$. Since the main goal is to compare these results with those obtained experimentally, the material and the load partial safety factors were fixed to 1.00 and average values for the material strengths were considered. The $f_{R3m,\,min}$ required to meet the ductility condition established in the MC 2010 may be calculated through Equation 2.4. Notice that a constant value of $f_{R3m,\,min}$ = 4.8 N/mm² is obtained regardless of $n_s$ or $e$ since $M_{cr}$ is a mechanical property of the cross – section (dashed line in *Figure 2.11b*).

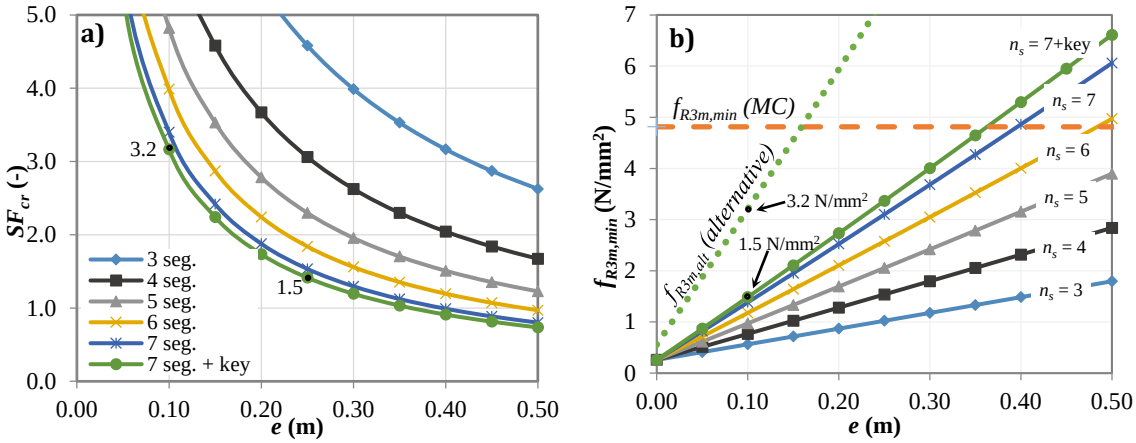


*Figure 2.11 a) Variation of $SF_{cr}$ and b) $f_{R3m,\,min}$ depending on eccentricity*

On the other hand, for the alternative design philosophy proposed in this study, the mechanical requirement of the FRC was estimated considering characteristic values of loads and mechanical properties, which were then reduced by partial safety factors. Since the critical situation is observed in a transient stage, the partial safety factors for the loads are 1.35 for the self-weight and 1.00 for the load of the upper segments (the eccentricity should be considered as an accidental geometric imperfection), whereas the partial safety factor for the compressive and for residual tensile strengths of the FRC ($\gamma_c$) is 1.50. The $M_d$ and the $f_{cd}$ calculated in this way are included in Equation 2.5 to assess the minimum average value of $f_{R3}$ for the alternative approach ($f_{R3m,alt}$), using $\psi$ equal to 0.7 as proposed in the MC 2010 . Only the curve corresponding to a pile of 7 segments plus the key is showed (dotted line in *Figure 2.11b*).

Again, it is observed that the sectional response estimated with the numerical model agrees with the experimental results. At the moment of testing, the $f_{R3m}$ of concrete of the segments was approximately 4.3 N/mm² (85% of $f_{R3m}$ at 28 days for $C_f$ = 60 kg/m³, see *Figure 2.7*). If $e_e$ = $e_i$ = 0.5 m, this strength is exceeded when more than 5 segments are placed on the pile (required $f_{R3m}$ equals 5.0 N/mm²). The results also reveal that values of

$f_{R3m}$ higher than $f_{R3m,min}$ calculated according with the MC 2010 are obtained in case of having stacked more than five segments ($n_s$ = 6 and $e$ ≥ 0.48 m; $n_s$ = 7 and $e$ ≥ 0.40 m; $n_s$ = 7 + key and $e$ ≥ 0.36 m). For the other scenarios, although the $f_{R3m}$ requirement might be less demanding, the $f_{R3m,\,min}$ would be used. For the eccentricity of 0.10 m considered in the project of Line 9 of Barcelona, the average residual strength calculated in service without any safety factor is 1.5 N/mm$^2$ ($n_s$ = 7 + key and $e$ = 0.10 m).

Notice that the ductility required by the MC 2010 would be fully activated only if a load approximately 3.2 times higher than the load expected during the transient stage ($n_s$ = 7 + key and $e$ = 0.10 m, Figure 2.11a) is applied. In fact, this requirement ($f_{R3m,\,min}$ = 4.8 N/mm$^2$) provides a minimum residual strength that is high enough even to satisfy the ULS design of the segment. The reason for such result lays on the fact that these segments were designed not to crack. Consequently, the cracking load becomes the reference for the assessment of both SLS and ULS in terms of simple bending. As this load is also the basis for the assessment of the ductility requirement from the MC 2010, indirectly the minimum residual strength obtained complies with the ULS.

On the contrary, the alternative design philosophy proposed in this work yields a minimum residual strength of 3.2 N/mm$^2$ (*Figure 2.11b*). Consequently, the ductility becomes active for a load 2.2 times higher than the load expected during the transient load stages, which is equivalent to an eccentricity $e$ = 0.22 m if $n_s$ = 7 + key (*Figure 2.11b*). Such difference is attributed to the safety factors introduced in the calculations. In this situation, the segment would be capable of showing ductility at a load level that is below the considered in the ULS and is more compatible with the requirements in the service stage, although a certain safety margin is maintained.

## 2.8 REPERCUSSION OF DUCTILITY CRITERIA

To evaluate the repercussion of the two approaches discussed in this study, the minimum average $f_{R3m}$ estimated following each of them was translated into required fibre content ($C_f$). For that, the values of $f_{R3m,\,min}$ calculated for a range of design eccentricities ranging from 0 to 0.15 m were divided by 0.85 to estimate the corresponding strength at 28 days. The latter was then used in Equation 2.7 to assess $C_f$. *Figure 2.12* shows the curves that relate $C_f$ and $e$ for the critical situation of a pile composed by 7 segments plus the key.

As expected, the requirement from the MC 2010 leads to a constant $C_f$ of 63.7 kg/m$^3$ (65 kg/m$^3$ for production purpose). This value is difficult to justify from the technical, practical and economic point of view taking into account the specific circumstances of Line 9 of Barcelona. Consequently, the direct application of the requirement from the MC 2010 would render the use of fibres as the only reinforcement almost unviable for the example considered. In contrast, the new philosophy proposed here yields a $C_f$ of 42.3 kg/m$^3$ (45 kg/m$^3$ for production purpose). This represents a reduction of approximately 31% in the fibre consumption and provides enough ductility with a safety margin for the design load considered during stocking (all segments in the pile and accidental eccentricity $e$ of 0.10 m).

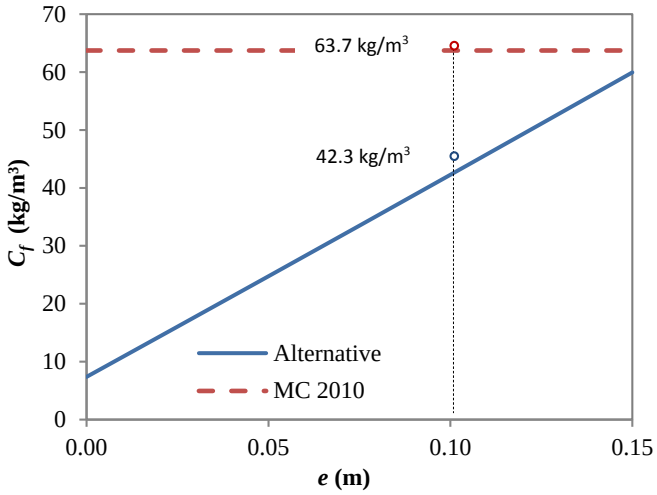


*Figure 2.12 Curves $C_f$ - e depending on the approach selected*

## 2.9 CONCLUSIONS

The analysis performed in this chapter sheds light on a fundamental aspect related to the design of FRC tunnel segments that might have a direct practical repercussion. The following conclusions may be derived from the work.

- The results from numerical simulations of the structural response of the segments under the storage conditions agree with the results obtained in the real-scale experimental programme. The good agreement obtained indicates that the constitutive equation derived from the bending test of small-scale beams is representative of the behaviour of the FRC in the real segment subjected to the typical transient loads. This suggests that, in most situations, it might be enough to resort solely to numerical analysis based on small scale-test instead of performing a complex experimental programme with real-scale segments.

- In tunnels with segmental linings subjected mainly to compression in service and designed not to crack in the transient stages, the direct application of the ductility requirements from the MC 2010 may lead to a higher $f_{R3}$ than the required value for the ULS. Such criterion may seem excessive taking into account that it responds to a transient stage and that the likelihood of cracking due to the applied loads is low (provided that $f_{ct,fl}$ is compatible with both the static and the dynamic loads expected and support configurations designed). If cracking occurs, the most probable scenario is that it will be the result of thermo-hygrometric induced stresses or a dynamic load very limited in time. In this context, the ductility required by the provisions from the MC 2010 hardly ever will be activated considering the typical load observed in the transient stages.

- The alternative approach proposed in this study could be applied to estimate the required $f_{R3}$ in tunnels that comply with 3 conditions: 1) the critical load occurring during the transient stages under controlled conditions; 2) the segments are designed not to crack and 3) are subjected to compression during service life. In this approach,

the ductility is calculated considering the design values of both the mechanical parameters of the FRC and the loads by using the partial safety factors proposed in the MC 2010. The ductility obtained on this way will be more compatible with the load observed in the transient stages.

- For the application of the tunnel from the Line 9 of Barcelona, the $f_{R3m,min}$ estimated according with the MC 2010 is 4.8 N/mm$^2$. This mechanical requirement is related to a bending moment $M_{cr}$, which is 3.20 times higher than the bending moment expected during the transient stages. Consequently, the ductility provided by the fibres will only be fully activated at load levels far above the average observed in reality. On the contrary, in the alternative approach proposed in this study, a minimum average $f_{R3}$ equal to 3.2 N/mm$^2$ is obtained. The letter is compatible with the loads expected during transient situations and the safety factors suggested in the MC 2010.

- Based on the results of the experimental programme, the $C_f$ estimated according with the MC 2010 and with the approach proposed here are 65 kg/m$^3$ and 45 kg/m$^3$, respectively. Even though ductility would be achieved in both of them for the load level expected in practice, the decrease in fibre consumption provided by the alternative approach could make the use of fibres viable without compromising the quality of the lining during the service life.

# 3. CONCRETE BLOCKS SUBJECTED TO CONCENTRATED LOADS WITH AN APPLICATION TO TBM CONSTRUCTED TUNNELS

## 3.1 INTRODUCTION

To generate enough thrust for a Tunnel Boring Machine (TBM) to excavate soil and advance, several jacks are typically used to apply force to the last installed ring that acts as a reaction frame. If the loads are excessively high, crack patterns might arise in traditionally reinforced and in fibre reinforced concrete segments, as presented in Figure 3.1 (Waal 1999) for different configurations of the thrust jacks. Although some of the cracks might be explained by an imperfect support of the segments (Cavalaro et al. 2011 & Cavalaro et al. 2012 & Cavalaro et al. 2013), others are related to the application of concentrated loads. In the latter case, compressive and splitting stresses appear under the pads of the jacks. These stresses are derived from a triaxial state that spreads over the disturbance zone through compression trajectories. These trajectories are internally balanced by tensile trajectories, leading to splitting stresses (i.e., bursting stresses) that cause the main vertical cracks through the depth of the segment. Similarly, as a result of the convex–deformed geometry, spalling stresses could appear and generate secondary cracks.

Even though the opening of secondary cracks should also fulfil the service limit state (SLS) requirements, bursting stresses are of special interest to the design of the structure

because they determine the reinforcement strategy. Currently, these crack patterns (see *Figure 3.1*) are typically controlled by using traditional steel bars. However, it has been proven that the use of a certain amount of structural fibres may enhance the performance in SLS (Walraven 2009), leading to cost and time savings (de la Fuente et al. 2011).

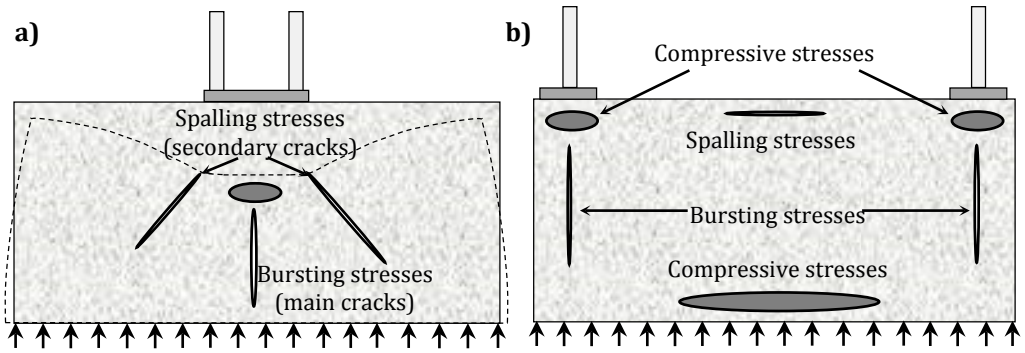


*Figure 3.1 General stress patterns for different thrust jack's configurations a) German, and b) Japanese and French systems*

It is well known that the application of concentrated loads induces a complex 3-D state of stresses, which is difficult to evaluate due to the existence of a disturbance zone beneath the load transfer area. The phenomenon was initially evaluated and applied to support systems (Ritter 1899 & Mörsch 1902 & Leonhardt 1965) and pre-stress transfer zones (Iyengare et al. 1966). Investigations for the particular case of tunnels constructed with a TBM and concrete segments (Waal 1999 & Cavalaro et al. 2012 & Kooiman 2000 & Blom 2002) are also in the literature. *Table 3.1* gathers experimental programmes from the literature related to the behaviour of concrete elements subjected to concentrated loads.

The studies presented in *Table 3.1* comprise concrete blocks (B) and precast concrete segments (PS). Some of these studies examined real tunnels (e.g., the Barcelona Metro Line 9 in Spain (Gettu et al. 2004), Hydraulic Tunnel of Montelirio in Panama (de Rivaz et al. 2008 & Caratelli et al. 2012), the Brenner Base Tunnel joining Italy and Austria (Hilar et al. 2012) and the Prague Metro Line (Hilar et al. 2012 & Beno et al. 2013), while the rest are associated with research projects (Hemmy et al. 2001 & Schnüntger et al. 2001 & Pohn et al. 2009 & Breitenbücher et al. 2014 & Abbas et al. 2014). Others also include plain concrete (PC), reinforced concrete (RC) or fibre reinforced concrete elements.

In general, the forces from a TBM's thrust jacks were emulated in the experimental programmes from *Table 3.1* as centred loads applied by laboratory testing machines, except in Gettu et al. (2004) and Breitenbücher et al. (2014), which also included the eccentricity of the load as a parameter. Although in most cases the elements were uniformly supported, several authors (Pohn et al. 2009 & Hilar et al. 2012 & Beno et al. 2013) tested an imperfect support between a placed ring and a segment being installed with a cantilevered configuration. Conversely, Breitenbücher et al. (2014) analysed the effect of different loaded area ratios and positions of the load.

The influence of the diameter ($\Phi_f$) and aspect ratio ($\lambda_f$) of the fibres were studied in several experimental programmes. Both parameters ranged from 0.20 mm to 1.00 mm and from

40 to 85, respectively. In almost all tests except for Pohn et al. (2009), steel fibres with hooked ends and amounts ranging from 35 to 80 kg/m$^3$ were used. Effects on the variability on the structural response due to the fibre distribution and orientation were studied by Sorelli et al. (2005) and Breitenbücher et al. (2014). A special mention should be made to the experimental programme conducted by Abbas et al. (2014) to evaluate the ultra-high performance steel fibre reinforced concrete (UHPSFRC) as a potential material to enhance both the mechanical and durability performance of tunnel segments. In that study, UHPSFRCs with compressive strengths from 150 to 170 N/mm$^2$ and 236 kg/m$^3$ (3% by volume) of straight steel fibres were studied.

*Table 3.1 Previous research focused on FRC elements subjected to concentrated loads*

| Elements | $f_c$ (MPa) | Dimensions (mm) | Material | $C_f$ (kg/m$^3$) | $\Phi_f/\lambda_f$ | Tests | Load | Num. sim. |
|---|---|---|---|---|---|---|---|---|
| PS (RP) | 60 | 3000x1000x300 (panels) | RC | - | - | 4 | Centred jack | 3D-FE (ANSYS) |
| | | | SFRC | 35 | 0.65/60 | | | |
| | | | | 60 | 0.65/60 | | | |
| | | | | | 0.92/65 | | | |
| B (RP) | 60 | 350x350x700 | SFRC | 35 | 0.65/60 | 12 | Centred line and point loads | 3D-FE (ANSYS) and strut-tie models |
| | | | | 60 | 0.92/60 | | | |
| PS (MT) | 50 | 900x520x175 (panels) | RC+SFRC | 30 | 1.00/65 | 4 | Centred & eccentric jack | 3D-FE elastic model (ANSYS) |
| | | | SFRC | 60 | | | | |
| PS (RP) | 75-100 | 3150x1420x300 | RC | - | - | 5 | Centred jack | 3D-FE (ABAQUS) and strut-tie models |
| | | | SFRC | 60 | 1.00/50 | | | |
| PS (HT) | 35 | 1840x1200x250 | SFRC | 40 | 0.75/80 | 1 | Centred jack | None |
| PS (RP) | 60 | 2359x1400x350 | PC | - | - | 9 | Centred jack on cantilevered supported segment | None |
| | | | SPFRC | 30+1 | 0.75/80 + PP fibres | | | |
| | | | | 40+1 | | | | |
| PS (RT) | 50 | 3400x1500x200 | RC | - | - | 2 | Centred jack | None |
| | | | SFRC | 40 | 0.35/85 | | | |
| PS (HT) | 35 | 1840x1200x250 | SFRC | 40 | 0.35/85<br>0.60/50<br>0.75/40 | 3 | Centred jack | Design with MC2010 |
| PT (MT) | 60 | 2570x1500x250 | SFRC | 40 | | 15 | Centred jack on uniformly and cantilevered supported segment | 2D-FE (ATENA) and 3D-FE for the full-scale tests on precast segments |
| B (RP) | 75-95 | 300x150x150 | PC | 50 | 0.75/80 | 96 | Different loaded-area ratios with varying positions of the concentrated load | 3D-FE (MSC-Marc) |
| | | | | - | - | | | |
| | | | | 40 | | | | |
| | | | | 60 | 0.75/80 | | | |
| | | | SFRC | 80 | | | | |
| | | | | | 0.90/65 | | | |
| | | | | 60 | 0.71/85 | | | |
| PS (RP) | 150-170 | 1000x500x100 (reduced scale) | UHPC | - | 0.55/55 - | 2 | Centred TBM jack simulation | None |
| | | | UHSFRC | 236 | 0.20/80 | | | |

Concerning the design, it should be noted that 3D finite element models with smeared crack has been the primary approach used by researchers (Hemmy et al. 2001 & Schnüntger et al. 2001 & Gettu et al. 2004 & Sorelli et al. 2005 & Hilar et al. 2012 & Beno et al. 2013 & Breitenbücher et al. 2014 & Abbas et al. 2014) to simulate the jack thrust of a TBM numerically. The most common software packages applied for this purpose were ABAQUS (1995), ANSYS (1998), ATENA (2013) and MSC-Marc (2008) (see *Table 3.1*). Other numerical studies have been performed by Burgers et al. (2007) and Tiberti et al. (2014) in which different fibre reinforcement ratios and load configurations were

evaluated. Particularly, in Burgers et al. (2007), a real failure of a segment used at the Metro Line 9 of Barcelona was reproduced numerically.

Analytical models based on the struts and ties models (STMs) have also been recommended as a safe alternative to evaluate the splitting stresses and the reinforcement requirements of element subjected to concentrated loads (Ramirez et al. 1991 & Reineck et al. 1982 & ACI-ASCE Committee 445, 2000), particularly for precast concrete segments (Toutlemonde 2000 & Toutlemonde et al. 2000 & Haring et al. 2002 & Groeneweg 2007 & Bakhshi et al. 2014). This simplified approach is interesting due to its easy implementation and adaptability to reproduce the stress patterns caused by TBM thrust. In Schnüntger et al. 2001, a study was performed to adjust the analytical expressions considering the fibre contribution in the resistant mechanism as well as to adjust the depth of the disturbance zone.

Despite the many studies in the literature, most study elements with similar height-to-length ratios. To cover the wide variety of dimensions and loading patterns, additional experimental assessments are yet required. These studies could support the calibration of analytical formulations to assess the cracking and the failure load depending on the dimensions of the elements.

## 3.2 OBJECTIVES

The objective of the chapter is to extend the study of elements subjected to concentrated loads by considering different height-to-length ratios with and without fibre reinforcement. The goal of this study is to validate simplified analytical formulations that may be applied for the verification of concrete segments in SLS and ULS. An experimental programme was also conducted with small-scale specimens; the associated results were used to validate the formulations derived using similar studies from the literature. Finally, an application of the formulation is proposed to the case study of Line 9 in Barcelona is presented. This study represents a contribution toward the development of simplified tools for the design of SLS and ULS segmented linings.

## 3.3 EXPERIMENTAL PROGRAMME

The experimental programme consisted of the assessment of the mechanical response of small-scale concrete specimens with different dimensions subjected to concentrated loads. To consider the typical variety of materials applied in segmented linings, specimens were cast with 4 concrete series with the compositions indicated in *Table 3.2.* The series PC-40 and PC-50 correspond to plain concrete with compressive strengths (UNE-EN 12390 2011) ($f_c$) of 40 N/mm$^2$ and 50 N/mm$^2$, respectively. The series SFRC-40 and SFRC-50 correspond to steel-fibre-reinforced concrete with equivalent strength class. Hooked–end steel fibres with 60 mm of length ($l_f$), 0.75 mm of diameter ($\Phi_f$) and yield modulus ($f_f$) of 1050 N/mm$^2$ were used in the latter type.

*Table 3.2 Composition of concrete series (in kg/m³)*

| Material | PC-40 | SFRC-40 | PC-50 | SFRC-50 |
|---|---|---|---|---|
| Cement CEM I 52,5R | 300 | 300 | 400 | 400 |
| Marble powder | 350 | 350 | 250 | 250 |
| Sand 0-3 (mm) | 510 | 510 | 510 | 510 |
| Aggregate 2.5/6 (mm) | 400 | 400 | 400 | 400 |
| Aggregate 6/15 (mm) | 520 | 520 | 520 | 520 |
| ADVA Flow 400 | 12 | 12 | 12 | 12 |
| Water | 150 | 150 | 178 | 178 |
| Steel fibres | - | 40 | - | 40 |

In total, 32 concrete blocks were cast with the dimensions shown in *Figure 3.2.* In this sense, $a$, $b$ and $h_T$ represent the length, width and height of the concrete blocks, respectively. $a_1$, $b_1$ and $h_1$ correspond to the length, width and height of the support plate, respectively. The concrete was poured directly into a four-compartment mould (see *Figure 3.3a*) placed on a vibrating table. As shown in *Figure 3.3b,* metal bushings were installed on both sides of the larger moulds.

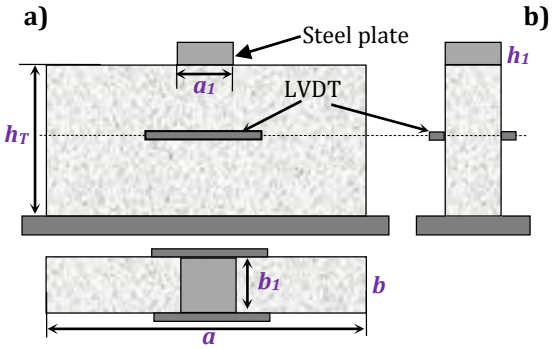


b)

| $a$ | $a_1$ | $b$ | $b_1$ | $h_T$ | $h_1$ |
|---|---|---|---|---|---|
| 200 | 150* | 150 | 150 | 300 | 50 |
| 250 | 150* | 150 | 150 | 300 | 50 |
| 400 | 150 | 150 | 150 | 300 | 50 |
| 750 | 150 | 150 | 150 | 300 | 50 |

* For the series SFRC40 with the length $a$ = 200 and 250 mm, the width of the plate is $a_1$ = 50 mm.

*Figure 3.2 Three-view plan schematic of the instrument set-up, and b) dimensions of the blocks and support plates*

In addition to the elements used in the concentrated load tests, 12 cylindrical specimens (Φ15×30 cm), 12 cylindrical specimens (Φ15×30 cm) and 16 cylindrical specimens (Φ15×15 cm) were cast and used to assess the compressive and tensile strengths using the Brazilian test (UNE-EN 12390, 2010) and the residual using the Barcelona test (UNE 83515 (2010) & Pujadas et al. 2014 & Blanco et al. 2014), respectively. All specimens were produced on the same day in the same ambient conditions. The specimens were stored under controlled conditions at a temperature of 20±1 °C and an average relative humidity HR ≥ 95% until testing.

During the tests, the blocks were supported by a rigid steel plate, and the load was applied by the system presented in *Figure 3.4*. Similarly, two Temposonic displacement sensors were fastened to the block in a horizontal orientation at the middle on both sides. The loading rate was 0.2 MPa/s, and the tests were stopped once failure was detected.

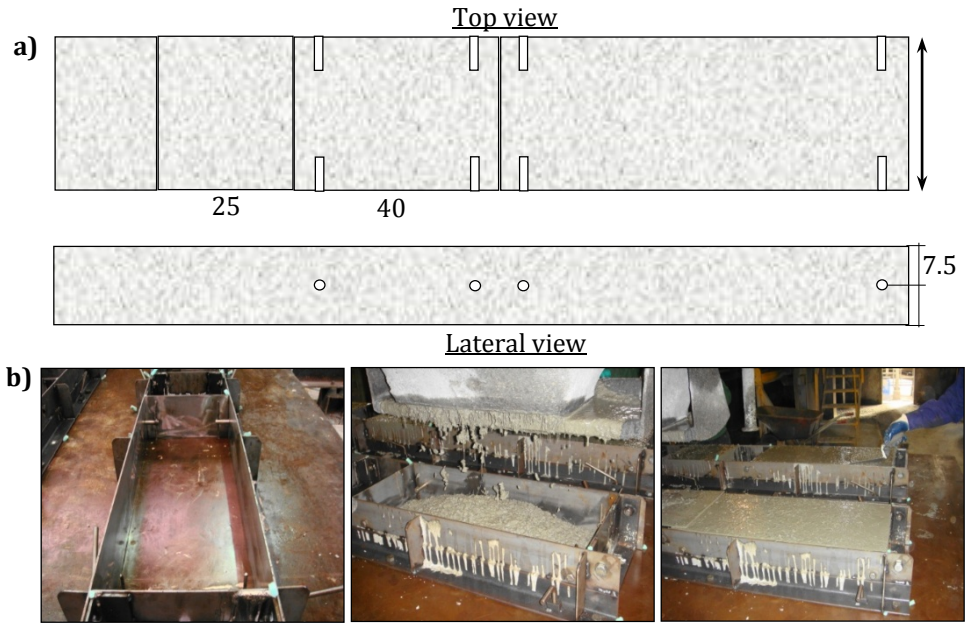


*Figure 3.3 Production of concrete blocks: a) dimensions of moulds (in mm), and b) different views during casting*

*Figure 3.4 Concentrated load test configuration*

## 3.4 TEST RESULTS AND ANALYSIS

*Table 3.3* shows the results of the characterization tests carried out 28 days after casting. $f_{cm}$ is the average compressive concrete strength, and $f_{ctm1}$ and $f_{ctm2}$ are the average tensile strengths obtained from the Barcelona and Brazilian tests, respectively.

*Table 3.3 Test results of the characterization specimens (in N/mm²)*

| Series | Compression Test | | Barcelona Test | | Brazilian Test | |
|---|---|---|---|---|---|---|
| | $f_{cm}$ | CV (%) | $f_{ctm1}$ | CV (%) | $f_{ctm2}$ | CV (%) |
| PC-40 | 43.7 | 1.1 | 4.33 | 1.7 | 4.33 | 2.5 |
| SFRC-40 | 39.4 | 1.9 | 3.99 | 5.4 | 4.74 | 9.2 |
| PC-50 | 53.3 | 0.9 | 4.09 | 5.4 | 4.40 | 5.6 |
| SFRC-50 | 51.8 | 0.9 | 4.32 | 1.9 | 4.49 | 2.4 |

As expected, the PC specimens presented slightly higher strengths presumably due to the

occluded air that the use of fibres leads to in SFRCs. The compressive strengths that were expected based on the materials' compositions were achieved (see *Table 3.2*). It is worth mentioning that the Barcelona tests presented lower values of the coefficient of variation (CV) than those from the Brazilian tests.

It was observed that most of the blocks cracked in three stages during the concentrated load tests. As shown in *Figure 3.5*, in the first stage, a crack is caused due to bursting according to the equilibrium conditions. This is the main crack that progresses through the depth of the specimen as the load increases. In the second stage, diagonal cracks (i.e., secondary cracks with angle $\beta$) appear as a result of compatibility demands on the deformed shape; they appear to start at the upper support plate and end at the bottom of the block and are likely caused by spalling stress. Finally, in the third stage, a cone wedge is formed beneath the load transmission plate due to the triaxial compressive stress.

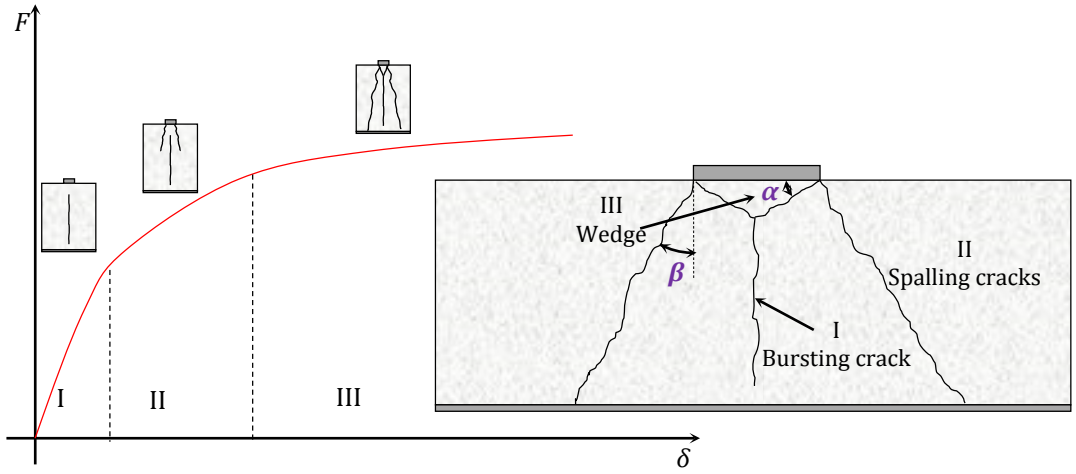


*Figure 3.5 Different crack patterns observed in the tests during the loading process*

This wedge penetrates through the main bursting crack, provoking the physical separation of two semi-blocks and decreasing the bearing load. However, the third stage was not always present in plain concrete blocks due to a brittle rupture in the second stage. This is mainly caused by the lack of reinforcement, which reduces internal equilibrium restoring capacity after the first bursting crack occurs.

The load-vertical displacement ($\delta$) curves of the concrete blocks grouped by the same block length are presented in the *Figure 3.6.* The curves correspond to the average values of each series. Similarly, *Table 3.4* shows the results of the first crack load ($F_{cr}$) and the maximum load ($F_{max}$). The nomenclature established to refer to the concrete blocks is "Concrete Type-$f_c$-$a$-$a/a_1$". More detail information can be found in the ***Annex A.***

*Figure 3.6a* and *Figure 3.6b* and *Table 3.4* show that the series SFRC-40-200-4.0 and SFRC-40-250-5.0 (grey-shaded), for which a 50x150x50 m$^3$ steel plate was used instead of the 150x150x50 mm$^3$ steel plate used for the other series, have a lower load bearing capacity than the series PC-40-200-1.3 and PC-40-250-1.7. Considering that both series present similar tensile concrete strengths (see *Table 3.3*), this effect could be attributed to the ratio

$a/a_1$ as it has been proven numerically (Leonhardt 1965) and experimentally Breitenbücher et al. (2014). In this regard, the decrease of $a_1$ leads to a stress concentration above the steel plate and an increase of the bursting stresses.

*Table 3.4 Experimental loads $F_{cr}$ and $F_{max}$ measured (in kN)*

| Series | Load | Length of the block ($a$) | | | | | | | |
|---|---|---|---|---|---|---|---|---|---|
| | | 200 mm | | 250 mm | | 400 mm | | 750 mm | |
| PC-40 | $F_{cr}$ | 401 | 412 | 398 | 421 | 640 | 625 | 708 | 780 |
| | $F_{max}$ | 1049 | 1038 | 976 | 1081 | 1287 | 1200 | 1340 | - |
| SFRC-40 | $F_{cr}$ | 396 | 415 | 372 | 376 | 611 | 650 | 672 | 647 |
| | $F_{max}$ | 536 | 570 | 535 | 571 | 1250 | 1305 | 1299 | 1360 |
| PC-50 | $F_{cr}$ | 417 | 417 | 416 | 452 | - | - | - | - |
| | $F_{max}$ | 1166 | 1107 | 1167 | 1108 | - | - | - | - |
| SFRC-50 | $F_{cr}$ | 435 | 423 | 520 | 533 | 630 | 652 | 712 | 718 |
| | $F_{max}$ | 1250 | 1150 | 1225 | - | 1485 | 1450 | 1604 | 1459 |

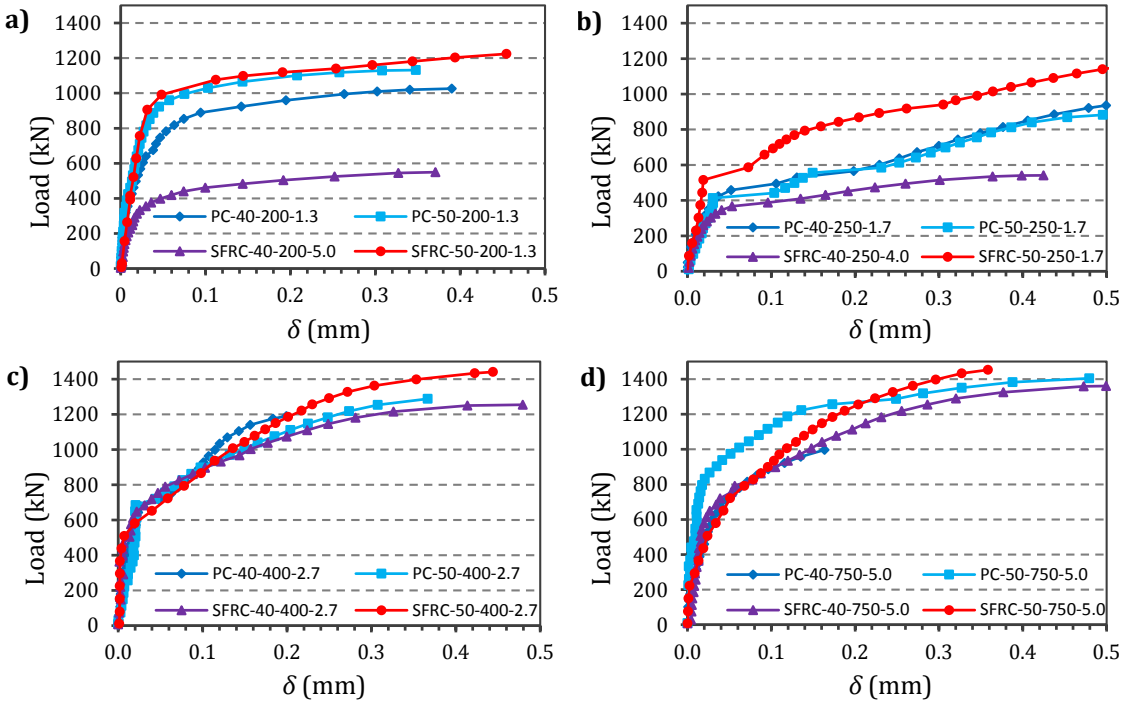


*Figure 3.6 Load - displacement curves of the concrete blocks*

Conversely, the results also show that the bearing capacity increases with the length of the block and that the load $F_{max}$ ranges from 2.0 to 3.0 times the load $F_{cr}$. These results reveal the high internal capacity of the system to redistribute stresses by means of both equilibrium and compatibility cracks. These load increases are also observed for both unreinforced and fibre reinforced concrete blocks. The use of 40 kg/m³ of steel fibres has also been shown to lead to slight differences in $F_{max}$ with respect to the PC series. However, PC blocks presented only 3 main cracks (1 bursting and 2 spalling cracks), as shown in *Figure 3.7a*, while SFRC blocks (see *Figure 3.7b*) exhibit this same crack pattern with more secondary cracks due to from the higher internal distribution capacity produced by the fibres. This fact is interesting in terms of crack width and service limit state of the precast segments during the TBM jack action.

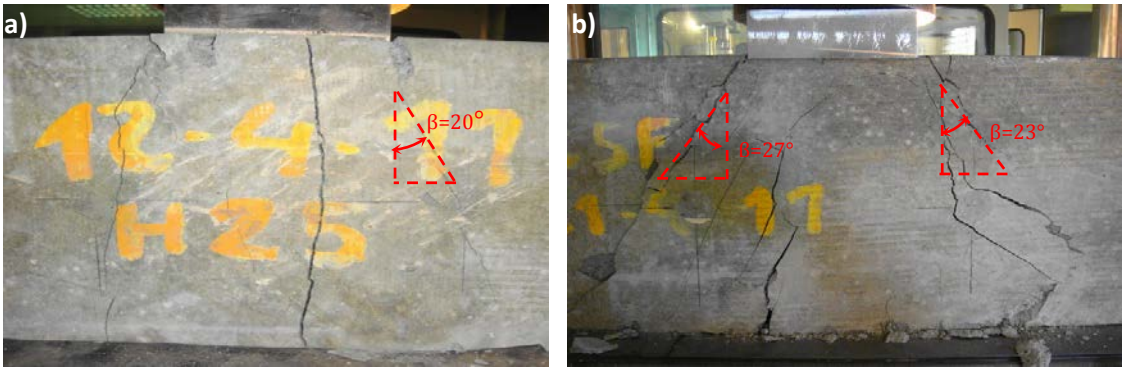


*Figure 3.7 Crack patterns observed in: a) a PC-40-750 block, and b) an SFRC-40-750 block*

To calibrate the model presented in this paper, additional measurements of the crack patterns were performed. Specifically, the angle $\beta$ of the secondary cracks starting beneath the steel plate were measured in all tested specimens, yielding an average value of 23° with a CV of 9.2%. Similarly, the dimensions of the cone wedge (see *Figure 3.8*) formed during the 3rd loading stage (see *Figure 3.5*) were also measured. It was observed that the height of the cone wedge ($h$) was approximately equal to the length of the support plate ($a_1$). The average value of the angle $\alpha$ formed between the upper face of the block and the lateral surface of the cone was 63° (CV = 2.2%).

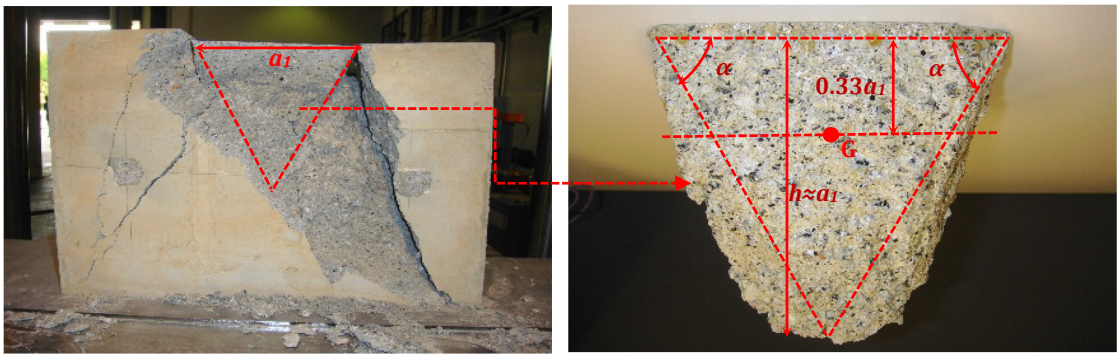


*Figure 3.8 Cone wedge formed during the last loading stage*

## 3.5 PROPOSED STRUT AND TIE MODELS TO ASSESS $F_{cr}$ and $F_{max}$

### 3.5.1 Introduction

Based on the analysis of the experimental results previously made, a strut-and-tie model (STM) was adopted to assess the value of the loads $F_{cr}$ and $F_{max}$. These depend on the relationship between the total block height ($h_T$) and its length ($a$). Thus, the concrete blocks were divided into two groups: *short blocks* ($h_T \geq a$) and *long blocks* ($h_T < a$).

In *short blocks*, $F$ can be distributed along a disturbance length, namely $h$, and reach a uniformly distributed stress pattern ($\sigma$) within the total length of the block $h_T$ (Mörsch 1902); therefore, this stress pattern is also uniform at the support of the block. Conversely, in long blocks, this stress pattern is non-uniform at the base.

According to this classification, the blocks with $a$ = 200 and 250 mm belong to the *short*

*block* group, and those with $a$ = 400 and 750 mm belong to the *long block* group. Therefore, the proposed model was discussed in accordance with these two groups.

### 3.5.2 Cracking Load $F_{cr}$

***Short blocks $h_T \geq a$***

In the *short block* series, the STM depicted in *Figure 3.9a* was used. This consists of compression members (i.e., struts) and tension members (i.e., ties), which were depicted by dashed and solid line, respectively. Considering the symmetry of the problem, $F$ can be decomposed into loads $F/2$ acting at a distance $a_1/4$ from the vertical symmetry axis.

Under the loading area, a confined zone was assumed to exist where the compressive stresses are uniform and constant; $k_1a_1$ was assumed to be the depth of this zone. The $k_1$ coefficient can be defined based on experimental results or in accordance with existing regulations. Additionally, $h$, which is also called the fictitious height or disturbance length, represents the required depth that guarantees a uniform distribution of stresses; $h \approx a$ according to Saint – Venant.

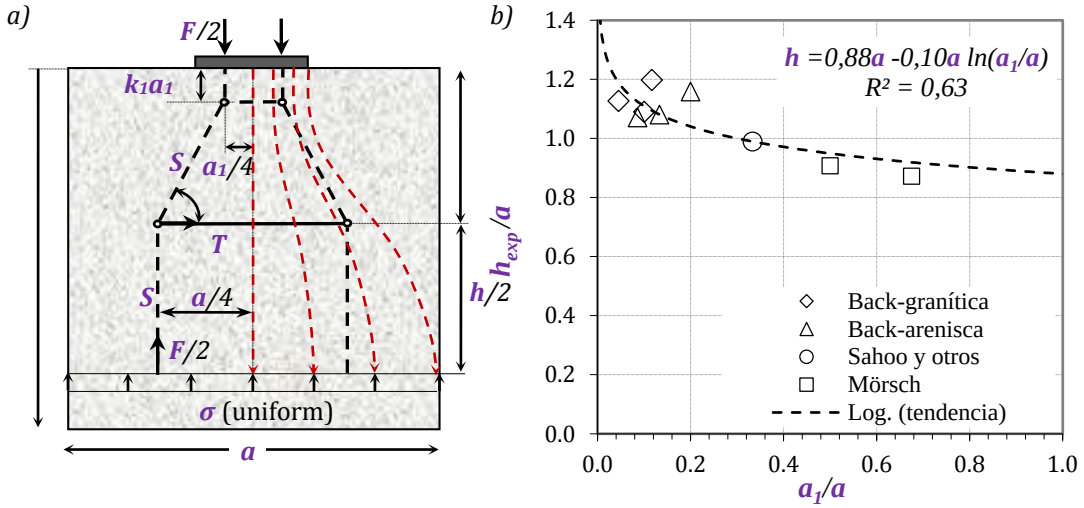


*Figure 3.9 a) Proposed STM for short blocks, and b) the determination of h*

The equilibrium equation resulting from the lattice system presented in *Figure 3.9a* results in *Equation 3.1* that permits the calculation of $T$.

$$T = \frac{F(a - a_1)}{4(h - 2k_1a_1)} \qquad \text{Equation 3.1}$$

Assuming a parabolic distribution of the tensile stresses acting perpendicularly along the vertical axis and establishing the proper boundary conditions, the maximum tensile stress $\sigma_{ct,max} = 3T/2A$ can be derived (García 2012) with $A = b(h\text{-}k_1a_1)$ being the area subjected to this stress pattern. Thus, from Equation 3.1 and $\sigma_{ct,max}$ , *Equation 3.2* can be obtained.

$$\sigma_{ct,max} = \frac{3T}{2b(h - 2k_1a_1)} \leq f_{ct} \qquad \text{Equation 3.2}$$

The cracking load $F_{cr}$ can be calculated by combining *Equation 3.1* and *Equation 3.2* and

letting that $\sigma_{ctmax} = f_{ct}$, obtaining *Equation 3.3*.

$$F_{cr} = \frac{8b(h - 2k_1a_1)(h - k_1a_1)}{3(a - a_1)} f_{ct} \qquad \text{Equation 3.3}$$

For this research project, $k_1$ = 0.33 was adopted because the parametric study of Bach (1903) showed that this value is the most representative the triaxial compressive state generated below the loading plate. A function $h = f(a, a_1)$ has also been calibrated from the experimental results presented in (Mörsch 1902 & Sahoo et al. 2011 & Infante 2006) (*Figure 3.9b*). In these studies, different concrete blocks with varying dimensions, concrete strengths and load types were investigated. The values of $F_{cr}$ obtained in these experiments in conjunction with Equation 3 have been used to calibrate *Equation 3.4.*

$$h = 0.88a - 0.10aln\left(\frac{a_1}{a}\right) \qquad \text{Equation 3.4}$$

*Equation 3.4* is consistent because for $a_1 \approx 0$ (i.e., a point load), the disturbance length is infinite while for $a_1 \approx a$, and the ratio $h/a$ tends to 0.88. Saint–Venant also proposed $h/a \approx 1$ independently of the loaded area ratio.

***Long blocks ($h_T < a$)***

For long blocks, according to the Saint-Venant principle, the stress pattern at the base of the block is non-uniform (see *Figure 3.10*) because $h > h_T$. Additionally, it has been observed experimentally that the mechanism can be represented by two blocks: (1) an active block with a length $a_3$ compressed within the two cracks inclined at an angle $\beta$, which is responsible the transmission of the external load $F$ transmission; and (2) two lateral blocks that confine the internal active block laterally and contribute to the transfer of the shear stresses either by the aggregate interlock mechanisms or by the action of the fibres.

The model proposed assumes that the maximum pressure $q_1$ is reached at the intersection of the base with the vertical symmetry axis. This pressure decrease linearly to $q_1$ at the edge of the active block. This stress distribution results in both $F/2$ forces, which are located close to the vertical axis; consequently, the internal equilibrium forces reduce its magnitude to $T$ with respect to those forces obtained in *short blocks*.

Additional hypotheses should be established to determine the magnitude of $T$: (1) there is a fictitious height $h > h_T$ in which the stress $q_a = F/a_3b$ is uniformly distributed; and (2) the support pressures $q_1$ and $q_2$ vary between $q_{a1} = F/a_1b$ and $q_a$. Assuming these hypotheses, *Equation 3.5* and *Equation 3.6* can be derived to assess $q_1$ and $q_2$, respectively.

$$q_1 = \frac{F}{a_1 b}\left[1 - \frac{h_T(a_3 - a_1)}{a_3 h}\right] \qquad \text{Equation 3.5}$$

$$q_2 = \frac{2F}{a_3 b} - q_1 \qquad \text{Equation 3.6}$$

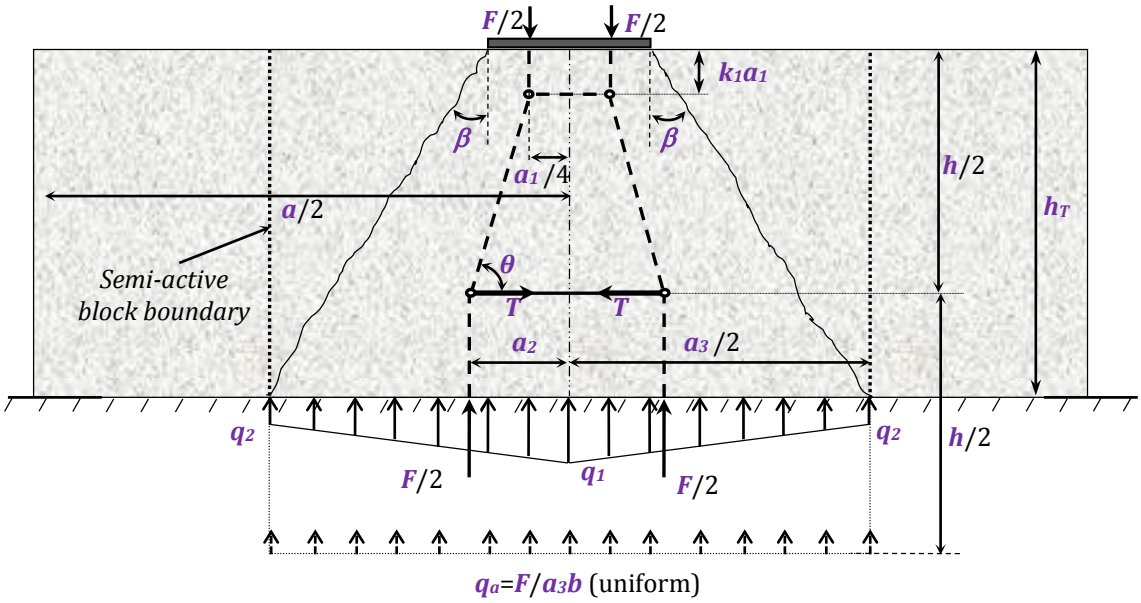


*Figure 3.10 Proposed STM for long blocks*

To obtain $q_2 < 0$ in *Equation 3.6*, the stress distribution can be assumed to be triangular; thus, the pressures become $q_2 = 0$ and $q_1 = 2F/a_3b$ and $a_2 = a_3/6$. Furthermore, by applying geometrical considerations, the restriction expressed by *Equation 3.7* can be established.

$$a_3 = a_1 + 2h_T tan\beta \leq a \qquad \text{Equation 3.7}$$

By imposing the resulting force from the non-uniform pressure pattern equal to $F/2$, *Equation 3.8* can be obtained. This allows the calculation of $a_2$.

$$a_2 = \frac{a_3}{6}\left(\frac{q_1 + 2q_2}{q_1 + q_2}\right) \qquad \text{Equation 3.8}$$

Following the same criteria established to derive *Equation 3.1*, *Equation 3.2* and *Equation 3.3* for *short blocks*, *Equation 3.9* can be deduced to obtain the value of $F_{cr}$ for long blocks.

$$F_{cr} = \frac{8b(h - 2k_1a_1)(h - k_1a_1)}{3(4a_2 - a_1)} f_{ct} \qquad \text{Equation 3.9}$$

Using the experimental values of $F_{cr}$ for long blocks in (Bach, 1903 & Mörsch, 1952 & Sahoo et. al. 2011), the calibrated *Equation 3.10* can be used to assess the value of $h$.

$$h = 0.71a - 0.22a_3 ln\left(\frac{a_3}{a}\right) \qquad \text{Equation 3.10}$$

### 3.5.3 Maximum load $F_{max}$

It has been observed experimentally that the blocks were divided into two main sections after cracking (see *Figure 3.11*). This causes a drastic change in the internal stress distribution that is difficult to assess analytically. In such a situation, the two parts are subjected to loads with an eccentricity $k_2a$, which leads to a flexural-compression state in

each independent part.

By imposing the classical formula of mechanics of the materials, the maximum compressive stress $\sigma_{cc,max}$ acting at the central part of the block can be assessed (*Equation 3.11*).

$$\sigma_{c,max} = \frac{F_{max}/2}{ba_3/2} + \frac{F_{max}/2\,(a_3/4 - k_2\,a_1/2)}{b(a_3/2)^3/12}\frac{a_3}{4} = \frac{F_{max}}{ba_3{}^2}(4a_3 - 6k_2a_1) \qquad \text{Equation 3.11}$$

Assuming that the failure of the block is reached when the maximum compressive stress equals the compressive strength of the concrete ($\sigma_{cc,max} = f_c$), the value of $F_{max}$ can be derived from *Equation 3.11* obtaining *Equation 3.12.*

$$F_{max} = \frac{ba_3{}^2}{4a_3 - 6k_2a_1} f_c \qquad \text{Equation 3.12}$$

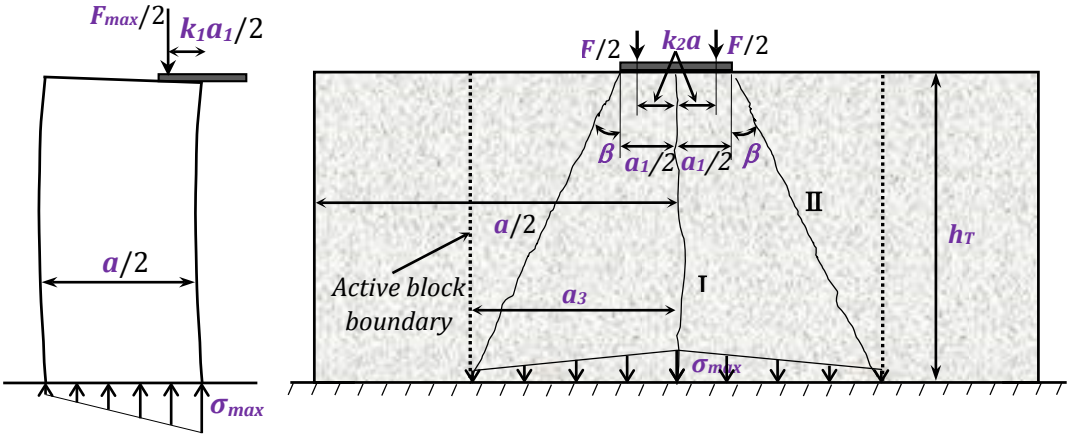


*Figure 3.11 Theoretical scheme of the fissure formed during the block test*

It should be highlighted that $F_{max}$ depends on the geometric variables ($b$, $a_1$ and $a_3$), the concrete compressive strength $f_c$ and the eccentricity factor $k_2$ of the load in the failure regime. It is also important to note that the contribution of the fibres is not taken into account in the failure state because of their minimal impact, as shown in *Table 3.4* by comparing the values of $F_{max}$ for PC and SFRC blocks. With larger amounts of fibres, the failure mechanism might change, and the contribution of the fibres should be considered in the analysis; otherwise, the value of $F_{max}$ assessed would be underestimated. Additionally, the precast segments are designed so that the cracking is not allowed during the placing operations.

In *Equation 3.12*, $a_3$ can be determined by *Equation 3.7*; $k_2$ should be derived from *Equation 3.13* (*Figure 3.12*), which has been calibrated with the experimental values of $F_{max}$ presented in Mörsch (1902) and considering *Equation 3.12*:

$$k_2 = e^{-0.70\frac{a_1}{a_3}} \qquad \text{Equation 3.13}$$

*Equation 3.13* is shown to be consistent with the physical phenomena: for a point load ($a_1$

≈ 0), the ratio $a_1/a_3 \approx 0$, and consequently, $k_2 \approx 1.0$, meaning that the load $F/2$ is applied at the internal edge of the plate in the failure regime. Contrarily, if $a_1 = a_3$ ($a_1/a_3 = 1.0$), then $k_2$ tends towards 0.5, and therefore, $F/2$ is applied at a distance $a_1/4$ from the vertical axis of the block, which coincides with the central point of the symmetry axis of the loading semi-plate.

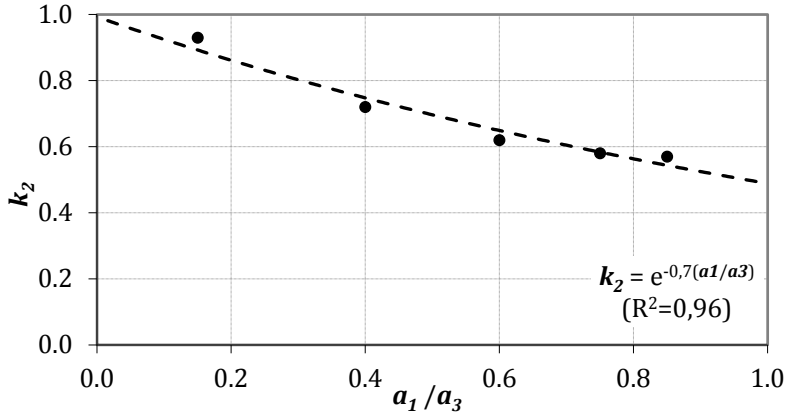


*Figure 3.12 Values of $k_2$ derived from the experimental values of $F_{max}$*

### 3.5.4 Comparing the experimental and theoretical values of $F_{cr}$ and $F_{max}$

*Table 3.5* and *Table 3.6* present both the experimental results and the theoretical values of $F_{cr}$ and $F_{max}$ estimated using *Equation 3.3* and *Equation 3.9* for $F_{cr}$ and *Equation 3.12* for $F_{max}$. The results presented in the *Table 3.5* highlight the suitability of the analytical model proposed to assess $F_{cr}$ of both *short* and *long blocks*. The STM leads to a maximum underestimation for $F_{cr}$ of 16.3% (SFRC-40-200-5.0) with respect to the experimental value; conversely, maximum overestimation of -17.9% (SFRC-40-250-4.0) is also calculated. The absolute average relative error of $F_{cr}$ was calculated to be 10.1%. Considering these results, it can be assumed that these are satisfactory in terms of design because, although there is a certain deviation of the proposed model, these errors are limited and lower than those inherent errors accepted for the materials' strengths. Despite being an SLS, safety factors for $F_{cr}$ applied during the design procedure usually exceed 1.5.

*Table 3.5 Comparison between theoretical and experimental average values for $F_{cr}$ (relative error %)*

| Specimen | Exp. | Th. | Specimen | Exp. | Th. |
|---|---|---|---|---|---|
| PC-40-200-1.3 | 407 | 379 (6.9) | PC-50-200-1.3 | 417 | 358 (14.1) |
| PC-40-250-1.7 | 409 | 425 (-3.9) | PC-50-250-1.7 | 434 | 401 (7.6) |
| PC-40-400-2.7 | 633 | 725 (-14.5) | PC-50-400-2.7 | - | - |
| PC-40-750-5.0 | 744 | 750 (-0.8) | PC-50-750-5.0 | - | - |
| SFRC-40-200-5.0 | 406 | 340 (16.3) | SFRC-50-200-1.3 | 429 | 378 (11.9) |
| SFRC-40-250-4.0 | 374 | 441 (-17.9) | SFRC-50-250-1.7 | 527 | 424 (19.5) |
| SFRC-40-400-2.7 | 631 | 668 (-5.9) | SFRC-50-400-2.7 | 641 | 724 (-12.9) |
| SFRC-40-750-5.0 | 660 | 691 (-4.7) | SFRC-50-750-5.0 | 715 | 748 (-4.6) |

It can be confirmed from the results of *Table 3.6* that the agreement between the experimental and theoretic results of obtained with the proposed STM are even better

with respect to those of $F_{cr}$. The maximum and minimum relative errors are 22.1% (SFRC-40-200-5.0) and 2.5% (PC-40-250-1.7), respectively, and the average is 9.8%. Therefore, taking into account the aforementioned for $F_{cr}$, these results also highlight the suitability of the analytical model to assess the value of $F_{max}$. The assessment of load is thus not relevant to the calculation of $F_{cr}$ in the design of precast concrete segments.

*Table 3.6 Comparison between theoretical and average experimental values for $F_{max}$ (relative error %)*

| Specimen | Exp. | Th. | Specimen | Exp. | Th. |
|---|---|---|---|---|---|
| PC-40-200-1.3 | 1044 | 980 (6.1) | PC-50-200-1.3 | 1137 | 1195 (5.1) |
| PC-40-250-1.7 | 1029 | 1003 (2.5) | PC-50-250-1.7 | 1138 | 1223 (7.5) |
| PC-40-400-2.7 | 1244 | 1156 (7.1) | PC-50-400-2.7 | - | - |
| PC-40-750-5.0 | 1340 | 1162 (13.3) | PC-50-750-5.0 | - | - |
| SFRC-40-200-5.0 | 553 | 431 (22.1) | SFRC-50-200-1.3 | 1200 | 1161 (3.3) |
| SFRC-40-250-4.0 | 553 | 500 (9.6) | SFRC-50-250-1.7 | 1225 | 1187 (3.1) |
| SFRC-40-400-2.7 | 1278 | 1041 (18.5) | SFRC-50-400-2.7 | 1468 | 1368 (6.8) |
| SFRC-40-750-5.0 | 1330 | 1047 (21.3) | SFRC-50-750-5.0 | 1532 | 1375 (10.2) |

## 3.6 APPLICATION TO LINE 9 IN BARCELONA

Because the formulations that estimate the cracking and ultimate loads have been proposed, an application is now considered regarding the segmented lining in Metro Line 9 in Barcelona. The detail information about the metro Line 9 in Barcelona has been described in Chapter 2 section 2.4. The ratio between the thickness and the diameter of the ring is approximately 31, whereas most tunnels have the same parameter between 20 and 25. The high slenderness of the ring from the Metro Line 9 in Barcelona in comparison with other tunnels may lead to the application of higher stress levels to the segment. Together with the possible eccentricity of the jacks, this might increase the risk of bursting cracks.

During the construction process, the load required to generate enough pressure to excavate the front face and to advance the TBM is generated by 15 pairs of thrust jacks. Each pair transmits the forces to a 20 mm thick steel plate, known as a pad. The pads transmit this force to the recently installed ring that acts like a reaction frame. Segments A1, A2, A3, A4, A5, B and C (*Figure 3.13a*) receive the load from two pads, whereas the key segment receives the load from only one pad. *Figure 3.13b and Figure 3.13c* depict a front view and a top view of the load application points.

Notice that a design eccentricity of 79 mm towards the centre of the ring is already considered in the project (*Figure 3.13c*). Such eccentricity is intentionally used to generate compressive forces in the longitudinal joints, thus reducing the risk of collapse when the segments are still inside the TBM, and only a small compression exists. The magnitude of the load applied by the thrust jacks during the construction process will depend on the properties of the ground excavated, the position of the segment inside the ring, and the curvature of the stretch, among other factors. In Infante (2006), there is an extensive study of the variability of the forces applied in Line 9 in Barcelona. The results suggest that the

average load during construction is 2600 kN/pad. However, in Cavalaro et al. (2012), the maximum load is found to be approximately 4660 kN/pad. The latter is taken as a reference for the calculations performed here.

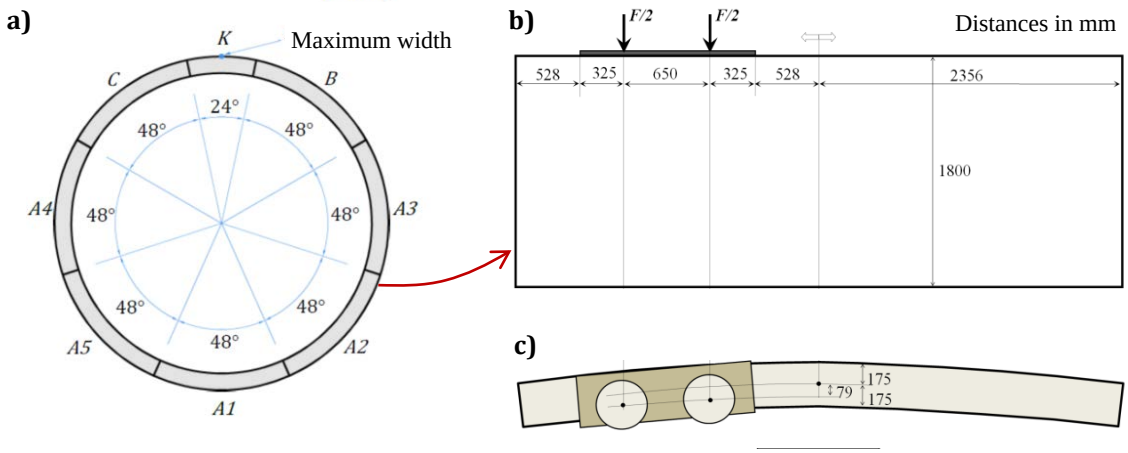


*Figure 3.13 a) Detail of ring front view, b) top view and c) load application in the segment*

Depending on the magnitude of the load and the support conditions of the segments, different types of damage could occur in the segments during construction. According with the study performed by the Japanese Society of Civil Engineers, most damage is associated with the handling of the segments and with the application of the thrust forces when the segments are leaving the shield Sugimoto (2006). Although not the most frequent type, one of the possible types of damage that might occur in this last situation is depicted in *Figure 3.14.*

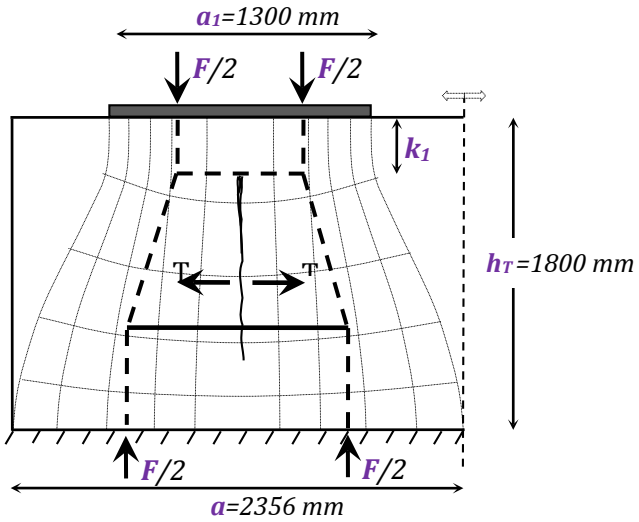


*Figure 3.14 Symmetric top view of a segment from Line 9 in Barcelona with a crack*

*Figure 3.14* shows only half of the top view of the segment from Line 9 in Barcelona with a crack parallel to the width that starts closer to the point of application of the load from the thrust jacks. The mechanism of crack formation in this case is similar to that described in Sections 3 and 4 of this study. Due to the dimensions of the segment and the reduced area of the pads, the segment behaves like a block subjected to concentrated loads. In fact, these loads produce tensile stresses that might crack and even produce a failure of the segments.

Notice that even if the support provided by the previous ring installed was perfect, failure might still take place.

The formulation developed here might be used to predict the safety factor (SF) in service and in ultimate limit states related with this type of damage. To perform this estimation following the project specifications, it is assumed that a segment should not crack in service. Additionally, the characteristic compressive ($f_c$) and tensile ($f_{ct}$) strengths of concrete are 50 N/mm$^2$ and 2.7 N/mm$^2$, respectively. The height of the segment $h_T$ is 1800 mm, the length of the load application $a_1$ equals that of the pad (i.e., 1300 mm), the eccentricity of forces $a_2$ is 574 mm, the length of the segment ($a$) considering the symmetry axis is 2356 mm, the coefficient $k_1$ that determines the length of the confined zone is 0.3 and the depth below which internal stresses become uniform ($h$) is 1981 mm.

Because $h_T$ is smaller than $a$, *Equation 3.9* is used to estimate a cracking load $F_{cr}$ of 7161 kN. Conversely, *Equation 3.12* is used to assess the maximum load $F_{max}$, which is 23559 kN. The SF in a service-limit state (SLS) is obtained by dividing $F_{cr}$ by the maximum load per pad. This gives an SF of 1.54. The same is performed for the ultimate limit state (ULS) using $F_{max}$. As a result, an SF of 5.06 is obtained.

Following Mösrch (1952), an SF of 2.0 is recommended to avoid the use of any reinforcement. Although smaller values are obtained in SLS, it is important to consider that the typical SF in service is assumed to be 1.0 and that more than enough safety margin remains regarding the ULS. It is also necessary to consider that the maximum load from the thrust jacks were used in the calculation and that a low risk of collapse is associated with this type of cracking once the ring leaves the shield. Based on these considerations, it is possible justify that no reinforcement is required; however, a combination of reinforcing bars and steel fibres were used in these precast segments due to the relatively high bending moments expected in some lengths of the tunnel.

An extensive experimental programme was performed in the Metro Line 9 in Barcelona to evaluate the possibility of replacing the traditional reinforced concrete segment by a fibre-reinforced concrete equivalent Infante (2006). During the experimental programme, 30 rings reinforced solely with steel fibres were installed in a curved stretch. The inspection of these segments showed that no longitudinal cracks occurred due to bursting stresses. This is consistent with the results obtained through the application of the analytical model.

## 3.7 CONCLUSIONS

An experimental investigation was performed to study the mechanical behaviour of concrete blocks with different dimensions with and without steel fibres under concentrated loads. Through the study, three simplified analytical formulations based on STM were proposed. To fully understand the proposed model, a case study at Metro Line 9 in Barcelona was discussed. The main conclusions of this study are described below:

- As a simple and accurate method for structural analysis, the strut-and-tie model shows a reliable ability to analyse concentrated loads on concrete blocks. The depth of the confined area of the blocks significantly affects the form of the proposed formulations to predict the mechanical behaviour of the concrete blocks.

- In blocks with greater length than height, only a portion of the blocks is responsible for transmitting the applied loads. The area that effectively contributes to the transmission of stress is defined by an angle equal to 23°, according to experimental results.

- From the comparisons of theoretical and experimental values of $F_{fis}$ and $F_{rup}$, it has been verified that the formulations proposed could predict the mechanical behaviour of the blocks in the experimental study.

- Due to its simplicity and accuracy, the formulations developed in this work could serve as a basis for predicting the mechanical behaviour of concrete blocks subjected to concentrated loads.

- The application of the formulations developed for Line 9 in Barcelona indicates that a safety factor of 1.51 and 5.06 exist in the SLS and the ULS, respectively. These results suggest that no specific reinforcement should be placed to resist the tensile forces that arise due to the concentrated loads applied by the thrust jack pads.

# 4. DESIGN PROCEDURE AND EXPERIMENTAL STUDY ON FRC SEGMENTAL RINGS FOR VERTICAL SHAFTS

## 4.1 INTRODUCTION

Structural fibres are commonly used in precast segments for the lining of tunnels constructed with tunnel boring machines (TBM). These structures usually remain under compression in service, presenting tensile stresses primarily during transient stages (demoulding, storage, transport, handling, and installation). Under these conditions, the partial or even the complete replacement of traditional bar reinforcement by an adequate amount of structural fibres becomes technical and economically attractive. De la Fuente et al. (2012) and Liao et al. (2015a) presented a set of real experiences in tunnels that were constructed with a TBM, and in which FRC is used as sole material to produce segments.

Currently, several codes and guidelines (DBV 1992 & CNR 2006 & RILEM TC 2003 & CPH 2008 & Model Code 2010) include fibre reinforced concrete (FRC) as a structural material; highlighted among them the MC 2010. Furthermore, many experimental campaigns from the literature as shown in *Table 4.1* (the abbreviation used is the same as in the *Table 3.1*). have focused on the production, full-scale bending tests, and numeric simulations of segments made of concrete with compressive strengths fc ranging from 20 to 150 $N/mm^2$ and structural fibre contents ($C_f$) ranging from 30 to 236 $kg/m^3$. Moreover, Plizari et al. 2010; de la Fuente et al. 2012; Bakshi et al. 2014 also present a set of real experiences in tunnels constructed with TBM in which FRC is used. These experiences have promoted the

application of FRC, demonstrating that the material is competitive at the structural level compared with other traditional solutions.

*Table 4.1 Experimental campaigns and numerical simulations collected from the scientific literature regarding FRC segments for tunnels created with a TBM*

| Elements | $f_c$(MPa) | Dimensions(mm) | Material | $C_f$(kg/m$^3$) | $\Phi_f/\lambda_f$ | No | Num. Sim. |
|---|---|---|---|---|---|---|---|
| PS (RT) | 75 | 3640×1500×200 | SFRC | 40 | 0.35/30 | 1 | None |
| | 45 | | RC | --- | --- | 1 | |
| PS (RP) | 60 | 2359×1400×350 | PC | --- | --- | 3 | None |
| | | | SFRC | 30 | 0.75/60 | 3 | |
| | | | | 40 | | 3 | |
| PS (RT) | 45 | 2406×900×200 | RC | --- | --- | 1 | None |
| | | | SFRC | 20 | 0.55/35 | 1 | |
| PS (MT) | 60 | 4700×1800×350 | SFRC | 40 | 0.75/60 | 2 | None |
| | | | | 50 | | 2 | |
| PS (MT) | 60 | 4700×1800×350 | SFRC+RC | 30 | 1.0/50 | 2 | Full-scale test & 3D-FE (ANSYS) |
| | | | SFRC | 45 | | 2 | |
| | | | | 60 | | 2 | |
| PS (MT) | 20 | Semi-circle 9700×1000×300 | PC | --- | --- | 1 | Full-scale test & 3D-FE (ANSYS) |
| | | | SFRC | 40 | 0.8/60 | 1 | |
| | | | PC | --- | --- | 1 | |
| | | | SFRC | 40 | 0.8/60 | 1 | |
| | | | PC | --- | --- | 1 | |
| | | | SFRC | 40 | 0.8/30 | 1 | |
| | | | PC | --- | --- | 1 | |
| | | | SFRC | 40 | 0.8/60 | 1 | |
| PS (RP) | 66 | 2120×1500×235 | RC | --- | --- | 1 | None |
| | 68 | | SFRC | 120 | 0.75/60 | 1 | |
| | 66 | 3180×1500×235 | RC | --- | --- | 1 | |
| | 68 | | SFRC+PF | 120+ | 0.75/60 | 1 | |
| | 140 | 1000×500×100 | UHPC | --- | --- | 1 | Full-scale test & 3D-FE (ABAQUS) |
| | 150 | 1000×500×100 | UHPFRC | 236 | 0.2/80 | 1 | |
| PS (MT) | 68 | 2438×1500×235 | SFRC | 57 | 0.75/60 | 6 | Full-scale test & 3D-FE (ABAQUS) |

Until now, the design of FRC segments has been addressed by means of numerical methods (Poh,J. et al. 2009 & de Waal, R.G.A. 1999 & Kooiman, A.G. 2000 & Caratelli, A. et al. 2012 & Bakhshi M. et al. 2013 & 2014 & Chiaia, B. et al. 2009a & 2009b). To the authors' best knowledge, no analytical expression that describes the design of segments reinforced only with fibres or with hybrid reinforcement (fibre + bars) is found in the literature. Furthermore, the authors have been unable to find any reference in which these types of segments are used in vertical shafts constructed with a vertical shaft machine (VSM). Like in many tunnels, in this case the segments are generally subjected to reduced stresses during the transitional phases and compression predominates during service. Therefore, despite the absence of previous experiences, the use of structural fibres instead of bars may also be competitive.

## 4.2 OBJECTIVES

The objective of this Chapter is to provide a response to the two absences mentioned in the previous paragraph. On one hand, the objective is to demonstrate that the complete replacement of the bar reinforcement by fibres is also possible in shaft linings constructed with VSM. On the other hand, the objective is to propose an analytical and general formulation to assess the minimum mechanical requirements that the FRC must fulfil in elements with complete or partial substitutions of the traditional reinforcement. First, the analytical formulation based on the MC 2010 is proposed for the structural design of FRC segments. This formulation is then applied to the redesign of the segments from Montcada Shaft, which was originally conceived with traditional reinforcement. After that, in the context of full-scale construction work (Montcada Shaft, Barcelona) and a research project, a characterisation campaign of conventional and self-compacting concretes reinforced with fibre quantities ($C_f$) between 30 and 60 kg/m$^3$ was performed to evaluate the optimum amount for the complete removal of the traditional reinforcement. Finally, an experimental campaign of full-scale segments subjected to bending was performed with both concrete types to verify the ductile behaviour until failure.

This study widens the field of application of FRC, demonstrating the feasibility of a new use. Moreover, it shows new formulations that might support engineers towards the optimal structural design of this type of structures or others constructed with FRC.

## 4.3 CHARACTERISATION OF FIBRE REINFORCED CONCRETE

### 4.3.1 Test method to characterize residual strength

The most common test to characterise post-cracking behaviour of FRC is three-point test according to the EN 14651(2005) standard for prismatic beams with dimension of 150mm × 150mm × 600mm (see *Figure 4.1a*). During the test, the applied load and crack mouth opening displacement (CMOD)/deflection of notched beam were recorded.

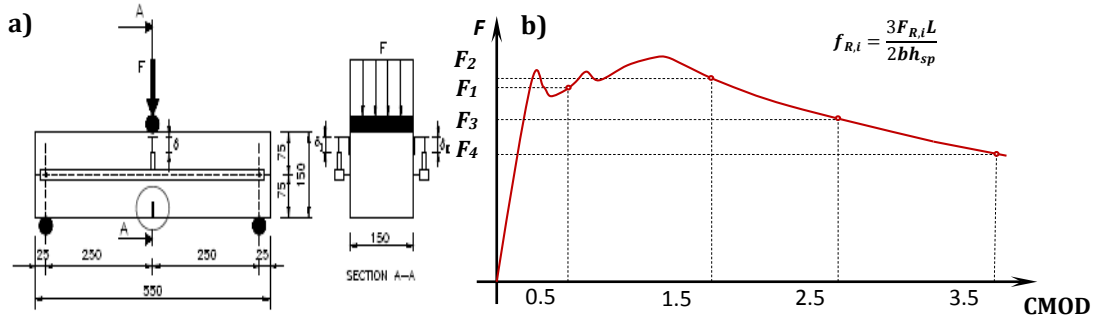


*Figure 4.1 Three-point test in notched prismatic beams: a) test configuration and b) F – CMOD generic curve*

The obtained *F* – CMOD curve (*Figure 4.1b*) can be used to deduce the material constitutive curve *σ*-*ε*. The stress σ is derived from the residual tensile strength $f_{Ri}$ using specific expression according to the standard.

### 4.3.2 Strength classification of the FRC

The classification proposed in MC 2010 is based on the characteristic values of the residual tensile strength for CMOD=0.5 mm ($f_{R1k}$) and CMOD=2.5 mm ($f_{R3k}$). In this regard, the FRC strength class is specified using $f_{R1k}$ to represent the strength interval and letter (*a*, *b*, *c*, *d,* or *e*) to represent the $f_{R3k}/f_{R1k}$ ratio:

1. The strength interval $f_{R1k}$ is established by using a number from the following series: 1.0 – 1.5 – 2.0 – 2.5 – 3.0 – 4.0 – 4.5 – 5.0 – 6.0 – 7.0 – 8.0 in N/mm$^2$.

2. The $f_{R3k}/f_{R1k}$ ratios are in accordance with the following series: *a)* if $0.5 \leq f_{R3k}/f_{R1k} < 0.7$; *b)* if $0.7 \leq f_{R3k}/f_{R1k} < 0.9$; *c*) if $0.9 \leq f_{R3k}/f_{R1k} < 1.1$; *d*) if $1.1 \leq f_{R3k}/f_{R1k} < 1.3$; and *e* if $f_{R3k}/f_{R1k} \geq 1.3$

In addition, MC 2010 establishes that when the goal is to replace, either partially or completely, the traditional passive reinforcement with an equivalent quantity of structural fibres in ULS, the following must be satisfied: $f_{R1k}/f_{Lk} > 0.4$ and $f_{R3k}/f_{R1k} > 0.5$.

## 4.4 DESIGN OF ELEMENTS SUBJECT TO REDUCED STRESS

### 4.4.1 Introduction

The classical design philosophy of reinforced concrete structures (also for pre-stressed structures) is to guarantee ductile behaviour of the section in which the fatigue mechanism appears. In this regard, in sections where the bending moment *M* is lower than the bending moment produced by cracking $M_{cr}$, the strategy to establish the minimum amount of reinforcement $A_{s,min}$ consists of ensuring that the ultimate strength moment $M_u$ is no less than $M_{cr}$ ($M_u \geq M_{cr}$; see *Figure 4.2*). This means that the strength capacity of the concrete matrix is maintained during the post-cracking phase.

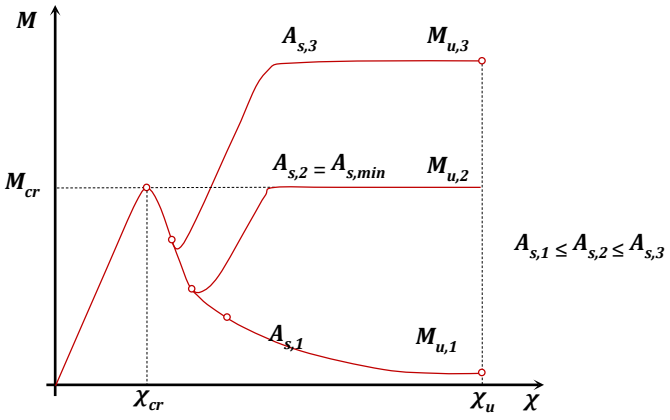


*Figure 4.2 Moment M – Curvature χ diagram to illustrate sectional response as a function of the degree of reinforcement*

This approach has been historically adopted in the MC 2010 and in other national codes to evaluate $A_{s,min}$. *Equation 4.1* shows the minimum amount of the traditional reinforcement

needed to fulfil the ductility requirements in rectangular sections. This equation is derived by matching the mean value of $M_{cr}$ ($M_{crm}$) with $M_u$, assuming that in ULS the arm ($z$) equals 0.8 of the height ($h$), the distance to the gravity centre of the bars in tension ($d$) equals 0.9 of $h$, and the partial safety factor of the steel bar ($\gamma_s$) is 1.15. In this regard, as discussed in (Levi, F. 1985), adopting mean values of $M_{cr}$ leads to $A_{s,min}$ on the safe side.

$$A_{s,\min} = 0.26 \frac{f_{ctm,fl}}{f_{yk}} bd \qquad \text{Equation 4.1}$$

In FRC elements, assuming mean values of $M_{cr}$ for this type of approach usually leads to high minimum fibre contents ($C_{f,min}$), which could be unfeasible at a technical and economic standpoint. In the case of segments for tunnel linings, an extensive discussion of this issue can be found in (Liao, L. et al. 2015a). Taking that into account, the design values of $M_{cr}$ and the tensile strength in flexion $f_{ct,fl}$ ($M_{crd}$ and $f_{ctd,fl}$, respectively) are assumed for the evaluation of $A_{s,min}$ of traditional reinforcement and the minimum residual strength $f_{R3k,min}$ of FRC needed to ensure the ductility of the segment in case the design value of the moment ($M_d$) exceeds $M_{crd}$ due to an external load during the transient stages.

### 4.4.2 Formulas to evaluate minimum reinforcement requirement

In contrast to bar-reinforced concrete sections (for which there are formulas such as *Equation 4.1* to evaluate $A_{s,min}$, for FRC sections and sections with hybrid reinforcement ($A_s$ + $C_f$) there are no analytical formulas to obtain $f_{R3,min}$ to satisfy the minimum ductility requirements. In this regard, the recommendations proposed in MC 2010 as well as in the classical approach is to ensure that $M_u \geq M_{cr,d}$.

A rectangular section with dimensions $b$ and $h$ with a hybrid reinforcement represented in *Figure 4.3* is considered. This would respond to a section of an FRC segment with localised reinforcement to confine the concrete during the jack thrust phase and to control possible cracking due to bursting and splitting (Hemmy, O. et al. 2001 & Burguers, R. 2006 & Burguers, R. et al. 2007 & Tiberti. G. et al. 2014 & Breitenbücher, R. 2014 & Bakhshi, M. et al. 2014 & Liao, L. et al. 2015b).

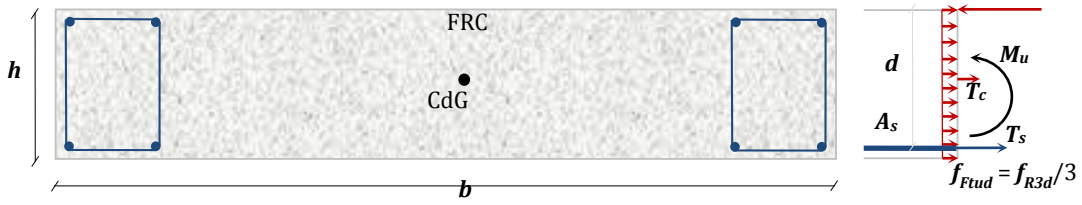


*Figure 4.3 Transversal section of a segment with hybrid reinforcement ($A_s$ + $C_f$)*

Notice that the longitudinal bars and the fibres contribute to the flexural strength of the cross-section. In this way, the $f_{R3}$ required will depend on the amount of traditional reinforcement used. To evaluate the characteristic value of $f_{R3}$ ($f_{R3k}$), a sectional analysis is proposed and the following hypotheses are assumed.

- The behaviour of FRC subjected to tensile stresses is simulated through the perfect plastic constitutive diagram proposed in MC 2010 and defined by the design value of the ultimate tensile residual strength of the material ($f_{Ftud}$) that should equal $f_{R3d}/3$. The value of $f_{R3d}$ should be obtained by the division of the corresponding characteristic value ($f_{Rk3}$) by the partial safety factor for the FRC under tension ($\gamma_{FRC}$).

- Since sections are weakly reinforced, the neutral line in bending for ULS is located near the upper fibre. The same is true for the resultant force $C_c$ of the compressive stresses, which should also be concentrated in the upper fibre.

- The passive reinforcement reaches the yielding limit and develops a tensile force $T_s = A_s \cdot f_{yd}$, where $f_{yd} = f_{yk}/\gamma_s$ ($f_{yk}$ and $f_{yd}$ are the characteristic and design values of the elastic limit of steel, respectively). The reinforcement near the upper fibre is not taken into account in the analysis. This hypothesis is on the safe side.

The equilibrium equations of the horizontal loads *Equation 4.2* and of the moments with respect to the section centre of gravity *Equation 4.3* are imposed. By combining *Equation 4.2* and *Equation 4.3*, *Equation 4.4* is obtained.

$$C_c - T_s - T_f = 0 \qquad \text{Equation 4.2}$$

$$M_u = C_c \frac{h}{2} + T_s\left(d - \frac{h}{2}\right) \qquad \text{Equation 4.3}$$

$$M_u = f_{Ftud}\frac{bh^2}{2} + A_s f_{yd} d \qquad \text{Equation 4.4}$$

Considering that for all the loading stages $M_d \leq M_{crd}$, only a minimum amount of reinforcement is required to ensure a ductile failure. In other words, the condition $M_u \geq M_{crd}$ should be imposed. $M_{crd}$ can be evaluated by a simple linear elastic calculation that, for rectangular sections, is mathematically represented through *Equation 4.5.*

$$M_{crd} = \frac{bh^2}{6} f_{ctd,fl} \qquad \text{Equation 4.5}$$

By combining Eq. 4 and Eq. 5 and considering the relationship $\xi = d/h$ and $\rho_s = A_s/A_c$ (the geometric quantity of passive reinforcement), *Equation 4.6* is obtained to assess $f_{R3k}$. In this equation, $\gamma_c$ is the partial safety factor for concrete.

$$f_{R3k\geq} \frac{\gamma_{HRF}}{\gamma_c}\left(1 - 6\rho_s \frac{\frac{f_{yk}}{\gamma_s}}{f_{ctk,fl}}\xi\right) f_{ctk,fl} \qquad \text{Equation 4.6}$$

The minimum geometric amount of reinforcement for sections only reinforced with traditional reinforcement ($\rho_{s,min}$) can be evaluated with *Equation 4.7.* This equation is derived by matching the $M_u$ (obtained through *Equation 4.4* for $f_{Ftud} = 0$ and $C_f = 0$) with $M_{crd}$ (obtained with *Equation 4.5*). By combining *Equation 4.6* and *Equation 4.7,* a closed

expression is achieved for the ratio $f_{R3k}/f_{ctk,fl}$ (see *Equation 4.8*) of FRC. Notice that the latter depends on the geometric amount of traditional reinforcement ($\rho_s$) actually used.

$$\rho_{s,\min} = \frac{h}{6d}\frac{\frac{f_{ctk,fl}}{\gamma_c}}{\frac{f_{yk}}{\gamma_s}} = \frac{1}{6\xi}\frac{f_{ctk,fl}}{f_{yk}}\frac{\gamma_s}{\gamma_c} \qquad \text{Equation 4.7}$$

$$f_{R3k}/f_{ctk,fl} \geq \frac{\gamma_{HRF}}{\gamma_c}\left(1-\frac{\rho_s}{\rho_{s,\min}}\right) \qquad \text{Equation 4.8}$$

*Figure 4.4* shows how the ratio $f_{R3k}/f_{ctk,fl}$ varies with the ratio $\rho_s/\rho_{s,min}$. The curve obtained was calculated by assuming that $\gamma_{FRC}$ and $\gamma_c$ are equal to 1.5. It is important to remark that when no traditional reinforcement is applied ($\rho_s = 0$), the FRC will be the sole responsible for providing the ductility. This is reflected in the result of Eq. 8 since $f_{R3k}$ becomes equal to $f_{ctk,fl}$. On the contrary, if the minimum amount of traditional reinforcement is used ($\rho_s = \rho_{s,min}$), the result of Eq. 8 becomes 0. This indicates that no contribution of the FRC for the ductility is required ($f_{R3k} = 0$), hence no fibre reinforcement is needed.

It is evident that the use of *Equation 4.8* leads to a minimum strength criterion that the FRC must fulfil. This criterion is independent of the type of fibre (material, shape, anchor type, and other specific factors for each commercial fibre). Once the fibre type has been chosen, the $C_f$ required must be evaluated through standardised tests that characterize the residual strength of FRC. Examples are the bending test on prismatic notched beams (EN 14651, 2005) or the Barcelona test (2010) on cylindrical specimens, which has been reported in numerous scientific papers (Chen, WF. 1970 & Molins, C. et al. 2009 & Carmona, S. et al. 2012 & Pujadas, P. et al. 2013 & Pujadas, P. et al. 2014) and recently included in ITATECH (2015) guidelines for the design of precast concrete segments.

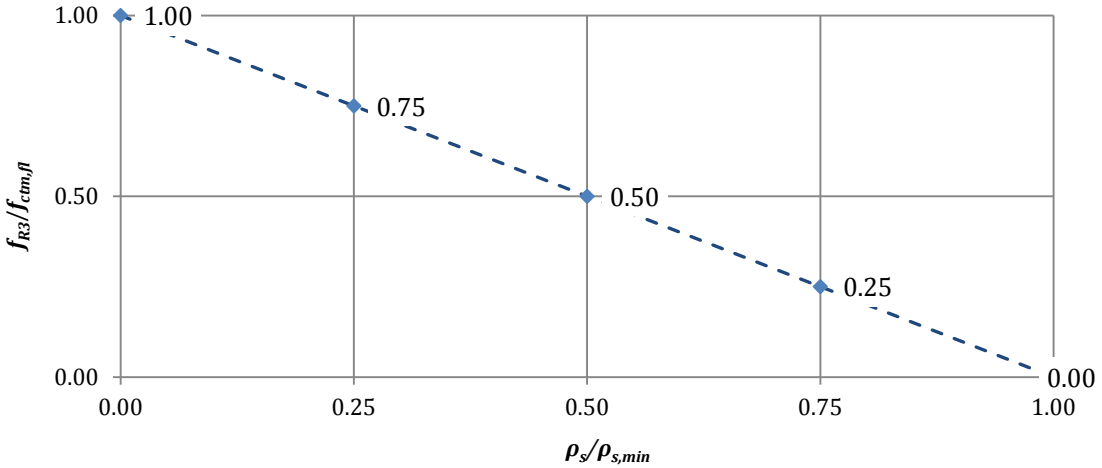


*Figure 4.4 $f_{R3,k}/f_{ctk,fl}$ ratio as a function of the $\rho_s/\rho_{s,min}$ ratio obtained with Equation 4.8. ($\gamma_c = \gamma_{FRC} = 1.50$)*

## 4.5 RE-DESIGN OF THE VERTICAL SHAFT MONTCADA

The construction of several vertical ventilation shafts is included in the project of the high-speed line that will connect Madrid, Barcelona and the border of France. One of the vertical shafts of this line is located in the municipality of Montcada and Reixac (Barcelona). The shaft has a depth of 59 m with, an inner diameter of 9.20 m (see *Figure 4.5a*) and will be constructed with a VSM (see *Figure 4.5b*). The ground excavated consists of 4 m of landfill material close to the surface, followed by 16 m of sand or gravel strata and 39 m of slate.

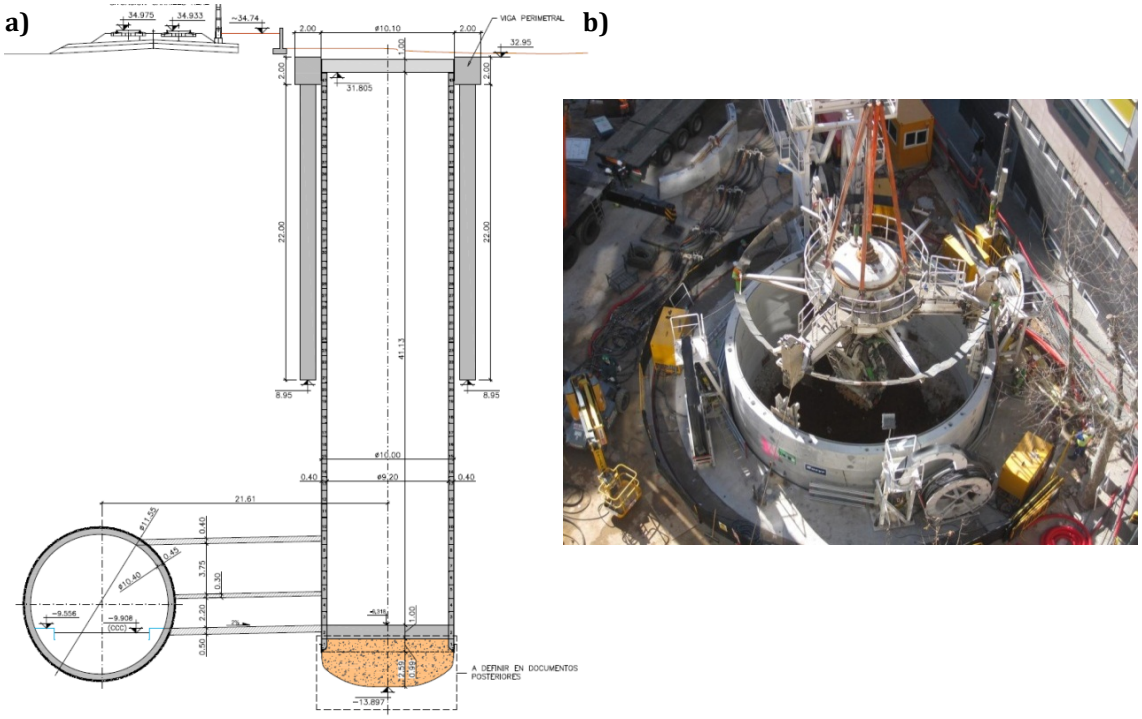


*Figure 4.5 a) Geometry of the Montcada shaft and b) the VSM use for the shafts of the AVE Madrid– French Border*

According with the original project, the rings are formed by four segments (see *Figure 4.6*) of C40 traditionally reinforced concrete ($f_{ck}$ = 40 N/mm²) with a thickness of 0.40 m and a width of 1.0 m. The main reinforcement is formed by two layers of 10Φ16 bars disposed along the width of the segment. Local and transversal reinforcements are also included in the original project. The concrete cover is 50 mm thick to ensure sufficient performance in the case of a fire and to comply with the requirements of EHE – 08 (2008).

The segments undergo different transient loading stages and support configurations during production: (1) demoulding (see *Figure 4.7a*); (2) provisional storage after production (see *Figure 4.7b*); (3) on-site storage (see *Figure 4.7c*) and (4) lifting for its placement (see *Figure 4.6d*). In the first two stages, the segment exhibits beam-type behaviour, whereas in the last two stages, the behaviour resembles that of a deep beam. For situations (1) and (2), the design requirement is that cracking does not occur considering a load safety factor $\gamma_{SW}$ of 1.50, which already takes into account the risk of impact or dynamic action.

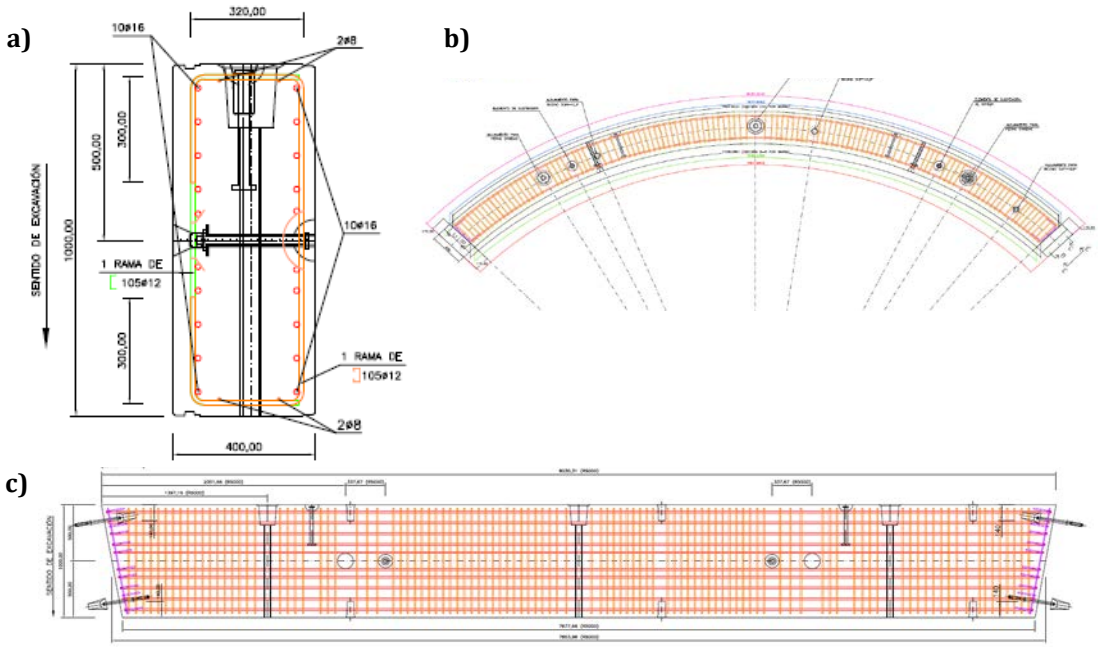


*Figure 4.6 a) Transversal section, b) front view, and c) plane view of the segment reinforcement for the Montcada shaft*

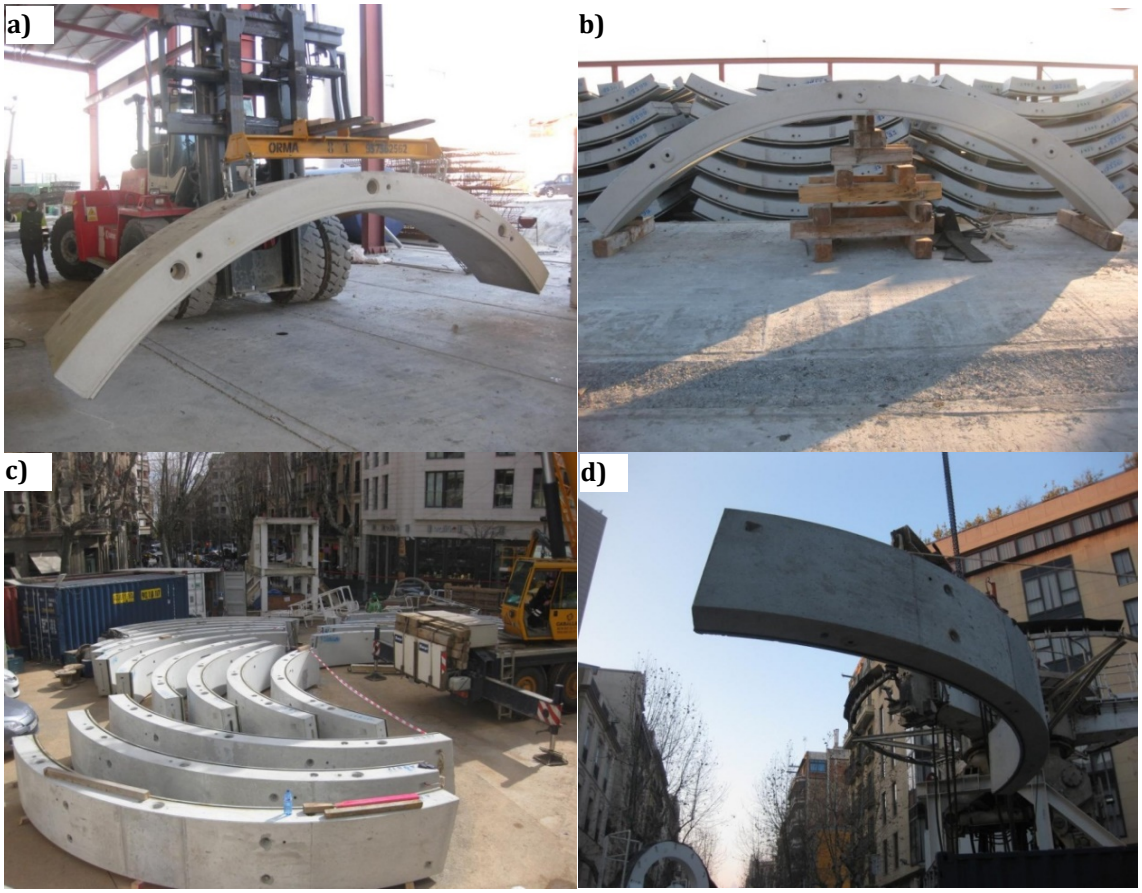


*Figure 4.7 a) Transport after mould release; b) provisional support under storage; c) support configuration in the work site; and d) lifting operation for the placement of the ring*

The interaction with ground during the service phase was simulated with PLAXIS® software and with STATIK® software considering the geomechanical parameters presented in *Table 4.2*. The models were used to estimate the characteristic values of bending moment, normal force and shear force ($M_k$, $N_k$, and $V_k$, respectively) for sections at depths of 15, 35, and 59 m. The characteristic values found are summarized in *Table 4.2* along with the corresponding design values obtained with load safety factor of 1.50.

*Table 4.2 Geomechanical parameters considered in the simulation with PLAXIS*

| Lithological unit | γ (kN/m³) | C (kN/m²) | Φ (°) | $K_o^{nc}$ () | $K_{o,x}$ () |
|---|---|---|---|---|---|
| Landfill | 16.0 | 0 | 28 | 0.53 | 0.53 |
| Sand | 21.0 | 10 | 35 | 0.50 | 0.50 |
| Gravel sand | 21.0 | 0 | 38 | 0.50 | 0.50 |
| Slates | 26.7 | 176 | 38 | 0.50 | 1.00 |

For the transient load stages, it was verified that $M_d < M_{crd}$ in the most unfavourable sections. Consequently, only minimum reinforcement is required. The goal of the investigation consists of completely removing the reinforcement, particularly the main reinforcement, using an adequate amount of structural fibres to ensure the requirements established in MC 2010.

Applying *Equation 4.8* proposed in this article and considering $\rho_s$ equal to 0 to account for the absence of traditional reinforcement, it is found that the FRC used should comply with a ratio $f_{R3k}/f_{ctk,fl} \geq 1.0$. Furthermore, it must comply with $f_{R1k}/f_{Lk} > 0.4$ and $f_{R3k}/f_{R1k} > 0.5$. Consequently, $f_{R3k} \geq 3.0$ N/mm² and 1.2 N/mm² < $f_{R1k}$ < 6.0 N/mm² (considering $f_{Lk} = f_{ctk,fl}$).

To verify if the FRC defined previously suffices the design requirements from *Table 4.3* during service, an AES nonlinear analysis model of sections (de la Fuente, A. et al. 2012) was used. This model simulates the FRC mechanical behaviour with the constitutive equations proposed for this material in MC 2010. The AES model was used to assess the normal stress-bending moment (*N*–*M*) interaction diagram shown in *Figure 4.8*. The design values from *Table 4.3* are also included in the same figure to evaluate if the cross-section performance complies with the ULS.

*Table 4.3 Stresses for the ring transversal section at different depths*

| Level | $M_k$ (mkN) | $M_d$ (mkN) | $V_k$ (kN) | $V_d$ (kN) | $N_k$ (kN) | $N_d$ (kN) |
|---|---|---|---|---|---|---|
| -15 m | 34 | 51 | 53 | 79 | 1174 | 1763 |
| -35 m | 63 | 95 | 97 | 145 | 2157 | 3235 |
| -59 m | 103 | 155 | 159 | 238 | 3532 | 5298 |

Notice that all points are within the N-M envelope. The results indicate that the cross-section operates under flexo-compression with dominant compressions. Consequently, the section does not crack when subjected to the design stresses and the FRC proposed is adequate for service phases. Therefore, it is possible to substitute the entire main tensile reinforcement by fibres.

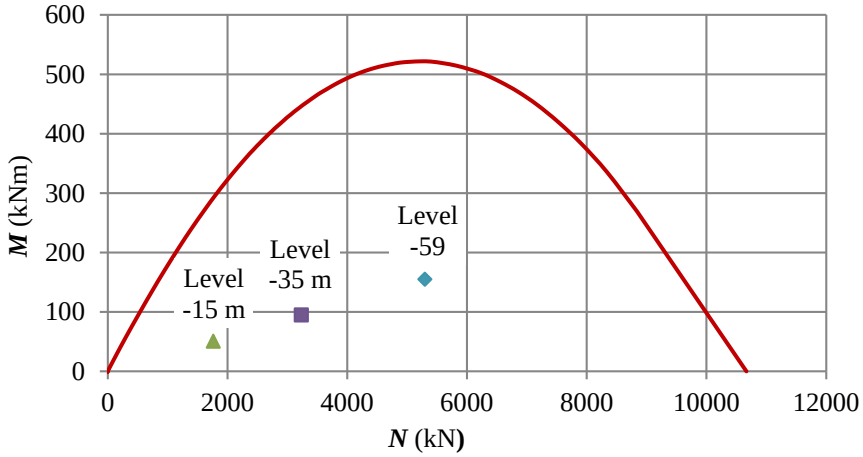


*Figure 4.8 N – M interaction diagram of the ring transversal section of the Montcada shaft*

## 4.6 EXPERIMENTAL PROGRAMME

### 4.6.1 Introduction

Once the mechanical requirements for FRC are set by considering the different load stages, the value of $C_f$ required to satisfy the established requirements must be evaluated. Thus, a characterisation and an optimisation of the experimental campaign for the material is proposed, in which two types of concretes are involved: conventional concrete (CC) and self-compacting concrete (SCC). The effect of fibre orientation to the post-cracking behaviour of precast segment would be investigated and three different fibre contents $C_f$ are used to evaluate the minimum value ($C_{f,min}$). Subsequently, four segments are produced with the two types of concrete by using the $C_{f,min}$.

### 4.6.2 Material characterisation and optimisation

Three batches of concrete with the fibre content of 30 kg/m³, 45 kg/m³ and 60 kg/m³ were produced in concrete plant both for CSFRC (numbered as CSFRC-30, CSFRC-45, CSFRC-60) and SCSFRC (numbered as SCSFRC-30, SCSFRC-45, SCSFRC-60). The composition of the mixture is presented in *Table 4.4*. The low carbon hooked-end steel fibre supplied by BASF was used. The fibre has a minimum tensile strength of 1000 N/mm², length of 50mm±1 mm, and the diameter of 1.0mm±0.1 mm.

*Table 4.4 Mix composition of CSFRC and SCSFRC [in kg/m³]*

| Mixtures | CSFRC | SCSFRC |
|---|---|---|
| Sand 0/5 | 817 | 1200 |
| Fine aggregate 5/15 | 404 | 500 |
| Coarse aggregate 12/20 | 810 | 200 |
| Water | 156 | 165 |
| CEM I 52.5 R | 312 | 380 |
| Superplasticizer | 2.19 | 4.56 |

In the fresh state, the consistency was characterised with the slump flow test (EN 12350-2, 2009) for the CSFRC and with the flow extent test (EN 12350-8, 2010) for the SCSFRC. Moreover, the content of occluded air and the density were measured using the tests described in (EN 12350-7, 2009) and in (EN 12350-6, 2009), respectively. The results of the fresh state tests are presented in *Table 4.5*. The FRSCC reached flow extents above the 60 cm established in the EN 12350-8 as a minimum for self-compacting concrete. It is also observed that the FRCC present an occluded air content approximately 2.5 smaller than the FRSCC. This may be the consequence of the higher amount and different type of superplasticizer, as well as, the higher mortar content used in the former to increase the flowability.

*Table 4.5 Test results on fresh state*

| Series | Cone test (cm) | Flow test (cm) | Air content (%) | Density (kg/m³) |
|---|---|---|---|---|
| CSFRC-30 | 3 | - | 1.8 | 2481 |
| CSFRC-45 | 5 | - | 2.1 | 2481 |
| CSFRC-60 | 3 | - | 2.2 | 2494 |
| SCSFRC-30 | - | 65 | 5.4 | 2394 |
| SCSFRC-45 | - | 65 | 5.5 | 2394 |
| SCSFRC-60 | - | 67 | 7.4 | 2319 |

To characterise the mechanical behaviour of each mixture in the *hardened state*, nine cylindrical specimens were moulded (ϕ150x150 in mm) to evaluate the compressive strength $f_c$ according with (EN 12390-3, 2009) at 1, 7, and 28 days of age. In addition to that, three prisms (150x150x600 in mm) were cast to perform the notched three-point test (EN 14651, 2005) and evaluate $f_L$ and $f_{Ri}$ at 28 days. Non-destructive inductive tests were also performed to evaluate the $C_f$ values following (Torrents, J. et al. 2012 & Cavalaro, S.H.P. et al. 2014 & 2015), as shown in *Figure 4.9a*. This test was conducted on cubic specimens (150x150 in mm) cut from the already tested prismatic specimens. These specimens were extracted respecting the distances indicated in *Figure 4.9b* to avoid the influence of the wall effect and of the cracked section. Notice that two cubic specimens are symmetrically extracted from each beam subjected to the bending test.

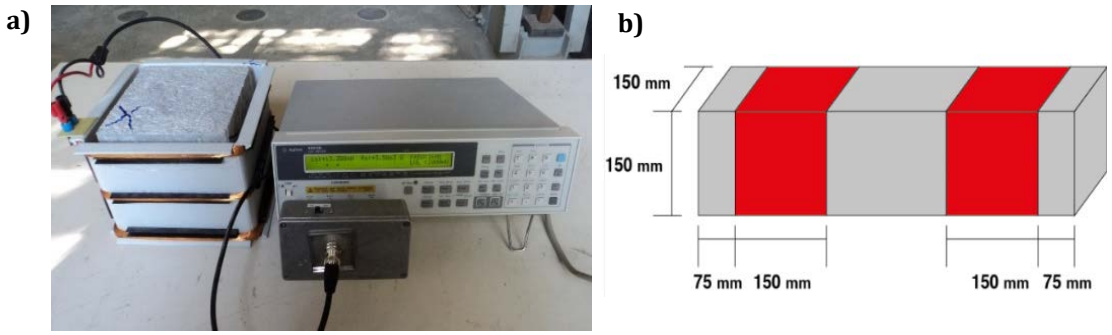


*Figure 4.9 a) Inductive test and b) cubic specimens cut from the tested prisms*

*Table 4.6* presents the values of $C_f$ for each cubic specimen, the mean values of $C_f$ ($C_{fm}$), and their coefficient of variation of the results (CV). *Table 4.7* shows the evolution of compressive strength and the strengths measured in the bending tests. *Figure 4.10*

presents the average F-CMOD curves obtained in the bending test for the concrete mixes tested. All the detail information of test results are presented in the ***Annex B.***

*Table 4.6 Values of $C_f$ and $C_{fm}$ in kg/m³ and CV (%) obtained with the inductive test*

| Series | $C_f$ (kg/m³) | | | | | | $C_{fm}$ | CV |
|---|---|---|---|---|---|---|---|---|
| | Specimen 1 | | Specimen 2 | | Specimen 3 | | | |
| | 1-1 | 1-2 | 2-1 | 2-2 | 3-1 | 3-2 | | |
| CSFRC-30 | 31.5 | 30.1 | 34.9 | 28.4 | 33.1 | 31.5 | 31.6 | 6.6% |
| CSFRC-45 | 54.3 | 43.4 | 41.9 | 41.4 | 51.5 | 39.8 | 45.4 | 12.1% |
| CSFRC-60 | 65.3 | 67.2 | 57.2 | 64.3 | 56.3 | 55.7 | 61.0 | 7.7% |
| SCSFRC-30 | 24.4 | 25.8 | 30.6 | 25.6 | 28.5 | 33.0 | 28.0 | 10.9% |
| SCSFRC-45 | 39.4 | 37.6 | 48.2 | 50.7 | 49.8 | 49.0 | 45.8 | 11.4% |
| SCSFRC-60 | 59.4 | 63.0 | 47.2 | 54.3 | 69.0 | 71.4 | 60.7 | 13.7% |

*Table 4.7 Average values of $f_c$, $f_L$, $f_{R1}$, and $f_{R3}$ (N/mm²) and CV (%)*

| Series | $f_{cm}$/CV | | | $f_{Lm}$/CV | $f_{R1m}$/CV | $f_{R3m}$/CV |
|---|---|---|---|---|---|---|
| | 1 days | 7 days | 28 days | 28 days | | |
| CSFRC-30 | 20.2/1.2 | 54.4/1.8 | 65.1/0.3 | 5.2/1.1 | 3.2/8.4 | 2.4/1.8 |
| CSFRC-45 | 19.7/2.4 | 54.6/0.8 | 63.9/1.5 | 5.8/3.8 | 5.1/20.3 | 3.9/22.2 |
| CSFRC-60 | 21.5/1.5 | 54.8/0.2 | 64.9/1.9 | 5.5/12.4 | 4.8/19.3 | 4.3/22.1 |
| SCSFRC-30 | 25.4/2.1 | 56.1/2.9 | 70.5/1.2 | 5.0/9.9 | 2.9/28.4 | 2.6/32.7 |
| SCSFRC-45 | 18.3/0.8 | 55.2/1.8 | 66.3/1.3 | 5.8/8.5 | 4.7/1.9 | 4.8/5.84 |
| SCSFRC-60 | 17.1/1.5 | 53.4/1.3 | 66.7/4.2 | 5.9/2.7 | 7.1/17.2 | 7.1/11.6 |

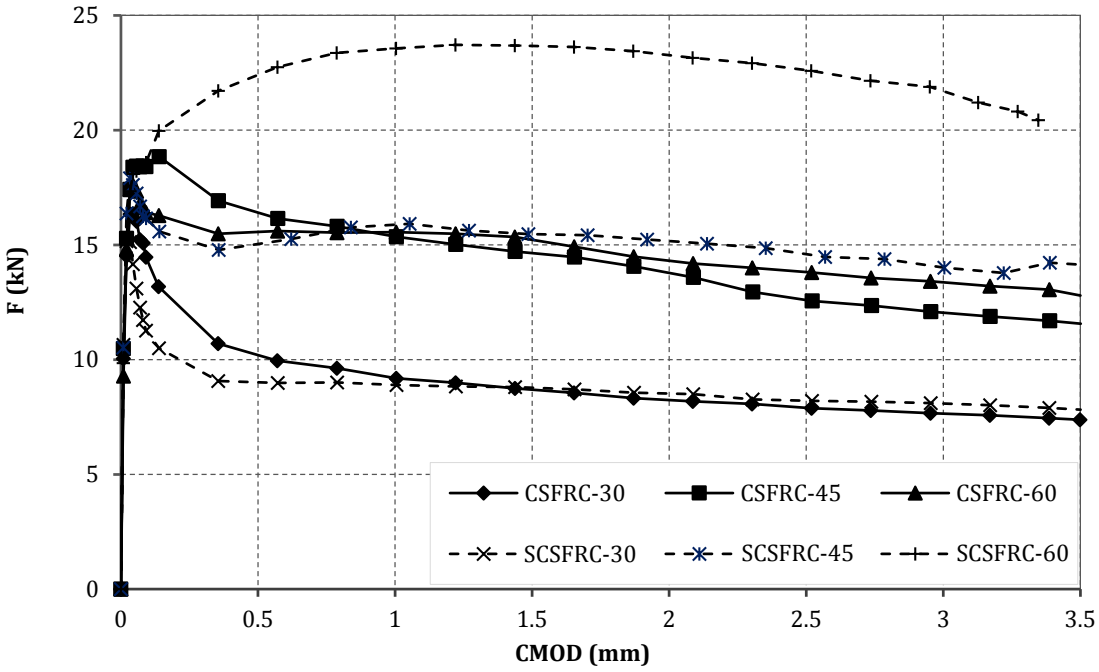


*Figure 4.10 Average F - CMOD relationship curves obtained from three-point bending tests*

Regarding the results presented in *Table 4.6* and *Table 4.7* and in *Figure 4.10*, the following can be concluded.

- The average fibre content measured with the inductive method approximates the nominal content of each mix. The coefficient of variation among samples is higher in the case of FRSCC than in the FRCC. This is probably the result of the bigger freedom of movement of the fibres in the mixture of FRSCC, which makes fibre distribution and content more sensible to variations in the casting procedure.

- In the short term, the values of $f_c$ is bigger than the minimum 15 N/mm$^2$ established in the project for demoulding segments. At 28 days of age, the values of $f_{cm}$ seem independent of the value of $C_f$, being around 5% higher for the FRSCC than for the FRCC. This slight difference may be attributed to the higher cement content in the former (*Table 4.4*). The minimum average value of $f_{ck}$ is 62.1 N/mm$^2$. Hence, all the compositions reached the C60 class (above the C40 established in the final project). It is important to remark that this is a common situation found in tunnels since the limiting strength is observed at early age for the demoulding, not at 28 day.

- The coefficient of variation of the results of the bending test is especially high for the FRCC mixes and for FRSCC with 30 kg/m$^3$. Values of approximately 25% are expected for this type of material (Blanco, A. et al., 2013), being caused by errors inherent to the test itself as well as the randomness in the distribution and orientation of the fibres (Pujadas, P. et al. 2014 & Blanco, A. et al. 2015 & Cavalaro, S.H.P. et al. 2014).

- The residual response measured in the bending test for FRCC and for FRSCC are similar, except in the mixes with 60 kg/m$^3$ of fibres. In this particular case, the mix with self-compacting concrete presents hardening, whereas the mix with conventional concrete presents softening with a behaviour close to that of FRCC-40. This may be partially attributed to the high scatter in the residual strength of mixes FRCC-40 and FRCC-60.

Following the same approach described in (Barros, J.A.O. et al. 2005 & de la Fuente, A. et al. 2012 & 2013), the relationships $f_{Rk1} - C_f$ and $f_{Rk3} - f_{Rk1}$ depicted in *Figure 4.11* are obtained. The $f_{Rk1} - C_f$ and $f_{Rk3} - f_{Rk1}$ relationships fit a linear tendency with $R^2$ bigger than 0.85 for FRSCC. For FRCC, the $R^2$ values are unacceptable due to the high scatter obtained in the results of residual strength. Therefore, to evaluate $C_{f,min}$, the linear regression obtained for FRSCC will be used. Introducing in this equation the requirements derived in section 4 gives a $C_{f,min}$ of 38 kg/m$^3$.

However, it is important to consider that the specimens used in the bending test would yield a flexural response higher than that expected in the real-size segment due to the scale effect associated with the height of the cross section. It is estimated that to achieve a $f_{ctk,fl}$ of 3.0 N/mm$^2$ in the real segment, a $f_{ctk,fl}$ of around 4.0 N/mm$^2$ would be needed in the small-scale bending test. Hence, it was finally established that $f_{R3k}$ bigger than 4.0 N/mm$^2$ is required. Using this value in the linear regression from *Figure 4.11* gives a $C_{f,min}$ of 48.6 kg/m$^3$. Therefore, for industrial reasons, a *fibre content* equal to 50 kg/m$^3$ was fixed regardless of the concrete type.

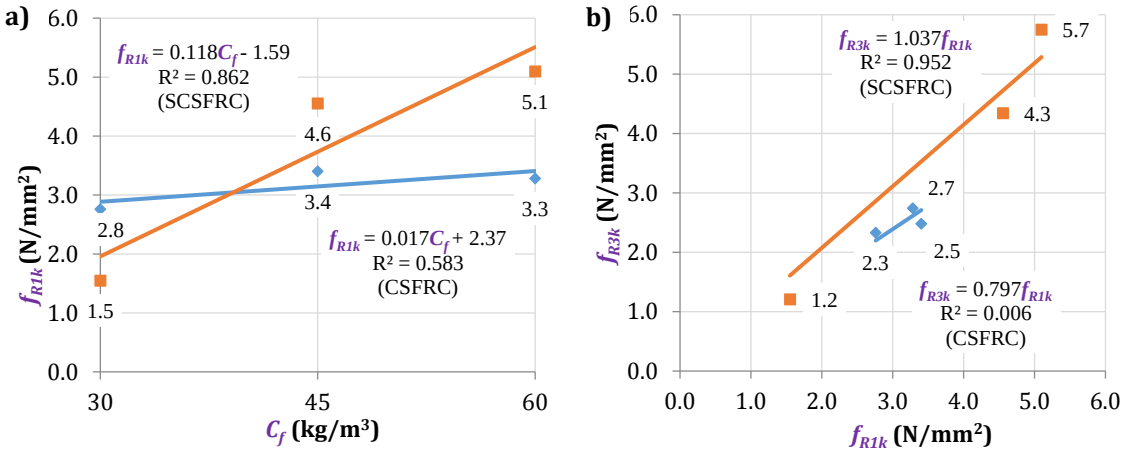


*Figure 4.11 a) $f_{R1k}$ – $C_f$ relationship and b) $f_{R3k}$ – $f_{R1k}$ relationship obtained with EN 14651 test*

### 4.6.3 Characterization of the structural behaviour of the segments

A conventional fibre-reinforced concrete segment (CSFRPS) and a self-compacting fibre-reinforced concrete segment (SCSFRPS) with $b$ = 1200 mm and $h$ = 350 mm were produced for a full-scale test intended to verify if the elements comply with the ductility requirements established. The compositions of the concrete presented in *Table 4.4* with a fibre content of 50 kg/m³, which was deduced from the section 4.5.2 was used to cast the segments. No additional reinforcement was included.

The concrete was poured with a hopper (see *Figure 4.12a*). The segment with conventional concrete was vibrated with internal and external vibrators. Both segments were cast on the same day and were unmoulded after 16 hours of casting (see *Figure 4.12b*). The segments were then placed over the support shown *Figure 4.12c* for their storage and transport. No surface cracks were detected in any of the visual inspections performed.

The segments were subjected to bending tests at 90 (CSFRPS) and 100 (SCSFRPS) days of age. The setup used is shown in *Figure 4.13a.* The segments were supported at the both ends. Prior to the test, the extremities of the segment had been cut to achieve a flat surface parallel to the reaction slab. The free-span ($l$) measured horizontally as a result of the cut was 5500 mm. Different materials were placed between the segment and the reaction slab in order to homogenize the contact and to reduce the friction. First, a 40-mm cement self-levelling mortar M20 was cast and left to cure over the reaction slab to regularize the surface. Over this layer, a 2-mm plastic sheet and a 2-mm Teflon sheet were placed. Finally, a neoprene layer with dimensions of 300x200x63 mm³ was allocated along the width of the segment.

The load was applied with a hydraulic piston at mid-span. The piston introduced a constant displacement rate of 0.9 mm/min towards the reaction slab. A thick steel beam and a neoprene sheet were placed between the piston and the segment to guarantee a uniform distribution of the load along the width of the segment. Displacement sensors were installed in the supports to measure the vertical and horizontal movements throughout the test. Furthermore, six LVDT were placed (three in each face (left and right)

of the central segment) to measure the width of the cracks near the loading zone, as shown in *Figure 4.13b, 13c.*


*Figure 4.12 Concrete pouring a), unmoulding operation b), and transport c) of the segments*

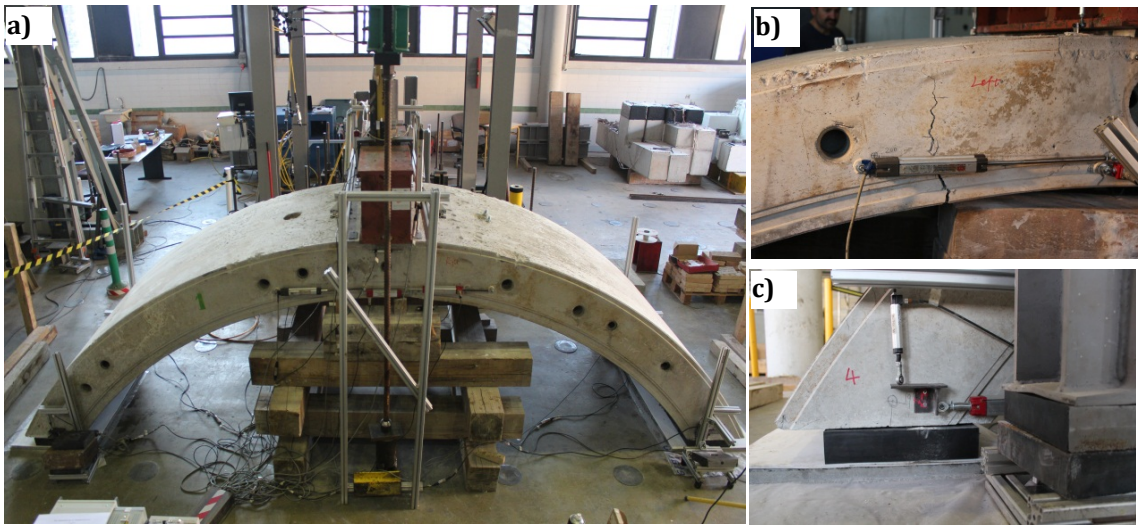


*Figure 4.13 a) Segment support configuration, b) LVDT to measure the width of the cracks due to bending, and c) detail of the support zone*

The results in terms of load ($F$) and crack width ($w$) are presented in *Figure 4.14a,* the $w$ used is the average value of left and right face crack width. A linear elastic behaviour is observed until reaching the cracking load ($F_{cr}$) of 61.5 kN and 68.0 kN for the CSFRPS and FRSCCS, respectively. Since the geometry is approximately equivalent in both tests, the

9.5% different in the values of $F_{cr}$ may be attributed to differences in the $f_L$ of each type of concrete.

a)

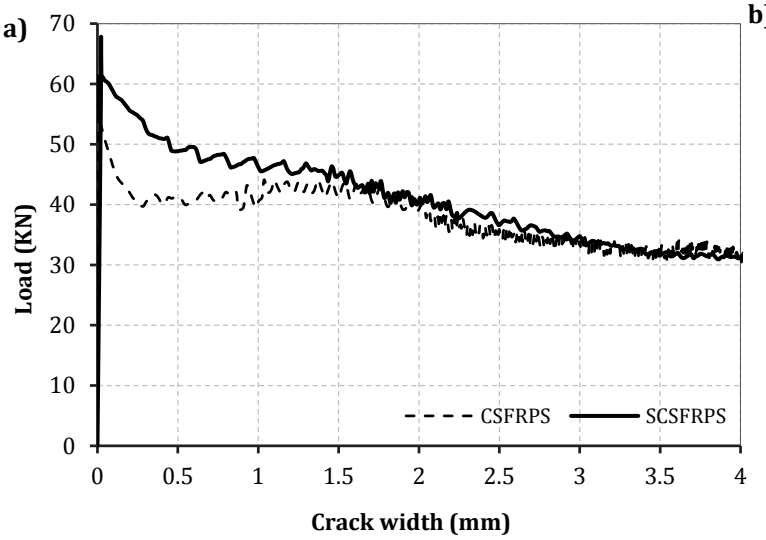


b)

| *w* (mm) | *F* (KN) | |
|---|---|---|
| | CSFRPS | SCSFRPS |
| 0.5 | 41.3 | 48.8 |
| 1.0 | 39.5 | 46.4 |
| 1.5 | 41.7 | 44.6 |
| 2.0 | 39.0 | 40.1 |
| 2.5 | 35.9 | 36.6 |
| 3.0 | 32.8 | 34.6 |
| 3.5 | 32.5 | 31.6 |
| 4.0 | 30.9 | 31.1 |

*Figure 4.14 a) Load (F) – crack width (w) curves and b) detail values obtained in the full-scale tests of the segments*

In both types of segment, a single main crack was formed (see *Figure 4.13b, 13c*). After that, a softening behaviour with a ductile response is observed. The results presented in *Figure 4.14b* also show that up to values of *w* close to 1.5 mm, the SCSFRPS presents a load that is, at most, 18.3% higher compared with that of CSFRPS. For *w* bigger than 1.5 mm, the response of both segments is equivalent in terms of *F*, thus confirming the general trend observed in the small scale experimental program from section 5.

After the test, the number of fibres present in the cracked section of each segment was counted (*see Figure 4.15*). In total 1026 fibres was found for the CSFRPS and 1082 fibres was found for the SCSFRPS. This slight difference (only 5%) in the number of fibres justify the equivalent mechanical behaviour obtained after cracking. It reflects that the influence of the rheology of concrete and the casting procedure on the fibre distribution was small, justifying the similar results obtained for conventional and self-compacting FRC.

*Figure 4.15 Grid generated to count the fibres in the fracture sections of the segments*

At the design standpoint and based on the discussions from sections 3 and 4, it is evident that both segments present ductile behaviour since large displacements are observed after reaching $F_{cr}$ (mean value of 64.8 kN for the two segments) with a gradual softening

response. Furthermore, considering the ultimate load ($F_u$) as that associated with a value of $w$ = 2.5 mm (in line with the value of $f_{R3}$ accepted in MC 2010 for the design in ULS), the results of *Figure 4.14b* indicate that $F_u$ reaches values of 35.9 kN for the CSFRPS and 36.6 kN for the SCSFRPS, where the mean value is 36.3 kN.

In this regard, the design performed in section 4 is still valid because *Equation 4.8* is presented with characteristic strength values, whereas the tests results must be considered as mean values. Thus, the $f_{ct,fl}$ of 4.0 N/mm$^2$ considered for the C60 leads to $M_{cr}$ = 98 kNm (in *Equation 4.5*). The bending moment associated with the self-weight is $M_{pp} = q \cdot l^2/8$ = 45 kNm ($q$ = 10.5 kN/m) The moment associated with force $F^*$ that would generate cracking under the design conditions is $M_{F^*,cr} = M_{cr} - M_{pp}$ = 53 kNm. Therefore, the cracking load under the setup configuration used could be calculated as $F^*_{cr} = 4M_{F^*,cr}/l$ = 38.5 kN and should be compared with $F_u$ = 36.3 kNm to be consistent with the proposed design strategy and to evaluate the suitability of *Equation 4.8.*

It is observed that $F^*_{cr}$ is 5.7% bigger than $F_u$. Therefore, the presented design would be slightly on the unsafe side in ULS for the $C_f$ established in section 5. However, this small difference may be disregarded as the segments were designed with characteristic values and partial safety coefficients ($\gamma_c = \gamma_{FRC}$ = 1.50) and given that the design was based on the value of $F_{cr}$ (64.8 kN) obtained in the small-scale tests. It is important to stress that, taking into account the effect of its self-weight, the estimated $f_{ct,fl}$ is of 5.1 N/mm$^2$ ($M_{cr}$ = 125 kNm), which is 27.5% bigger than the 4.0 N/mm$^2$ considered in the design for C60 concrete. The $M_d$ values estimated for the transient load phases are lower than that of the project $M_{cr}$ (98 kNm). Consequently, given the increment of $f_{ct,fl}$, the cracking risk is even lower.

Considering the hypotheses and design criterion presented in section 3 and the experimental campaign performed on the material and the segments, it was decided to modify the project reinforcement presented in *Figure 4.11*. In the new design, part of the segments were reinforced solely with 50 kg/m$^3$ of the structural metal fibres.

## 4.7 CONCLUSIONS

This study addressed the design and the characterisation of fibre-reinforced concrete segments to be used in the vertical shafts constructed with VSM. This type of structural element primarily works under compression during the service phase and the only tensile stresses that appear in the segments are produced during the transitional phases and have a low cracking risk. Therefore, the main bending reinforcement usually responds to minimum quantities of traditional reinforcement ($\rho_{s,min}$). The replacement of this reinforcement by an adequate quantity of structural fibres ($C_f$) is a real possibility that may bring technical as well as economic advantages. The following conclusions are derived from this study.

- The $f_{R3}/f_L$ ratio is linearly related with the $\rho_s/\rho_{s,min}$ ratio, which also takes into account the partial safety coefficients $\gamma_c$ and $\gamma_{FRC}$ through the analytical equation (*Equation 4.8*) proposed here. This equation helps to establish the minimum FRC requirements for hybrid sections (fibres + bars) subjected to reduced stresses (lower than the cracking

moment $M_{cr}$). This expression represents an important contribution for the design of FRC elements and has been proposed in the document by *fib committee* 1.4.1. "*Tunnels in fibre reinforced concrete*".

- Based on the experimental campaign and the application of *Equation 4.8* for the redesign of the segment from the Montcada shaft (Barcelona), it was observed that the value of $C_f$ that allowed the complete replacement of the reinforcement proposed in the initial project (minimum by mechanic criteria) is 50 kg/m$^3$.

- The mechanical behaviours of the CSFRPS and the SCSFRPS cast with 50 kg/m$^3$ of fibres in the full-scale bending tests were both ductile. Furthermore, an essentially equivalent response was obtained in both segments for cracking when $w \geq 1.5$ mm, which shows the reduced influence of rheology in fresh-state concrete on the behaviour in ULS. In this regard, the number of fibres in the failure sections differs by less than 5% for each segment, thus justifying the similar results.

# 5. STUDY OF ANISOTROPY PROPERTY OF THE FRC SEGMENTS

## 5.1 INTRODUCTION

In the past decades, the application of steel fibre reinforced concrete (SFRC) in civil engineering has grown rapidly due to the remarkable advantages of this material (di Prisco et al. 2000 & Walraven 2009 & Plizzari et al. 2006 & de la Fuente et al. 2012 & Burguers et al. 2007 & Liao et al. 2015a). It has been demonstrated that the addition of fibres could improve the mechanical performance of concrete considerably, especially in terms of the post-cracking behaviour. This contribution depends on the fibre content and orientation within the concrete element. Generally, a hypothesis of uniform distribution of fibres within SFRC is assumed for design purposes. The mechanical response and the fibre distribution is considered equivalent that of small scale specimens used in the flexural tests to obtain the constitutive models for the design. However, this analogy cannot be guaranteed due to differences in the procedures of casting and dimension of the elements. Therefore, it is significant to know the fibre distribution and mechanical response in concrete elements and to compare it with the measured in the small scale specimens.

In response to growing popularity of FRC, several design codes/recommendations have been published in recent years (DBV 1992 & CNR 2006 & RILEM TC 2003 & CPH 2008). In spite of many works being published indicated that the average distribution of fibres has a significant effect on the mechanical behaviour of FRC structure, the recommendations available for the design of FRC didn't take into account the influence of fibre distribution.

However, the fib Model Code (2010) proposed an orientation factor in the design of FRC that might affect the serviceability and ultimate residual strengths of concrete in certain situations. Although this new philosophy makes a step forward in the design of FRC, no specific guidelines on the quantification of such orientation factor is proposed (Blanco et al. 2015). Laranjeira (2010) studies revealed that even for the same type of element the orientation factor might be different due to many uncertain reasons.

Several studies (Edgington et al. 1979 & Stroeven 1977 & 1979 & Soroushian et al. 1990 & Toutanji et al. 1998) indicated that a preferential orientation of the steel fibres exist in slabs and might be favourable in controlling crack propagation. Despite that, few studies from the literature focus on the fibre orientation and resulting anisotropy in tunnel segments. Mora (2008) characterized the mechanical response of cores extracted from different direction of tunnel segments. The results showed a marked anisotropy. However, no all conclusions derived by the authors are based on the mechanical response of the cores, not on the explicit assessment of the fibre distribution.

## 5.2 OBJECTIVES

In this chapter, the assessment of fibre distribution in conventional steel fibre reinforced precast concrete segment (CSFRPS) and self-compacting steel fibre reinforced precast concrete segment (SCSFRPS) by means of inductive test and Barcelona test were conducted. For that, initially different types of specimens with varied fibre distribution were compared, and this would provide further evidence for what is required for the consideration of fibre distribution in the design of SFRC elements. Then, a large number of cores are extracted from the segments and tested with the inductive method to assess the fibre content and orientation. After that, the post cracking response of these cores was assessed with the Barcelona test. Based on the results obtained, a conceptual model of fibre distribution is proposed

## 5.3 EXPERIMENTAL PROGRAMME

### 5.3.1 Preparation of samples

The tunnel lining segments and the small scale specimens used for the study of the fibre distribution are the same as the described in the experimental programme from Chapter 4. The descriptions about the materials, the concrete mixes and the production process are described in sections 4.5 and 4.6.2 of Chapter 4.

#### ***Cylindrical cores***

Before the extraction, the position of the cores was marked at the outer surface of the segment (see *Figure 5.1a*). Each mark consisted of a number of references, a circumference that coincided with the perimeter of the core and an arrow that indicated the direction parallel to the circumferential length, that is, perpendicular to the axis of the tunnel. With these marks it is possible to identify the exact position and alignment of the core after extraction, which is necessary for a proper assessment of the fibre orientation.

A HILTI model DD 200 core rig was used to drill the cores through the full thickness of segments. The core extraction was always perpendicular to the contact face of segment (See *Figure 5.1b*). The internal diameter of the core bit was 150mm±1mm.

The cores were then cut with a disk saw to fulfil the requirements of the Spanish standard UNE 83515. First, both extremities were cut to obtain a cylinder with approximately 300 mm of length. Then, the remaining part was cut at the middle position to obtain cylinders with the length of 150 mm (See *Figure 5.1c*). These parts were identified as "upper" or "lower" considering the position of the segment during the casting process. Therefore, the upper core should be located close to the outer surface of the lining, while the lower core should be located closer to the inner surface.

All cores were marked according with the convention of axes shown in *Figure 5.1d.* According with this convention, the R-axis is parallel to the radius of the ring, the Y-axis is parallel to the width of the segment and the T-axis is tangent to the circumferential surface along the length of the segment. This consideration is relevant since a variation of the angle formed between the casting direction (Z) and the local coordinate system adopted for each core exists depending on the position inside the segment. For example, in cores extracted close to the middle-length of the segment the casting direction is parallel to the R-axis and orthogonal to the T-axis. Conversely, for cores extracted close to the extremities, the casting direction (Z) forms complementary angles with the R-axis and T-axis. This has to be taken into account when analysing the fibre orientation inside the segment.

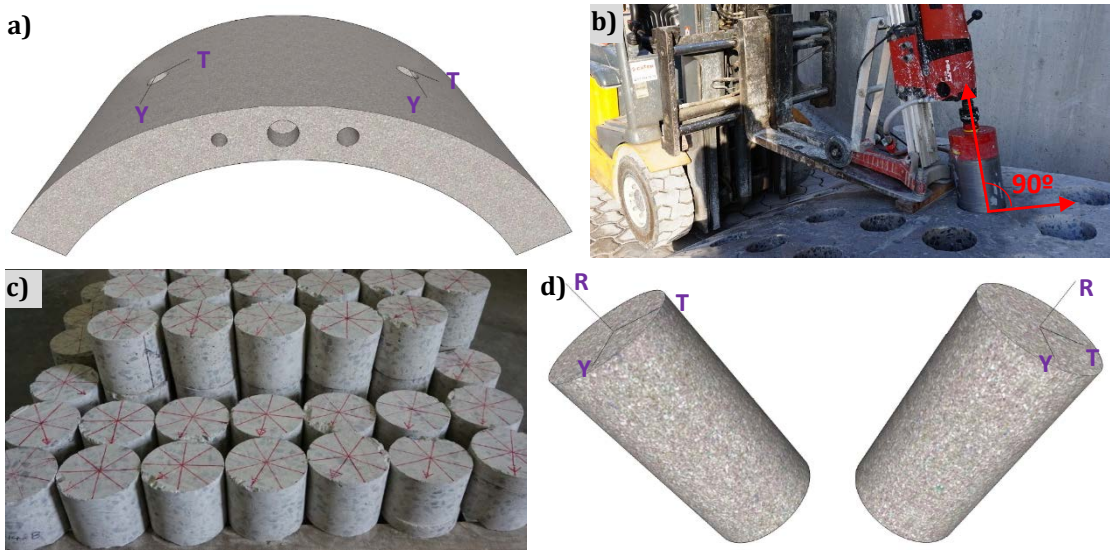


*Figure 5.1 a) Mark cores, b) Core drilling, c) final samples and d) convention adopted for the axes*

As explained in previous chapters, only one CSFRPS referred as C_A was characterized. On the other hand, three SCSFRPS were tested. These are called S_A, S_B and S_C. Notice that C_A and S_A were brought to the LTE Luis Agulló from the UPC for the full-scale mechanical test. After that, cores were extracted from uncracked areas. Conversely, segments S_B and S_C remained at the production plant.

Considering the harsh field environmental conditions and the technical difficulties to perform the extraction, cores were obtained solely from complementary halves of segments S_B and S_C. Taking into account the symmetric extraction and the fact that they share the same concrete mix, cores drilled from S_B and S_C segments were noted as S_D. The location of each core extracted is depicted with a cross in *Figure 5.2* along with the convention of axes used. In total, 80, 110, 24, 24 samples were obtained from C_A, S_A, S_B and S_C, respectively.

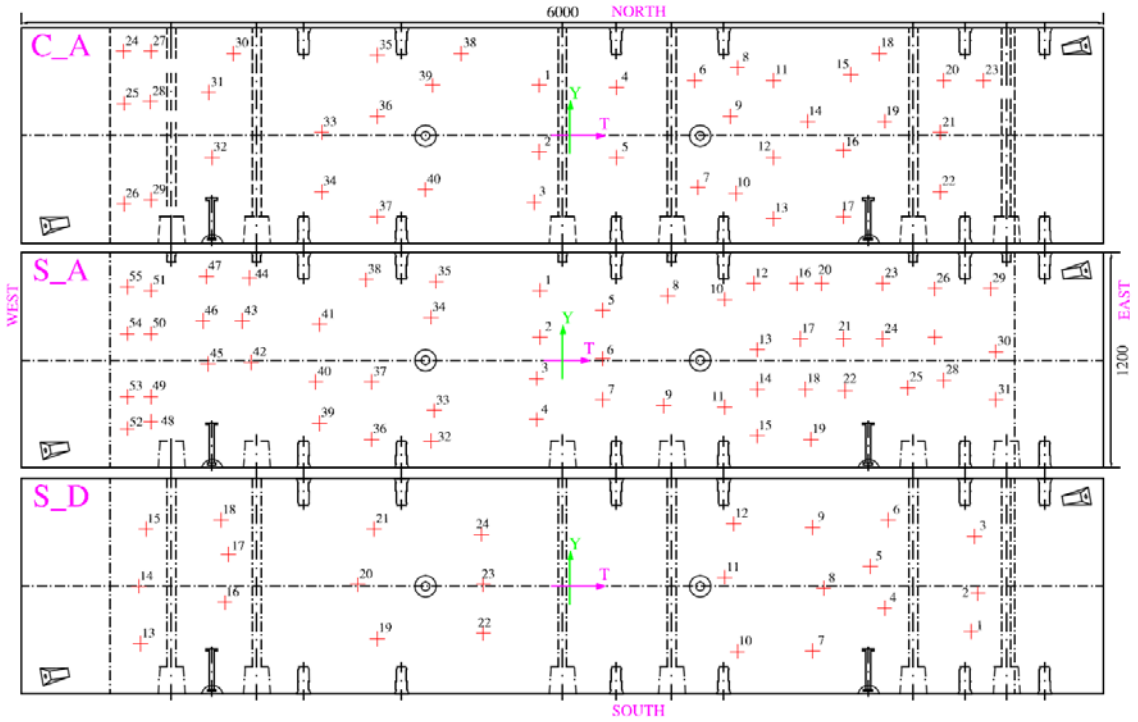


*Figure 5.2 Location of cores*

## ***Cubic samples***

During the production of the segments, specimens were also cast in cubic moulds with 150 mm of side. Moreover, cubic specimens of the same size were extracted from the small scale beam previously used for used in the bending test. This was done in accordance with the procedure described in Liao et al. (2014) and shown in *Figure 5.3a.*

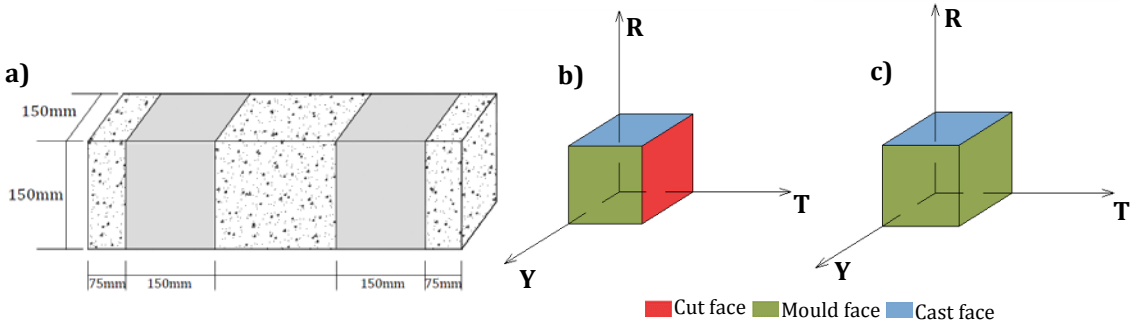


*Figure 5.3 a) Extraction of cubic specimens from the small scale beams, b) convention of axes used in extracted cubes and c) in cast cubes*

Cut was performed perpendicular to the length of the beams, 75 mm apart from the extremities with the intent of reducing the influence wall-effect that exists close to the mould. With the remaining central part, cuts were made to obtain 2 cubes from each beam. Then, the axes were marked following the convention from *Figure 5.3b.* In the case of moulded cubic specimens, the convention of axes used is shown in *Figure 5.3c.* All samples were stored at the temperature of 20 °C±1 °C and relative humidity no less than 95% until the preparation for testing.

### 5.3.2 Description of tests

In order to evaluate the fibre content and orientation the inductive test was performed. After that, the mechanical performance of each specimen was assessed with the Barcelona test. This way, the parameters related with the fibre distribution and their contribution in the residual strength are known for each specimen. All the detail information of test results are presented in the ***Annex C.***

***Inductive test***

The inductive test proposed by Torrents et al. (2012) and improved by Cavalaro et al. (2014a, 2014b) is used to quantify the amount and the distribution of fibres in steel fibre reinforced concrete in cubic and cylindrical specimens. The test consists of placing a SFRC specimen inside an energized coil. The magnetic nature of the steel fibres produce a change in the mutual inductance measured at the coil depending on the content and the alignment of the fibres with the axis of the coil (see *Figure 5.4a*). The inductance change is assessed for the specimens in different positions.

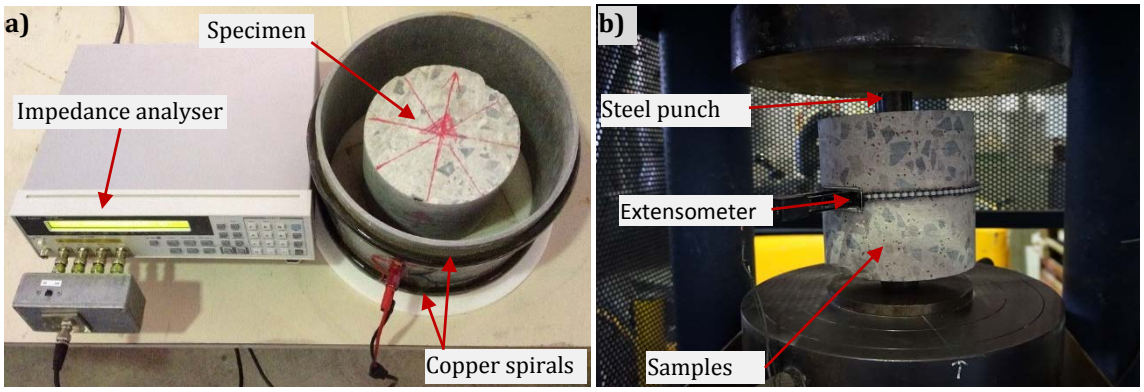


*Figure 5.4 a) Inductive test and b) Barcelona test*

Usually the sum of the measurements is linearly related with the fibre content ($C_f$) through a calibration curve that depends solely on the type of fibre. This curve is obtained experimentally by comparing the summed inductance and the content assessed by crushing one or two specimens and weighing the fibres. On the other hand, the comparison between the inductance measured in different directions is related with the fibre orientation number (η), which represents the average cosine formed by all fibres with the axis of the coil.

In the case of cylindrical specimens, it is also possible to obtain the maximum ($\eta_{max}$) and the minimum ($\eta_{min}$) orientation number, as well as their corresponding angles regarding the coordinate system adopted ($\theta_{max}$ and $\theta_{min}$, respectively). Another parameter assessed for cylindrical specimens is the isotropy factor Ω that ranges from 0 - for a perfectly anisotropic fibre distribution to 1 - for a perfectly isotropic fibre distribution.

***Barcelona test***

The Barcelona test is a modified double punching test to evaluate the residual tensile strength of fibre reinforced concrete Molins et al. (2006). Studies demonstrate that the test may be applied indistinctively to cubic and cylindrical specimens.

The test consists of applying a compressive load to a concentrated area of the cross-section. As depicted in *Figure 5.4b*, cylindrical metallic punches with a diameter equal to a quarter of the diameter of the specimen are used to concentrate the load. During the test, the plates of the press approach each other at a constant displacement rate of 0.5 mm/min and the force applied is registered. The relative displacement of the plates of the press is used to estimate the crack opening according with the formulation proposed by Pujadas et al. (2013). The peak load $F_{max}$ as well as the load corresponding to the total crack width of 0.5 mm, 1.0 mm, 1.5 mm, 2.5 mm and 3,5 mm were recorded as $F_{0.5}$, $F_{1.0}$, $F_{1.5}$, $F_{2.5}$ and $F_{3.5}$.

By combining the inductance value measured, the location of cracks and the load obtained, it is possible to evaluate the relationship between fibre distribution and the mechanical properties of the concrete.

## 5.4 RESULTS AND ANALYSIS

This section presents the results of the fibre distribution and mechanical response. To simplify the analysis, a study of the different variables contemplated in the experimental programme is performed. In this sense, the influence of the type of specimen, the type of concrete, the position along the thickness or the in plane position were evaluated.

### 5.4.1 Influence of the type of specimen

*Figure 5.5a* shows the fibre content measured depending on the type of specimen. For this analysis, the average of all specimen of the same type was calculated regardless of the type of concrete. Approximately the same value was obtained in all of them, with a difference of only 0.7% difference between the results for specimen from cubic moulds and for the cores extracted from the segments. The overall average content is close to 52 kg/m$^3$, which is slightly above the theoretical content established in the previous Chapter.

*Figure 5.5b* shows the average orientation numbers for the axes X (or T for the cores extracted from the segments), Y and Z (or R for the cores extracted from the segments) depending on the type of specimen. Contrarily to the observed in the case of the content, a significant difference is found in terms of the fibre orientation. These are differences are

related with the wall effect caused by each type of formwork and the flow of concrete during the cast procedure. For instance, specimens from cubic moulds have the same orientation number in the X and Y axes, while 37% smaller values are calculated in Z axis. These results suggest that fibres tend to be disposed in the plane perpendicular to the casting direction (Z), presenting a symmetric influence of the walls of the formwork in the other directions.

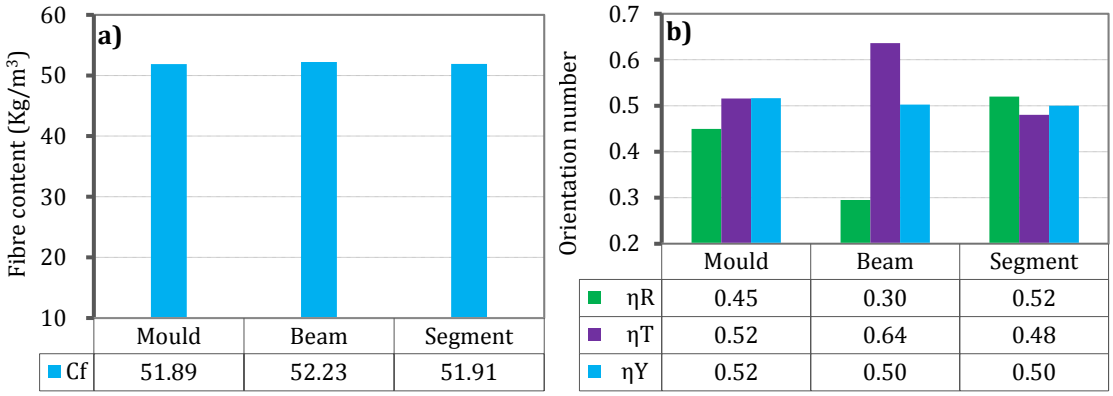


*Figure 5.5 a) Fibre content and b) orientation number depending on type of specimen*

Conversely, the specimens from the small-scale beams show a strong fibre orientation along X-axis, which coincides with the length of the beam. Orientation numbers obtained in the Y and Z-axis are nearly 31% and 58% smaller, respectively. It is evident that the predominant wall effect in the X direction and the flow of concrete condition the fibre orientation. For the cores extracted from the segments, the average orientation numbers in the axes C, Y and R are approximately the same.

The comparison of the fibre distribution throughout the types of specimens suggests that the post-cracking performance at a sectional level might not be equivalent. In this sense, the mechanical response of the bending test tends to governed by the orientation number at X-axis. This should be higher than the measured with the moulded cubic specimens characterized with the Barcelona test and in the cores extracted from the segments, which are more influenced by the orientation numbers in the axes X and Y. Therefore, in terms of fibre distribution, the moulded specimens used for the Barcelona Test could be more representative of the segments than the beam used in the bending test.

### 5.4.2 Influence of the concrete type

Another parameter that might influence the fibre distribution and, hence, the mechanical response is the consistency of the concrete used to cast the segments. The rheological properties of the concrete determine how the material will flow over and fill the formwork during the production process.

*Figure 5.6a* presents the average content of fibres obtained for all cores extracted from the segment with conventional (C) and from the segments with self-compacting concrete (S). Again, it is observed that the fibre content is approximately the same in both of them. This

is reasonable since the difference in flowability should not affect the fibre content regarded that no significant segregation occurs in the batches.

*Figure 5.6b* shows the orientation number for C and S. Notice that a rather isotropic fibre orientation is obtained for C. This is probably a result of the low consistency of the concrete (consistency close to 0 mm) that limits the freedom of movement of the fibres. On the contrary, a slightly preferential orientation is found in the radial direction for segments S and the smallest orientation numbers occur in the tangential direction (T).

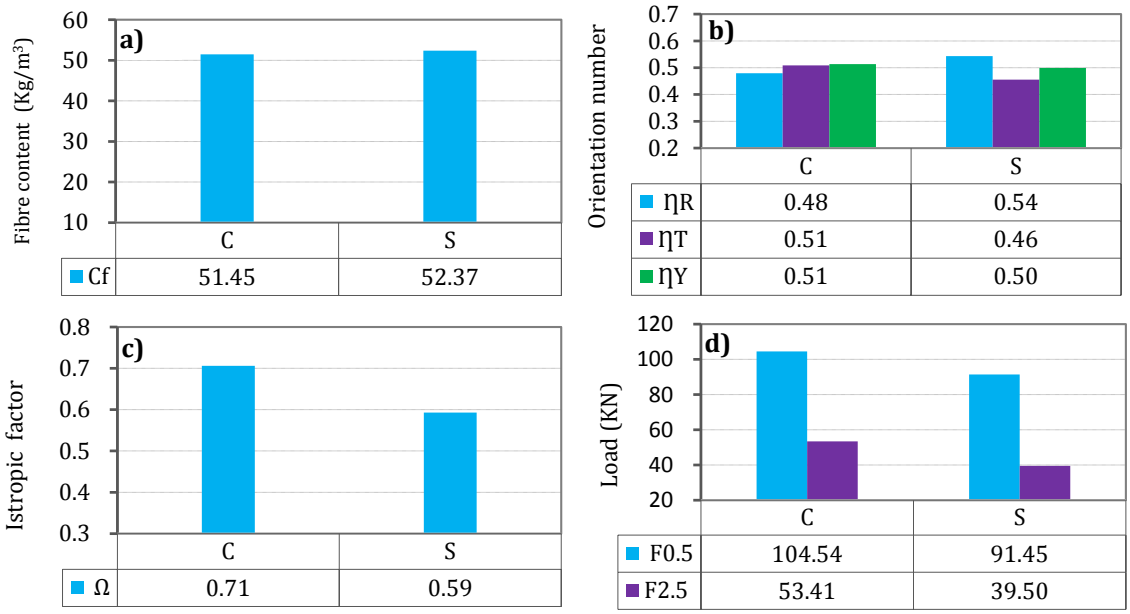


*Figure 5.6 Global comparison depending on concrete type*

This may be attributed to the higher flowability of the concrete, providing more freedom of movement to the fibres that might be more influenced by the flow of concrete. The segment has a circumferential length several times bigger than the width. Moreover, the opening for the casting of the segment extends over the whole width of the formwork. When the concrete is poured, an extensional flow regime will be established, covering rapidly the width of the segment. Consequently, a predominant flow along the circumferential length takes place, affecting the orientation of the fibres as a bigger distance has to be covered. Since in extensional flows fibres tend to align perpendicular to the stream flow, a reduction in the orientation number parallel to the circumferential length could be expected in the self-compacting concrete.

Even though this explanation justifies why a bigger orientation number is observed in the Y-axis than in the T-axis, it is not so evident why it could contribute partially to the high orientation numbers in the radial axis (R). To understand this result, it is necessary to take into account the influence of the curvature of the segment in the case of self-compacting concrete.

As mentioned in previous chapters, the casting was performed with a skip that had to be reloaded 4 times to fill up the formwork. The concrete from the first skips rapidly distributed and accumulate at the extremities of the formwork due to the curved shape of

the segment. In other words, a layered distribution of the material occurs. The surface tension of the free surface acts similarly to a wall effect, favouring the disposition of the fibres in the horizontal plane. Given that at the extremities the horizontal plane forms an angle different from 90° with the radial direction, an increase in the contribution of the fibres in R-axis follows close to the extremities.

The phenomenon described also affect the isotropy factor (Ω) of the materials, depicted in *Figure 5.6c.* The segment with conventional concrete presents a higher value, indicating a higher degree of isotropy than the segment with self-compacting concrete. The repercussion of the differential fibre orientation on the mechanical performance is shown in *Figure 5.6d.* The latter presents the residual load measured for total crack openings of 0.5 mm and 1.5 mm in the Barcelona Test. It is evident that the residual load for the specimens extracted from the segment with conventional concrete is between two and three times as big as that measured for the specimens extracted from the segments with self-compacting concrete for the same total crack opening.

This result might seem contradictory given the fact that the performance of the segment with conventional concrete presented a post-cracking residual load than that measured for the segment with self-compacting concrete in the full-scale test. The apparent contradiction between the Barcelona test and the full-scale test may be explained by two reasons.

The full-scale test only provides information of a cracked section located at the middle-length of the segment, whereas the cores characterized with Barcelona Test were extracted from different points and usually presented two or three cracks. The higher anisotropy of the self-compacting concrete suggests that the number of fibres bridging the cracks may vary depending on their direction. In the Barcelona Test, cracks bridged by a smaller number of fibres would tend to open more and with smaller load levels than those bridged by more fibres. Consequently, the post-cracking response measured during the Barcelona test would be predominantly influenced by the weakest cracked planes, being influenced by the smallest orientation number in the plane perpendicular to the cracks.

Notice that the minimum orientation number for the cores extracted from the conventional concrete segments in the axes Y and C is 0.51. However, for the cores extracted from the segments with self-compacting concrete the minimum value is 0.46. Therefore, a smaller post-cracking response should be expected in the latter. The same trend is not observed in the full-scale tests because in this case only one crack is formed with a preferential direction.

### 5.4.3 Variation depending on the position along the thickness

*Figure 5.7* shows the average values of fibre content, orientation number isotropy factor and residual load depending on the position of the core along the thickness of the segment with regard to the position during production. The letter “O” is appended to the nomenclature in order to indicate the cores closer to the outer surface of the segment. Similarly, the letter “I” indicates the cores close to the inner surface.

The analysis of *Figure 5.7a* shows that the difference between the results of fibre content for inner and outer cores is negligible for the segment with conventional concrete. Slightly bigger differences are observed in the analysis of the segments with self-compacting concrete, in which the cores close to the outer surface present a fibre content 5.4% lower than those close to the inner surface. This suggests a small segregation of the fibres as a result of the higher mobility provided by the self-compacting concrete. Despite that, the fibre contents measured remain above the theoretical content established for the experimental programme.

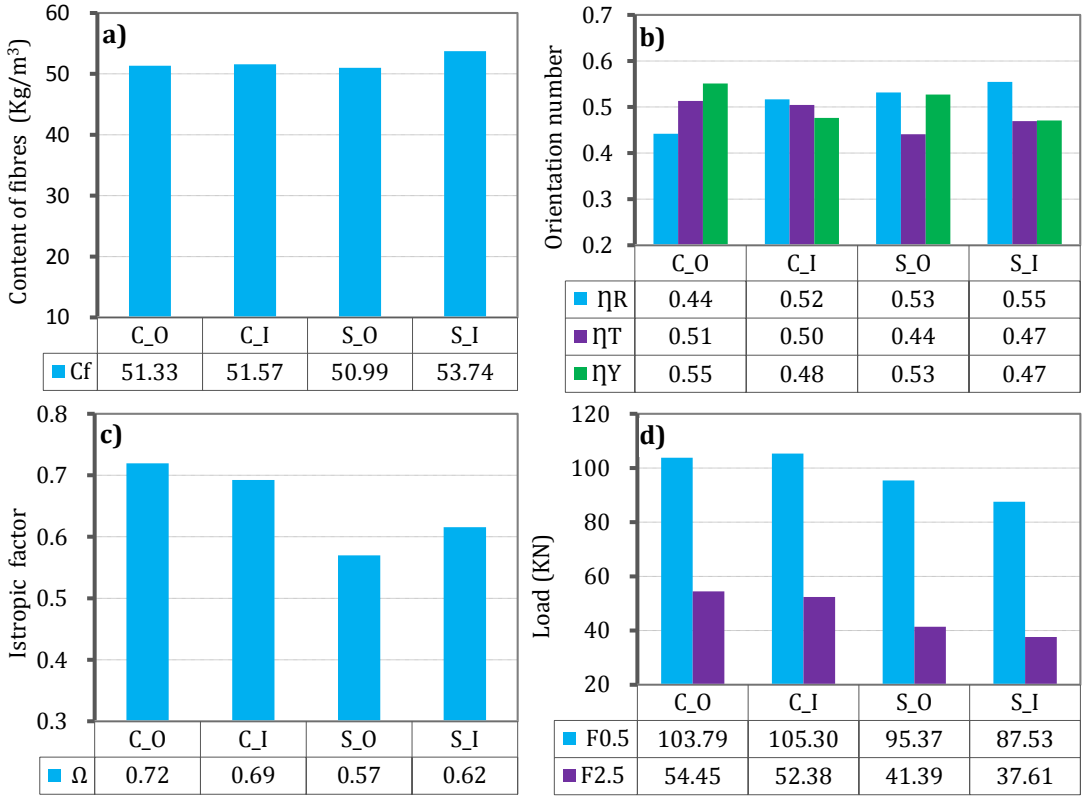


*Figure 5.7 Local comparison depending on the position along the thickness*

Taking into considered the orientation number (see *Figure 5.6b*), no clear trend is observed. Regarding the isotropy factor (see *Figure 5.7c*) and the residual load measured with the Barcelona Test (*see Figure 5.6d*), similar values are obtained for the cores extracted close to the outer surface and the inner surfaces.

### 5.4.4 Variation depending on the in-plane position

In order to evaluate the influence of the in-plane position over the fibre orientation and mechanical response, the segments are divided in the zones. The analysis is performed separately for the T-axis (see *Figure 5.8a*) that presented 5 zones with 500 cm of length and for the Y-axis (see *Figure 5.8b*) that had 3 zones with approximately 120 cm. In each case, the average of all the cores located within the limits of each zone is calculated for the different parameters studied. This consideration simplifies the interpretation of the

results and the identification of trends. The extremities cut from the segments for the execution of the full-scale tests were not included in the study, being depicted in discontinuous line in *Figure 5.8*.

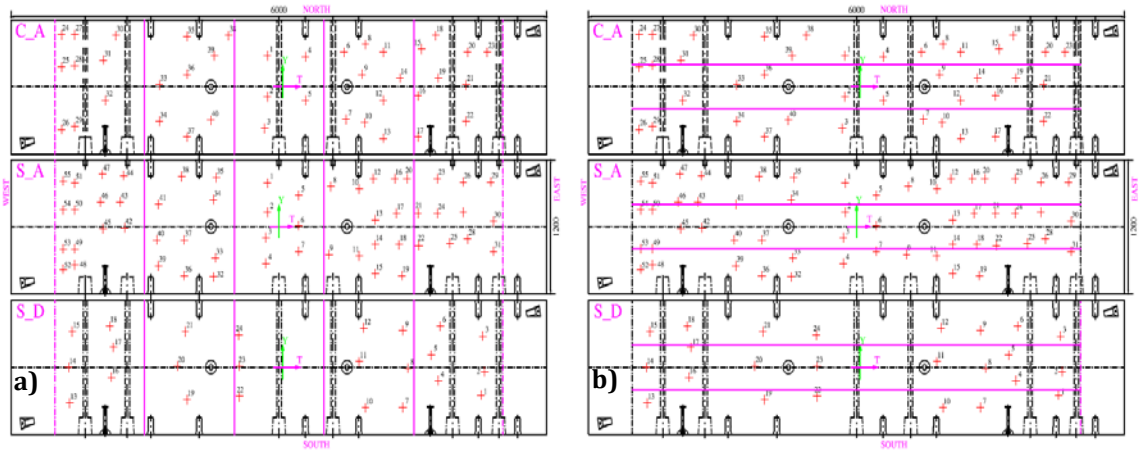


*Figure 5.8 Zones defined for the analysis of the influence of the position along a) the T-axis and b) Y-axis*

## ***Influence of zones along T-axis***

*Figure 5.9a* presents the variation of the average fibre content at the different zones defined along the T-axis. It is observed that practically over the whole extent of the segment the content measured complies with the theoretical value. The variation measured along the T-axis is slightly higher in the case of the segment with self-compacting concrete, which might be consequence of the higher risk of segregation of the material.

*Figure 5.9b* depicts the variation of the isotropy factor. In the case of the segment with convention concrete, values around 0.7 are obtained regardless of the position along the T-axis. In the segment with self-compacting concrete, smaller values are observed for all zones, except Z1. In addition to that a higher variability on the isotropy factor is observed. The results obtained suggest that the influence of the casting procedure on the orientation of the fibres is almost negligible for the segment with conventional concrete due to the low flowability and the internal restrictions to the movement of the fibres. On the contrary, the higher flowability of self-compacting concrete provides more freedom of movement to the fibres, making the material more sensible to the influence of the casting procedure.

*Figure 5.9c, 5.9d* and *5.9e* show the orientation numbers in the axes R, T and Y, respectively. This parameter remains almost constant and around 0.50 for the Y-axis, indicating similar fibre orientations regardless of the position and concrete type. Conversely, important variations are observed in the orientation numbers estimated for the T-axis. The higher values are observed close to the centre of the segment and the smaller close to the extremities. The opposite trend is observed for the fibre orientation in the R-axis, which presents higher values close to the extremities and lower values close to the centre of the segment.

Not only the trend is similar, but also the variation of the orientation depending on the position of the core. For instance, the orientation number in the R-axis decreases from the extremities to the centre of the segment by approximately 0.15. On the contrary, the orientation number in the T-axis increases from the extremities to the centre of the segment by 0.15. This confirms that the curvature of the segment produces a change in the angle formed by the R and T axis with the casting direction. Consequently, part of the contribution of the fibres moves from one axis to the other. Notice that the behaviour measured for the segment with conventional concrete and for the self-compacting concrete are virtually the same.

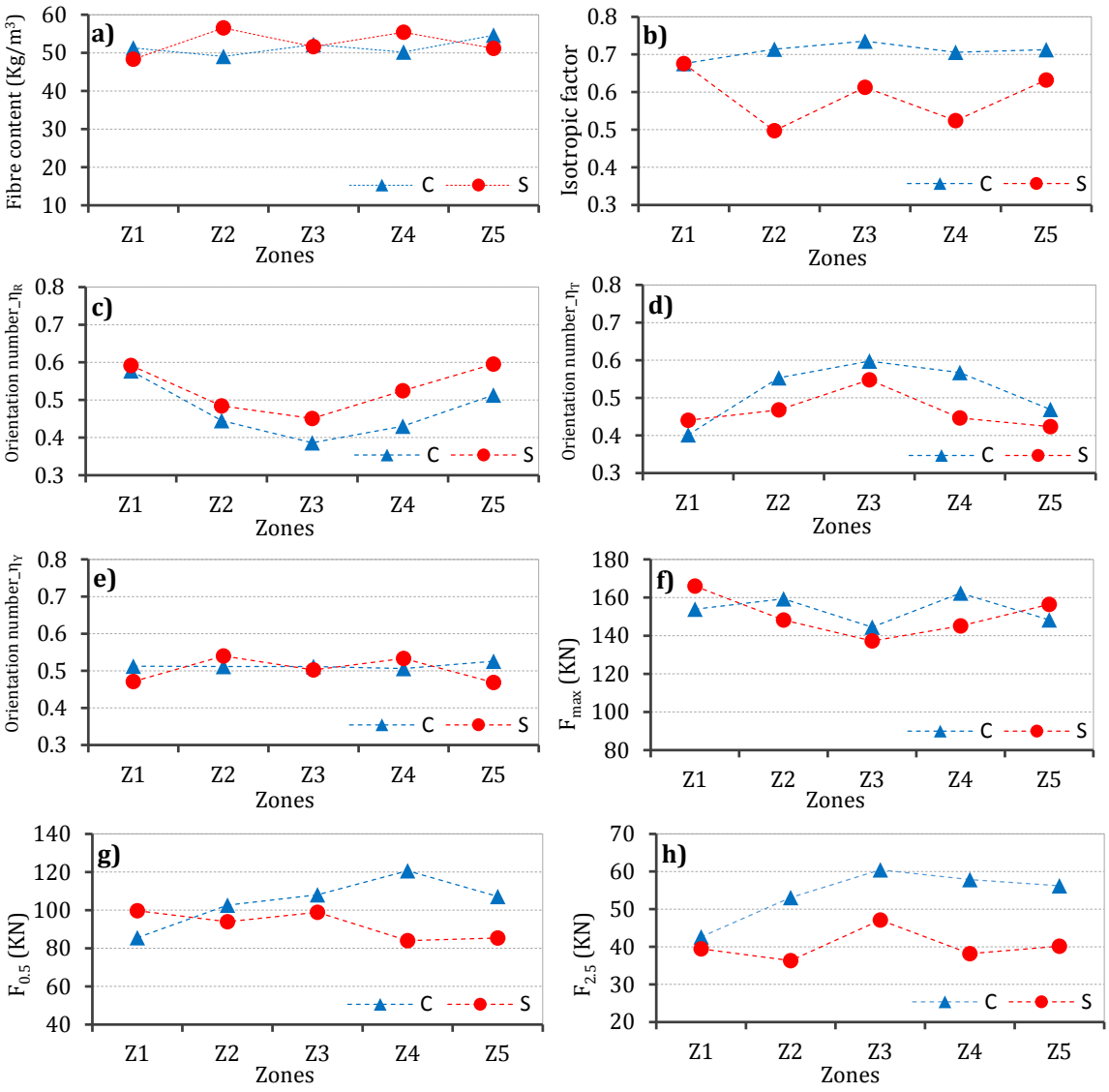


*Figure 5.9 Local comparison depending on the position along the T-axis*

The maximum load ($F_{max}$) and the residual loads for crack openings of 0.5 mm ($F_{0.5}$) and 2.5 mm ($F_{2.5}$) are presented in *Figure 5.9f, 5.9g* and *5.9h,* respectively. Both the segment with conventional concrete and the segment with self-compacting concrete show a decrease of $F_{max}$ at the central part, even though the reduction is more evident in the latter. The value of $F_{max}$ is associated with the characteristics of the concrete matrix, not being

affected by the contribution of the fibres. Consequently, the variations observed should be related with differences in concrete, probably influenced by the casting procedure.

For instance, the extremities of the segment are subjected to a higher dead load applied by the self-weight of the material placed close to the central part. Moreover, the vibration time of the extremities located at the extremities is usually higher than at the centre of the segment. This could lead to a better compaction and to a lower content of occluded air, contributing to the increase in the strength of the material.

The $F_{0.5}$ and the $F_{2.5}$ show a behaviour opposite to that of $F_{max}$. In fact, the residual load presents lower values close to the extremities of the segment and higher values at the central part. In this case, the orientation of the fibre clearly plays a more important role than the variations in the plain concrete properties. The justification is obtained by analysing the in-plane orientation numbers in the axes Y and T, depicted in *Figure 5.9d* and *Figure 5.9e,* respectively. Although the orientation number in Y remains constant an important reduction occurs in T close to the extremities. This reduces the total in-plane fibre contribution, leading to a consequent reduction of the residual loads.

### ***Influence of zones along Y-axis***

The influence of the position along the Y-axis on the fibre content, orientation numbers, isotropy factor and mechanical response are presented in *Figure 5.10*. Notice that zones Z1 and Z3 are influenced by the wall effect, whereas Z1 extends over the central part of the segment. The different boundary conditions have no influence on the fibre content (see *Figure 5.10a*), which is practically the same in all zones.

*Figure 5.10b* shows the variation of the isotropy factor depending on the Y-axis. The results suggest that the level of isotropy of the segment with conventional concrete almost constant throughout the width. On the other hand, the segments with self-compacting concrete have an isotropy factor 12.5% smaller in zones Z1 and Z3 if compared with that of Z2. This indicates that the wall effect indeed has led to preferential orientations of the fibres.

A similar conclusion is obtained after analysing the orientation numbers (*Figure 5.10c, 5.10d* and *5.10e*). The only exception is found for the curve of the orientation number in the T-axis for the segment with conventional concrete that presents slightly higher values in zones Z1 and Z3 than in Z2. This might be the result of the influence of wall-effect of the formwork. Interestingly, however, the variation is not observed in the case of self-compacting concrete is not evidenced by the results.

The value of $F_{max}$ is shown in *Figure 5.10f* depending on the position along the Y-axis. Similar results are obtained regardless of the zone characterized. This was expected since the influence of the casting procedure in the average properties of the plain concrete should not be as evident along the Y-axis in the study along the T-axis (Figure 5.9). Indeed, the influence of the self-weight of the concrete is not present in this case and the time of vibration may be considered approximately the same.

The $F_{0.5}$ and the $F_{2.5}$ are presented in *Figure 5.10g and Figure 5.10h.* Their analysis show again that the residual loads show a trend that seems to be related with the in-plane orientation numbers, especially in the T-axis depicted in *Figure 5.9.* The only exception is observed for $F_{0.5}$ measured at zone $Z_2$ of segment with conventional concrete.

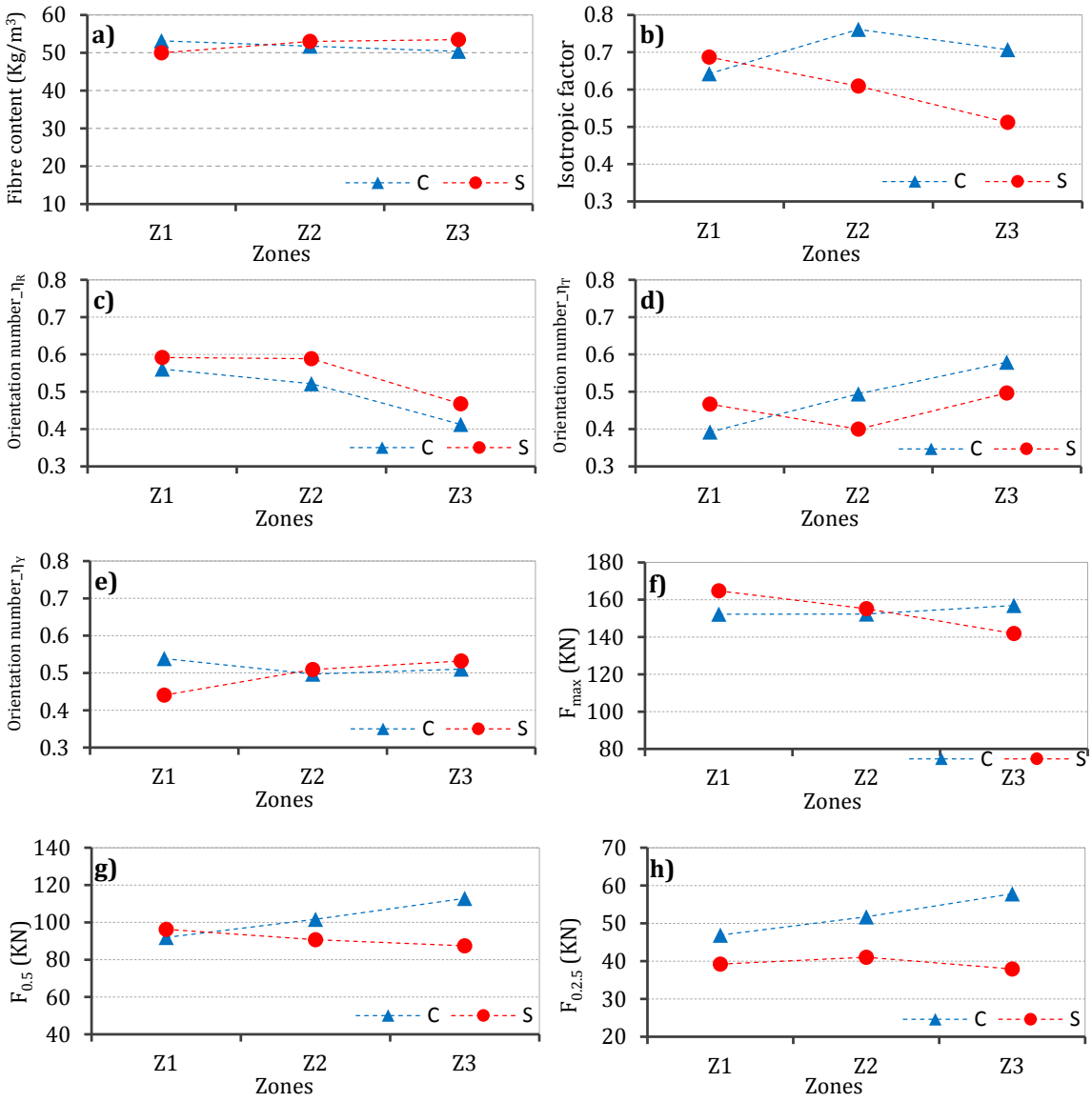


*Figure 5.10 Local comparison depending on the position along the Y-axis*

## 5.5 CONCEPTUAL MODEL FOR THE ANISOTROPY

Based on the results obtained in the experimental programme, a conceptual model is proposed to illustrate the expected anisotropy depending on the position inside the segments. As shown in *Figure 5.11*, the proposal is made in terms of the fibre orientation considering the average values obtained from the previous analysis. Between parentheses, the values for ηR, ηY and ηT are presented in this order for the segment with conventional (C) and self-compacting concrete (S).

*Figure 5.11* present a similar fibre orientation in the circumferential direction along the T-axis, $\eta_R$ presents the smallest values close to the top of the segment and the biggest values

close to the extremities. The opposite happens in the case of $\eta_T$, whereas remains constant $\eta_Y$ (0.51). This approximate conceptual model could be verified by other numbers showed at the bottom of the Zone-axis, and the result reveals that for both types of precast segments, the anisotropy in terms of the fibre orientation in T-axis tends to show the same fibre orientation pattern.

Regarding the fibre orientation along the width of the segment (Y-axis), constant values are assumed for $\eta_R$, $\eta_Y$ and $\eta_T$. Notice that certain differences depending on the flowability of concrete are expected, such differences are especially evident in $\eta_R$, and $\eta_T$.

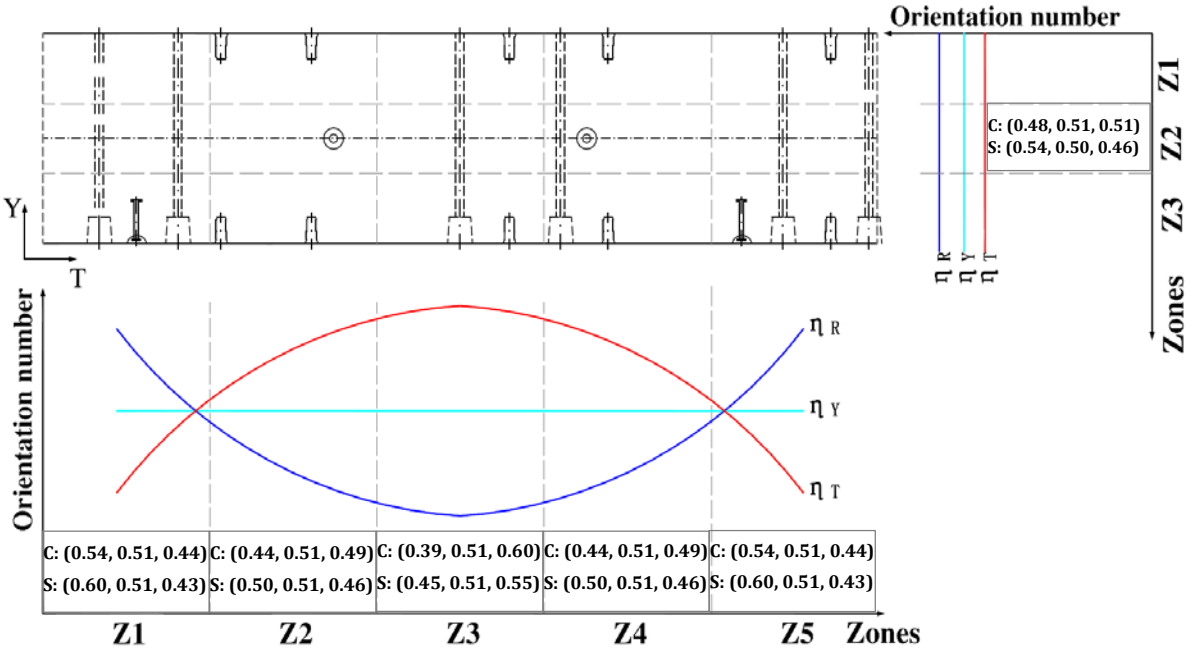


*Figure 5.11 Conceptual model for anisotropy in terms of fibre orientation a) CSFRPS and b) SCSFRPS*

## 5.6 CONCLUSIONS

In this chapter, an extensive experimental programme was conducted in order to understand the fibre orientation within two types of precast concrete segments. The following conclusions could be derived from the study.

- The results confirm the good quality of the conventional concrete and the self-compacting concrete. All specimens tested have approximately the same fibre content regardless of the position of extraction, thus indicating that segregation has negligible incidence in the materials used.

- The comparisons of the results from the different types of specimens shows that cast cubic specimens have a fibre distribution that is more representative of the cores extracted from the real-scale segment. On the contrary, the specimens extracted from the beam used in the small scale tests, show a marked preferential orientation along the axis of the beam.

- The orientation numbers assessed at the centre of the segment with conventional was similar to those assessed at the centre of the segment with self-compacting concrete. This might explain the similarities found in the mechanical response of both segments in the full-scale test.

- In general, the segment with conventional concrete and low flowability shows a higher level of isotropy than segments with self-compacting concrete. The higher flowability required in the latter increases the freedom of movement of the fibres in the concrete mass. Consequently, the fibre orientation becomes more sensible to the casting procedure. The main parameter that affected the orientation number was the flow of the concrete in the formwork.

- Regarding to the post-cracking mechanical behaviour of concrete, samples drilled from the segment with conventional concrete showed better performance than those of self-compacting concrete. This may be attributed to the higher anisotropy of the latter, and the mechanisms observed during the Barcelona Test, which provides results on the safe side.

- The biggest variations in the properties of the FRC are observed when specimens from different positions along the T-axis. The influence of the position along the thickness or along the Y-axis is considerably smaller and could even be neglected if no segregation occurs.

- A conceptual model was proposed to illustrate the anisotropy of the segments in terms of fibre orientation and the mechanical response. Even though the validity of this proposal is limited to the materials, dimensions and procedures applied in this study, it provides an innovative view considering concrete with different flowability. This model might serve as a reference for designers of tunnels segments.

# 6. CONCLUSIONS AND FUTURE PERSPECTIVES

## 6.1 GENERAL CONCLUSIONS

The application of SFRC in tunnelling has increased worldwide due to the numerous advantages of this composite material. However, several aspects related to the structural design as well as the fibre distribution required further investigation. For the above reasons, this doctoral thesis was proposed focusing on 4 specific topics: (1) the design of SFRPCS considering the ductility requirements of the Model Code 2010; (2) concrete blocks subjected to concentrated loads with an application to TBM constructed tunnels; (3) the design procedure and experimental research on SFRPCS supporting rings for vertical shafts and (4) the anisotropy property of the SFRPCS. The following points present the general conclusions that corresponded to the general objectives proposed in each of the 4 topics mentioned.

- The critical analysis of the ductility requirements from the MC 2010 showed that they could lead to over conservative design of certain types of tunnels segments. The alternative approach proposed here mitigates this issue, leading to a design more compatible with the conditions found in tunnels subjected to compression during the service life. The examples studied confirm that this alternative approach maintain acceptable ductility levels, leading to a reduction in the amount of fibre required. This also makes the reinforcement through the inclusion of fibre a competitive option in comparison with the use of traditional bar reinforcement.

- The results of experimental program validate the analytical formulation proposed to evaluate the SLS and ULS of structural elements subjected to concentrated loads. This formulation represents a contribution towards a more precise analysis of the tunnel segments with and without fibre subjected to the concentrated loads of the thrust jacks of the TBM.

- The re-design approach proposed in Chapter 4 allows an accurate assessment of the fibre content in segments with either conventional or self-compacting concrete. The validity of this approach was demonstrated by the results of the full-scale test conducted with the segments. The considerations proposed lead to a ductile failure of the segments.

- The casting procedure induces significant fibre anisotropy inside the segments. Based on the extensive experimental program conducted in Chapter 5, a fibre distribution profile was proposed in case of segments with conventional and self-compacting concrete. Even though the validity of this proposal is limited to the materials, dimensions and procedures applied in this study, it provides an innovative view considering mixes with different flowability.

## 6.2 SPECIFIC CONCLUSIONS

The specific conclusions correspond to the specific objectives defined in Chapter 1. The most relevant specific conclusions are presented below for each one of the 4 topics addressed in the thesis.

*Critical analysis of the design of FRC precast segments based on the MC 2010*

- The results from numerical simulations of the stocking process of the segments are consistent with the results obtained in the full-scale experimental program. The good agreement obtained indicates that the constitutive equation derived from the small-scale bending test on prismatic beams is able to represent the behaviour of the FRC in the real segment. This suggests that, in most situations, it might be enough to resort solely to numerical analysis based on small-scale tests instead of performing a complex experimental program with full-scale segments.

- In tunnels linings subjected mainly to compression in service and designed not to crack in the transient stages, the direct application of the ductility requirements from the MC 2010 may lead to a higher $f_{R3}$ than the required value for the ULS. Such criterion may seem excessive taking into account that it responds to a transient stage and that the likelihood of cracking due to the loads applied is small. If cracking occurs, the most probable scenario is that it will be very limited in time. In this context, the ductility provisions from the MC 2010 hardly ever will be activated considering the typical load observed in the transient stages.

- The alternative approach proposed in this Chapter could be applied to estimate the required $f_{R3}$ in tunnels that comply with 3 conditions: 1) the critical load occurs during the transient stages under controlled conditions; 2) the segments are designed not to crack and 3) the lining is subjected to compression during the service life. In this approach, the ductility is calculated considering the design values of both the mechanical parameters of the FRC and the loads by using the partial safety factors proposed in the MC 2010. The ductility obtained this way will be more compatible with the load observed in the transient stages.

- In the case study of Metro Line 9 of Barcelona, the $f_{R3m,min}$ estimated in accordance with the MC 2010 is 4.8 N/mm$^2$. This mechanical requirement was related to a bending moment $M_{cr}$ 3.20 times higher than the bending moment expected during the transient stages. Consequently, the ductility provided by the fibres will only be fully activated at load levels far above the observed in reality. On the contrary, in the alternative approach proposed in this study, a minimum average $f_{R3}$ equal to 3.2 N/mm$^2$ was obtained.

- Based on the results of the experimental program, the $C_f$ estimated according with the MC 2010 and with the alternative approach are 65 kg/m$^3$ and 45 kg/m$^3$, respectively. Even though ductility would be achieved in both of them for the load level expected in practice, the decrease in fibre consumption provided by the alternative approach could make the use of fibres viable without compromising the quality of the lining during the service life.

*Concrete blocks subjected to concentrated load*

- The STM is a simple and reliable method to the analysis of concentrated loads on concrete blocks. The depth of the confined area of the blocks influences the form of the formulations proposed to predict the mechanical behaviour of the concrete blocks.

- In blocks with length greater than the height, only a portion of the blocks was responsible for transmitting the applied loads. The area that effectively contributes to the transmission of stress was defined by an angle equal to 23°, according to experimental results.

- The comparison of theoretical and experimental values of $F_{fis}$ and $F_{rup}$ indicates that the formulations proposed can predict the mechanical behaviour of the blocks from the experimental study.

- The application of this formulation in the case study of Metro Line 9 in Barcelona indicates a safety factor of 1.51 and 5.06 in the SLS and the ULS, respectively. These results suggested that no specific reinforcement is required to resist the tensile forces that arise due to the concentrated loads applied by the thrust of jack pads.

*Re-design of FRC precast segments*

- By imposing the ductility conditions and through a sectional analysis considering the hypotheses in MC 2010 to simulate FRC post-cracking behaviour, the $f_{R3}/f_L$ ratio can be linearly compared with the $\rho_s/\rho_{s,min}$ ratio. This is represented in *Equation 4.8*, which also takes into account the partial safety factors $\gamma_c$ and $\gamma_{FRC}$. This equation helps to establish the minimum FRC requirements for hybrid sections (fibres+bars) subjected to reduced stresses (lower than the cracking moment $M_{cr}$). This expression has been proposed in the document generated by fib committee 1.4.1.

- Based on the experimental characterisation and the application of the pre-design approach, a content of fibres equal to 50 kg/m$^3$ is required for the total replacement of the conventional reinforcement proposed initially for the Montcada shaft (Barcelona).

- The mechanical behaviours measured in the full-scale bending tests of the CSFRPS and of the SCSFRPS were ductile. Furthermore, similar crack openings were measured in both of them. . A small influence of the fresh state rheology on the load resisted at ULS was observed. This may be justified by the reduced difference (only 5%) on the number of fibres in the cracking plane of each segment.

*Anisotropy property of the FRC precast segments*

- The results from the experimental program confirmed the good quality of the conventional concrete and the self-compacting concrete. Approximately the same fibre content was observed in all specimens tested regardless of the position of extraction. This indicates that the effect of segregation can be ignored in the materials used in the experimental program.

- The cast cubic specimens have a fibre distribution that is more representative of the cores extracted from the real-scale segment. On the contrary, the specimens extracted from the beam used in the small-scale tests show a preferential orientation along the axis of the beam.

- Generally, the segment with conventional concrete and low flowability showed a higher level of isotropy than segments with self-compacting concrete. The higher flowability required in the latter increased the freedom of movement of the fibres in the concrete mass. Consequently, the fibre orientation became more sensible to the casting procedure. The main parameter that affected the orientation number was the flow of the concrete in the formwork.

- Despite that, it was found that the orientation numbers at the centre of the segment with conventional was similar to those found at the centre of the segment with self-compacting concrete. This justifies the similarities found in the mechanical response of both segments in the full-scale test.

- Samples drilled from the segment with conventional concrete showed better post-cracking mechanical response than those of self-compacting concrete. This may be attributed to the higher anisotropy of the latter, and the mechanisms observed during the Barcelona Test that provides results on the safe side.

- The biggest variations in the properties of the FRC occur along the T-axis of the segment. The variations along the thickness or along the Y-axis were considerably smaller and may even be neglected if no segregation occurs.

## 6.3 FUTURE PERSPECTIVES

In spite of the achievements reported previously, several issues regarding the topics presented in this doctoral thesis still remain. For that reason, suggestions for future research are proposed in this section.

More studies should focus on the minimum ductility required and on the optimization of design of tunnel or shaft segments. In this sense, studies related to the constitutive model of SFRC are recommended. Additionally, the combined effect of rebar and steel fibres in full-scale segments could be explored in future studies. It would also be interesting to perform an in-depth analysis comparing the sustainability of the different reinforcement alternatives available nowadays depending on the geology of the soil or the geometry of the tunnel.

Even though the STM proposed to calculate loads $F_{cr}$ and $F_{max}$ shows a reliable accuracy, more studies about the local mechanical response of segments could be performed. These studies should include more complex models capable of capturing the crack formation process. Furthermore, the behaviour of concrete blocks subjected to line loads that simulate the external loads on the segments should also be assessed.

Although a conceptual model was proposed for the fibre distribution, it is necessary to go deeper on this topic. Advanced models could be used to simulate the casting procedure and the fibre distribution inside the segment. Moreover, it would be interesting to evaluate the influence of different casting procedures on the mechanical behaviour of the segments.

# REFERENCES

**ABAQUS STANDARD. (1995).** User's Manual, Hibbitt, Karlsson & Sorensen, Pawtucket.

**Abbas, S., Soliman, A., Nehdi, M. (2014).** Structural behaviour of ultra-high performance fibre reinforced concrete tunnel lining segments. FRC 2014 Joint ACI-fib International Workshop. Fibre Reinforced Concrete Applications. 24-25 July 2014, Montreal, Canada. pp.: 532 - 543.

**ACI 544. (2014).** Fibre-Reinforced Concrete: Design and Construction of Steel Fibre-Reinforced Precast Concrete Tunnel Segments.

**Aire, C., Carmona, S., Aguado, A., Molins C. (2015).** Double-Punch Test of Fibre-Reinforced Concrete: Effect of Specimen Origin and Size. ACI Materials Journal; 112 (2); pp.: 199-208.

**ANSYS REV. 5.5. (2013).** User Manual, Swanson Analysis Systems, Houston.

**Arnau, O., Molins, C. (2011).** Experimental and analytical study of the structural response of segmental tunnel linings based on an in situ loading test. Part 2: Numerical simulation. Tunn. Undergr. Space Technol; 26 (6); pp.: 778-788.

**Bach, Carl. (1903).** Tests with granite articulations and Sandstone (in German). Published by the Association of German Engineers.

**Bakhshi, M, Nasri, V. (2014).** Developments in design for fibre reinforced concrete tunnel segments. FRC 2014 Joint ACI-fib International Workshop. Fibre Reinforced Concrete Applications. 24-25 July 2014, Montreal, Canada. pp.: 441 - 452.

**Bakhshi, M., Nasri, V. (2013).** Structural design of segmental tunnel linings. In Proceedings of 3rd International Conference on Computational Methods in Tunnelling and Subsurface Engineering. EURO TUN 2013. 17–19 April 2013, Ruhr University Bochum, Germany.

**Bakhshi, M., Nasri, V. (2014).** Guidelines and Methods on Segmental Tunnel Lining Analysis and Design – Review and Best Practice Recommendation. In Proceedings of the World Tunnel Congress 2014. May 9-15, 2014. Iguassu Falls, Brazil.

**Bakhshi, M., Nasri, V. (2014).** Review of international practice on critical aspects of segmental tunnel lining Design. In Proceedings of the 2014 North American Tunnelling (NAT) Conference. 22-25 June 2014, Los Angeles, USA. pp.: 274-282.

**Barros, J.A.O., Cunha, V.M.C.F., Ribeiro, A.F., Antunes, J.A.B. (2005).** Post-cracking behaviour of steel fibre reinforced concrete. Mater. Struct; 38(1); pp.: 47-56.

**Beno, J., Hilar, M. (2013).** Steel fibre reinforced concrete for tunnel lining–verification by extensive laboratory testing and numerical modelling. Acta Polytechnia 53(4), pp.329-337.
**Blanco, A. (2013).** Characterization and modelling of SFRC elements. PhD Thesis, UPC, Barcelona, Spain.

**Blanco, A., Pujadas, P., Cavalaro, S.H.P., de la Fuente, A. y Aguado, A. (2014).** Constitutive model for fibre reinforced concrete based on the Barcelona test, Cement and Concrete Composites; 54; pp.: 327-340.

**Blanco, A., Pujadas, P., de la Fuente, A., Aguado, A. (2010).** Comparative analysis of constitutive models of fibre reinforced concrete. Hormigon. y Acer; 61(256); pp.: 83-101.

**Blanco, A., Pujadas, P., de la Fuente, A., Cavalaro S., Aguado, A. (2013).** Application of constitutive models in European codes to RC–FRC. Constr. Build. Mater; 40; pp.: 246–259.

**Blanco, A., Pujadas, P., de la Fuente, A., Cavalaro, S., Aguado, A. (2015).** Assessment of the fibre orientation factor in SFRC slabs. Composite Part B; 68(2); pp.: 343-354.

**Blanco, A., Pujadas, P., de la Fuente, A., Cavalaro, S., Aguado, A. (2013).** Application of constitutive models in European codes to RC–FRC. Constr. Build. Mater; 40; pp.: 246–259.

**Blazejowsky, M. (2012).** Flexural behaviour of steel fibre reinforced concrete tunnel linings. Electronic Thesis and Dissertation Repository. University of Western Ontario, Canada.

**Blom, C.B.M. (2002).** Design philosophy of concrete linings in soft soils, ISBN 90-407-2366-4, Delft University of Technology, Netherlands.

**Breitenbücher, R., Meschke, G., Song, F., Hofman, M., Zhan, Y. (2014).** Experimental and numerical study on the load-bearing behaviour of steel fibre reinforced concrete for precast tunnel lining segments under concentrated loads. FRC 2014 Joint ACI-fib International Workshop. Fibre Reinforced Concrete Applications. 24-25 July 2014, Montreal, Canada. pp.: 417 - 429.

**Burgers, R., Walraven, J.C., Plizzari, G.A., Tiberti, G. (2007).** Structural Behaviour of SFRC Tunnel Segments during TBM Operations. Underground Space. the 4th Dimension of Metropolises: Proceedings of the World Tunnel Congress 2007 and 33rd ITA/AITES Annual General Assembly, London, England. pp.: 1461–1467.

**Burguers, R. (2006).** Non-linear FEM modelling of steel fibre reinforced concrete for the analysis of tunnel segments in the thrust jack phase. Master Thesis, Delft University of Technology, Netherlands.

**Burguers, R., Walraven, J., Plizzari, G.A., Tiberti, G. (2007).** Structural behaviour of SFRC tunnel segments during TBM operations. In: World Tunnel Congress ITA-AITES, Prague, Czech Republic. pp.: 1461–1467.

**Camós, C., Casas, J.R., Molins, C. (2014).** An attempt to the determination of the partial safety factor for SFRC members subjected to bending forces. In 8th RILEM International Symposium on Fibre Reinforced Concrete: challenges and opportunities, 19-21 September 2014, Guimaraes, Portugal. pp.: 1059-1069.

**Caratelli, A., Meda, A., Rinaldi, Z. (2012).** Design according to MC2010 of fibre-reinforced concrete tunnel in Monte Lirio, Panama. Struct. Conc; 13(3); pp.: 166-173.

**Caratelli, A., Meda, A., Rinaldi, Z., Romualdi, P. (2011).** Structural behaviour of precast tunnel segments in fibre reinforced concrete. Tunn. Undergr. Space Technol; 26(2); pp. 284–291.

**Carmona, S., Aguado, A., Molins, C. (2012).** Generalization of the Barcelona test for the toughness control of FRC. Mater Struct; 45(7); pp.: 1053–69.

**Cavalaro, S H P., Blom, C B M, Walraven, J C, Aguado, A. (2011).** Structural analysis of contact deficiencies in segmented lining. Packer behaviour under simple and coupled stresses. Tunn. Undergr. Space Technol; 26 (6); pp.: 734-749.

**Cavalaro, S.H.P, López, R., Torrents, J.M., Aguado, A. (2015).** Improved assessment of fibre content and orientation with inductive method in SFRC. Materials and Structures; 48(60; pp.: 1859-1873.

**Cavalaro, S.H.P., Aguado, A. (2012).** Packer behaviour under simple and coupled stresses. Tunn. Undergr. Space Technol; 28; pp.: 159-173.

**Cavalaro, S.H.P., Blom, C.B.M., Aguado, A., Walraven, J. (2011).** New Design Method for the Production Tolerances of Concrete Tunnel Segments. J. Perform. Constr. Facil; 26(6); pp.: 824–34.

**Cavalaro, S.H.P., Blom, C.B.M., Walraven, J., Aguado, A. (2012).** Formation and accumulation of contact deficiencies in a tunnel segmented lining. Appl. Math. Mod; 36(9); pp.: 4422-4438.

**Cavalaro, SHP, Aguado, A. (2014).** Intrinsic scatter of FRC: an alternative philosophy to estimate characteristic values. Mater Struct. DOI 10.1617/s11527-014-0420-6.

**Cavalaro, SHP, Lopez, R, Torrents, JM, Aguado, A. (2014).** Assessment of fibre content and 3D profile in cylindrical SFRC specimens. Mater Struct. DOI 10.1617/s11527-014-0521-2.

**Cervenka V., Jendele, L., Cervenka, J. (2013).** ATENA Program documentation. Prague, Czeck Republic.

**Chen, WF. (1970).** Double punch test for tensile strength of concrete. ACI Mater J; 67(2); pp.: 993–5.

**Chiaia, B., Fantilli, A.F., Vallini, P. (2009).** Combining fibre-reinforced concrete with traditional reinforcement in tunnel linings. Eng. Struct; 31(7); pp.: 1600-1606.

**Chiaia, B., Fantilli, A.P., Vallini, P. (2009).** Evaluation of minimum reinforcement ratio in FRC members and application to tunnel linings. Mater. Struct; 42(3); pp.: 339-51.

**CNR DT 204/2006. (2006).** Guidelines for the Design, Construction and Production Control of Fibre Reinforced Concrete Structures, Italian National Research Council - CNR.

**CPH-2008. (2008).** EHE-08: Spanish Structural Concrete Standard. Annex 14: Recommendations for the use of fibre reinforced concrete.

**DBV–Recommendation (German Concrete Association). (1992).** Design principles of steel fibre reinforced concrete for tunnelling works. pp.: 19-29.

**de la Fuente A., Blanco A., Pujadas P., Aguado A., (2012).** Advances on the use of fibres in precast concrete segmental linings. Engineering and Concrete Future: Technology, Modelling & Construction. In International Federation for Structural Concrete (fib). Fib Symposium, 22- 24 April 2012, Tel – Aviv, Israel. Text in Proceedings, pp.: 691-694.

**de la Fuente, A., Aguadoa, A., Molins, C., Armengoub, J. (2012).** Numerical model for the analysis up to failure of precast concrete sections. Computers & Structures; 106-107; pp.: 105-114.

**de la Fuente, A., Blanco, A., Pujadas, P., Aguado, A. (2012).** Experiences in Barcelona with the use of fibres in segmental linings. Packer behaviour under simple and coupled stresses. Tunn. Undergr. Space Technol; 27(1); pp.: 60-71.

**de la Fuente, A., Escariz, R.C., de Figueiredo, A.D., Aguado, A. (2013).** Design of macro-synthetic fibre reinforced concrete. Constr. Build. Mater; 43; pp.: 523-532.

**de la Fuente, A., Escariz, R.C., de Figueiredo, A.D., Molins, C., and Aguado, A. (2012).** A new design method for steel fibre reinforced concrete pipes. Constr. Build. Mater; 30; pp.: 547-555.

**de Rivaz, B. (2008).** Steel fibre reinforced concrete (SFRC): The use of SFRC in precast segment for tunnel lining. In: World Tunnel Congress ITA-AITES September 22–24, 2008, Agra, India. pp.: 2007–2017.

**de Waal, R.G.A. (1999).** Steel fibre reinforced tunnel segments, ISBN 90-407-1965-9, Delft University of Technology, Netherlands.

**di Prisco, M., Plizzari, G., Vandewalle, L. (2009).** Fibre reinforced concrete: New design perspectives. Mater Struct; 42(9); pp.: 1169-69.

**Edgington, J., Hannant, D.J. (1972).** Steel fibre reinforced concrete. The effect on fibre orientation of compaction by vibration, Mater. Struct; 5 (25); pp.: 41-44.

**EN 12350-2. (2009).** Testing fresh concrete: Slump-test.

**EN 12350-6. (2009).** Testing fresh concrete: Density.

**EN 12350-7. (2009).** Testing fresh concrete: Air content. Pressure methods.

**EN 12350-8. (2010).** Testing fresh concrete. Self-compacting concrete: Slump-flow test.

**EN 12390-3. (2009).** Testing hardened concrete: Compressive strength of test specimens.

**EN 14651. (2005).** Test method for metallic fibered concrete. Measuring the flexural tensile strength (limit of proportionality (LOP), residual strength).

**ERMCO. (2012).** Guidance to fibre concrete: Properties, Specification and Practice in Europe.

**Ferrara, L., Faifer, M., Muhaxheri, M., Toscani S. (2012).** A magnetic method for non-destructive monitoring of fibre dispersion and orientation in steel fibre reinforced cementitious composites—part 1: method calibration. Materials and Structures; 45; pp.: 575–589.

**fib Bulletins 65-66. (2010).** Model code 2010 Final Draft, 2010. fédération internationale du béton (fib), Lausanne, Switzerland.

**García, M. (2012).** Experimental program on concrete blocks subjected to concentrated loads. M.Sc. Thesis, UPC, Barcelona, Spain. [In Spanish].

**Gettu, R., Aguado, A., Ramos, G., García, T. (2003).** Viability analysis of the use of fibres as the unique concrete reinforcement for the precast segments of Barcelona's metro L9. Final Report, UPC Barcelona, Spain, pp.: 49.

**Gettu, R., Barragán, B., García, T., Ramos, G., Fernández, C., Oliver, R. (2004).** Steel Fibre Reinforced Concrete for the Barcelona Metro Line 9 Tunnel Lining. In 6th RILEM Symposium on FRC, 20-22 September, Varenna, Italy. pp.: 141-156.

**Groeneweg, T.W. (2007).** Shield driven in ultra-high strength concrete: reduction of the tunnel lining thickness. Master Thesis, Delft University of Technology, Netherlands.

**Grunewald, S. (2004).** Performance based design of self-compacting fibre reinforced concrete. Delft University Press, Netherlands.

**Haring, F.P. (2002).** Stresses in assembly phase and serviceability phase in the lining of shield driven tunnels. Delft University of Technology, Netherlands.

**Hemmy, O. (2001).** Brite Euram Program on Steel Fibre Concrete, Subtask: Splitting of SFRC induced by local forces, "Investigation of tunnel segments without curvature", University of Braunschweig, Germany.

**Hilar, M., Vítek, P. (2010).** Experimental loading tests of steel fibre reinforced and traditionally reinforced precast concrete segments for tunnel linings. Tunn. Undergr. Sp. Technol; 21(4); pp.: 54-65.

**Infante, R.M. (2006).** Evaluación de las Necesidades de Refuerzo de Armadura de las Dovelas Prefabricadas del Sostenimiento de la Línea 9 del Metro de Barcelona Sometidas al Empuje de la Tuneladora. Minor Thesis, UPC, Barcelona, Spain.

**ITATECH Activity Group Support. (2015).** ITATECH design guidance for precast fibre reinforced concrete segments, July. Draft Report.

**Iyengar, K.T.S.R.; Yogananda, C.V. (1966).** A three dimensional stress distribution problem in the end zones of pre-stressed beams. Magazine of Concrete Research; 18; pp.: 75-84.

**Kooiman, A.G. (2000).** Modelling steel fibre reinforced concrete for structural design. Ph.D. thesis, Delft University of Technology, Netherlands.

**Laranjeira, F. (2010).** Design-oriented constitutive model for steel fibre reinforced concrete. Ph.D Thesis, UPC, Barcelona, Spain.

**Lee, G.-P., Bae, G.-J., Moon, D.-Y., Kang, T.-S., Chang, S.-H. (2013).** Evaluation of steel fibre reinforcement effect in segment lining by full scale bending test. J of Korean Tunn Undergr Sp Assoc; 15(3); pp.: 215-223.

**Leonhardt, F. (1965).** Über die Kunst des Bewehrens von Stahlbetontragwerken. Beton- und Stahlbetonbau 60, H.8, pp.: 181; H.9, pp.: 212.

**Levi, F. (1985).** On minimum reinforcement in concrete structures. ASCE J. Struct. Eng. ; 111(12); pp.: 791–796.

**Liao L., de la Fuente, A., Cavalaro S., Aguado, A., Carbonari, G. (2015).** Experimental and analytical study on concrete S.H.P. blocks subjected to concentrated loads. Tunn. Undergr. Sp. Technol; 49; pp.: 295-306.

**Liao, L., Cavalaro, S., de la Fuente, A., Aguado, A. (2014).** Complementary Use of Inductive Test and Bending Test for the Characterization of SFRC. Applied Mechanics and Materials; 580-583; pp.: 2213-2219.

**Liao, L., de la Fuente, A., Cavalaro S., Aguado, A. (2015).** Design of FRC tunnel segments considering the ductility requirements of the Model Code 2010. Tunn. Undergr. Sp. Technol.; 47; pp.: 200-210.

**MARC USER'S GUIDE. (2008).** U.S. A.

**Mashimoto, H., Isago, N., Kitani, T. (2004).** Numerical approach design of tunnel concrete lining considering effect of fibre reinforcements. Tunnelling and Underground Space Technology. Underground Space for Sustainable Urban Development. Proceedings of the 30th ITA-AITES WTC 2004, 22 – 27 May, Singapore.

**Molins, C., Aguado, A., Mari, A. R. (2006).** Quality control test for SFRC to be used in precast segments, Tunn. Undergr. Sp. Technol; 21(3-4); pp.: 423-424.

**Molins, C., Aguado, A., Saludes, S. (2009).** Double punch test to control the energy dissipation in tension of FRC (Barcelona test). Mater Struct; 42(4); pp.: 415–25.

**Molins, C., Arnau, O. (2011).** Experimental and analytical study of the structural response of segmental tunnel linings based on an in situ loading test: Part 1: test configuration and execution Tunn. Undergr. Sp. Technol; 26 (6); pp.: 764-777.

**Mörsch, Emil. (1902).** Reinforced Concrete, Theory and Application. Stuggart, Germany.
**Mösrch, E. (1952).** Teoría y Práctica del Hormigón Armado. Ed. G. Gili S.A., Buenos Aires. pp.: 448.

**Plizzari, G.A., Tiberti, G. (2006).** Steel Fibbers as reinforcement for precast tunnel segments. Tunn. Undergr. Sp. Technol; 21 (3-4); pp.: 438-439.

**Plizzari, G.A., Tiberti, G. (2007).** Structural behaviour of SFRC tunnel segments. In: Proceedings of the 6th International Conference on Fracture Mechanics of Concrete and Concrete Structures. Catania, Italy, June 17-22, 2007, pp.: 1577-1584.

**Pohn J., Tan KH, Peterson, GL., Wen, D. (2009).** Structural testing of steel fibre reinforced concrete (SFRC) tunnel lining segments in Singapore, WTC 2009, Budapest, Hungary.

**Pujadas, P. (2013).** Caracterización y diseño del hormigón reforzado con fibras plásticas. Ph.D Thesis, UPC, Barcelona, Spain.

**Pujadas, P., Blanco, A., Cavalaro, S., de la Fuente, A., Aguado, A. (2013).** New analytical model to generalize the Barcelona test using axial displacement. J Civ Eng Manage; 19(2); pp.: 259–71.
**Pujadas, P., Blanco, A., Cavalaro, S.H.P., de la Fuente A., Aguado A. (2014).** Multidirectional double punch test to assess the post–cracking behaviour and fibre orientation of FRC. Constr. Build. Mater; 58; pp.: 214-224.

**Pujadas, P., Blanco, A., Cavalaro, S.H.P., de la Fuente, A., Aguado A. (2014).** Fibre distribution in macro–plastic fibre reinforced concrete slab – panels. Constr. Build. Mater; 64; pp.: 496-503.

**Ramirez, J. A., Breen, J. E. (1991).** Evaluation of a Modified Truss-Model Approach for Beams in Shear. ACI Structural Journal; 88 (5); pp.: 562–571.

**Reineck, K.-H. (1982).** Models for the Design of Reinforced and Pre-stressed Concrete Members. CEB Bulletin 146, Paris, pp.: 43-96.

**RILEM TC 162-TDF. (2003).** Test and design methods for steel fibre reinforced concrete—σ–ε design method: final recommendation. Mater Struct; 36(262); pp.: 560–567.

**Ritter, W. (1899).** Construction Techniques of concrete. Schweizerische Bauseitung, Zurich.

**Sahoo, D.K., Singh, B., Bhargava, P. (2011).** Minimum reinforcement for preventing failure in bottle-shaped struts. ACI Structural Journal; 108(2); pp.: 206-216.

**Schnüntger, g., Erdem, E. (2001).** Brite Euram Program on Steel Fibre Concrete, Subtask: Splitting of SFRC induced by local forces, Ruhr-University, Bochum, Germany.

**Schnütgen, B. (2003).** Design of precast steel fibre reinforced tunnel elements, Proceedings of the RILEM TC 162-TDF Workshop, Test and design methods for steel fibre reinforced concrete – background and experiences, Bochum, Germany. pp.: 145-152.

**Sorelli, L., Toutlemonde, F. (2005).** On the design of steel fibre reinforced concrete tunnel lining segments. In 11th International Conference on Fracture, Turin, Italy, 20-25 March. pp.: 6.

**Soroushian, P., Lee, C.-D. (1990).** Distribution and orientation of fibres in steel fibre reinforced concrete, ACI Mater. J.; 87 (5); pp.: 433-439.

**Stroeven, P. (1977).** The analysis of fibre distributions in fibre reinforced materials, J. Microscopy 111, pp.: 283-295.

**Stroeven, P. (1979).** Morphometric of fibre reinforced cementitious materials, Part II: Inhomogeneity, segregation and anisometry of partially oriented fibre structures, Mater. Struct; 12; pp.: 9-20.

**Sugimoto, M. (2006).** Causes of shield segment damages during construction. International Symposium on Underground Excavation and Tunnelling. Bangkok, Thailand.
**Tiberti, G., Minelli, F., Plizzari, G. A., Vecchio, F.J. (2013).** Influence of concrete strength on crack development in SFRC members. Cement and Concrete Composites; 45; pp.: 176-185.

**Tiberti, G. (2009).** Concrete tunnel segments with combined traditional and fibre reinforcement: optimization of the structural behaviour and design aspects, Ph.D. Thesis. Under press.

**Tiberti, G., Plizzari, G. A. (2008).** Concrete tunnel segments with combined traditional and fibre reinforcement. Tailor Made Concr. Struct. ISBN 978–0–415–47535–8; pp.: 199–206.

**Tiberti, G., Plizzari, G. A. (2014).** Structural behaviour of precast tunnel segments under TBM thrust actions. World Tunnelling Congress: Tunnels for a Better Life, 9– 5 May, Foz do Iguaçu, Brazil.

**Torrents, J.M., Blanco, A., Pujadas, P., Aguado, A., Juan-Garcia, P., Sanchez-Moragues, MA. (2012).** Inductive method for assessing the amount and orientation of steel fibres in concrete. Mater Struct; 45(10); pp.: 1577–1592.

**Toutanji, H., Bayasi, Z. (1998).** Effect of manufacturing techniques on the flexural behaviour of steel fibre-reinforced concrete, Cem. Concr. Res; 28 (1); pp.: 115-124.

**Waal, R.G.A. de. (1999).** Steel fibre reinforced tunnel segments. ISBN 90-407-1965-9, Delft University of Technology, Netherlands.

**Walraven, J. (2009).** High performance fibre reinforced concrete: progress in knowledge and design codes. RILEM Materials Structures; 42 (9); pp.: 1247-1260.

**Y, Ding. (2011).** Investigations into the relationship between deflection and crack mouth opening displacement of SFRC beam. Constr. Build. Mater; 25 (5); pp.: 2432–2440.

**Yang, WY., Wenwu, C., Chung, TS., Morris, J. (2005).** Applied numerical methods using Matlab. John Wiley & Sons Inc., Hoboken, New Jersey, U.S.A.

# ANNEX A: PARAMETERS INVOLVED IN THE STM PROPOSED MODELS

## A.1 INTRODUCTION

Strut-and-tie modelling (STM) is a simple and effective method which can be used as a quick tool to analyse the discontinuous region (D-region) in concrete structures. In the section 3.5, Chapter 3 of this doctoral thesis, STMs were proposed to assess the crack load and the maximum load of concrete blocks with different height-to-length ratios, thus to validate simplified analytical formulations that may be applied for the verification of concrete segments in SLS and ULS.

This Annex would display the information of the parameters involved in the assessment of the crack load ($F_{cr}$) and the maximum load ($F_{max}$) according to the STM proposed when concrete blocks subjected to concentrated loads.

## A.2 PARAMETERS INVOLVED IN THE STM PROPOSED MODELS

The detail information of those parameters in terms of the dimension of support plate and concrete blocks, as well as mechanical parameters of the STMs are presented in the Table A.1 and Table A.2.

Table A.1 *Values of the parameters involved in the assessment of $F_{cr}$ according to the STM proposed*

| Specimen | k1 [] | a (mm) | a1 (mm) | a2 (mm) | a3 (mm) | q1 (N/mm2) | q2 (N/mm2) | b (mm) | hT (mm) | h (mm) | fct (N/mm2) | Fcr (kN) |
|---|---|---|---|---|---|---|---|---|---|---|---|---|
| PC-40-200-1.3 | 0.33 | 200 | 150 | - | - | - | - | 150 | 300 | 182 | 4,33 | 379 |
| PC-40-250-1.7 | | 250 | | - | - | - | - | | | 233 | | 425 |
| PC-40-400-2.7 | | 400 | | 89 | 400 | 15.92 | 8.27 | | | 370 | | 725 |
| PC-40-750-5.0 | | 750 | | 90 | 405 | 16.57 | 8.12 | | | 376 | | 750 |
| PC-50-200-1.3 | 0.33 | 200 | 150 | - | - | - | - | 150 | 300 | 182 | 4,09 | 358 |
| PC-50-250-1.7 | | 250 | | - | - | - | - | | | 233 | | 401 |
| PC-50-400-2.7 | | 400 | | 89 | 400 | 15.04 | 7.81 | | | 370 | | 685 |
| PC-50-750-5.0 | | 750 | | 90 | 405 | 15.65 | 7.67 | | | 376 | | 708 |
| SFRC-40-200-5.0 | 0.33 | 200 | 50 | - | - | - | - | 150 | 300 | 204 | 3,99 | 340 |
| SFRC-40-250-4.0 | | 250 | | - | - | - | - | | | 260 | | 441 |
| SFRC-40-400-2.7 | | 400 | 150 | 89 | 400 | 14.67 | 7.62 | | | 370 | | 668 |
| SFRC-40-750-5.0 | | 750 | | 90 | 405 | 15.27 | 7.49 | | | 376 | | 691 |
| SFRC-50-20-5.0 | 0.33 | 200 | 150 | - | - | - | - | 150 | 300 | 182 | 4,32 | 378 |
| SFRC-50-25-4.0 | | 250 | | - | - | - | - | | | 233 | | 424 |
| SFRC-50-40-2.7 | | 400 | | 89 | 400 | 15.88 | 8.25 | | | 370 | | 724 |
| SFRC-50-75-5.0 | | 750 | | 90 | 405 | 16.53 | 8.11 | | | 376 | | 748 |

*Table A.2 Values of the parameters involved in the assessment of $F_{max}$ according to the STM proposed*

| Specimen | $k_2$ [] | $a$ (mm) | $a_1$ (mm) | $a_3$ (mm) | $b$ (mm) | $h_T$ (mm) | $f_c$ (mm) | $F_{max}$ (kN) |
|---|---|---|---|---|---|---|---|---|
| PC-40-200-1.3 | 0.59 | 200 | 150 | 200 | 150 | 300 | 43.7 | 980 |
| PC-40-250-1.7 | 0.66 | 250 | | 250 | | | | 1003 |
| PC-40-400-2.7 | 0.77 | 400 | | 400 | | | | 1156 |
| PC-40-750-5.0 | 0.77 | 750 | | 405 | | | | 1162 |
| PC-50-200-1.3 | 0.59 | 200 | 150 | 200 | 150 | 300 | 53.3 | 1195 |
| PC-50-250-1.7 | 0.66 | 250 | | 250 | | | | 1223 |
| PC-50-400-2.7 | 0.77 | 400 | | 400 | | | | 1409 |
| PC-50-750-5.0 | 0.77 | 750 | | 405 | | | | 1417 |
| SFRC-40-200-5.0 | 0.84 | 200 | 50 | 200 | 150 | 300 | 39.4 | 431 |
| SFRC-40-250-4.0 | 0.87 | 250 | | 250 | | | | 500 |
| SFRC-40-400-2.7 | 0.77 | 400 | 150 | 400 | | | | 1041 |
| SFRC-40-750-5.0 | 0.77 | 750 | | 405 | | | | 1047 |
| SFRC-50-200-5.0 | 0.59 | 200 | 150 | 200 | 150 | 300 | 51.8 | 1161 |
| SFRC-50-250-4.0 | 0.66 | 250 | | 250 | | | | 1187 |
| SFRC-50-400-2.7 | 0.77 | 400 | | 400 | | | | 1368 |
| SFRC-50-750-5.0 | 0.77 | 750 | | 405 | | | | 1375 |

# ANNEX B: THREE POINT BENDING TEST RESULTS OF THE SFRC BEAMS

## B.1 INTRODUCTION

Regarding the mechanical properties of SFRC, normally it is characterised by the estimation of the post-cracking behaviour subjected to different tests. The most traditional and popular one adopted in Europe is Bending test. This test could be carried out in two different ways depending on its performance and configuration. One is by applying a punctual force on the centre of the specimen span (three-point bending test) and the other is by applying two forces on two thirds of the span (four-point bending test).

In the section 4.5, Chapter 4 of this doctoral thesis, the post-cracking behaviour of the SFRC beams were characterised by means of three point bending test. This Annex would present the detail information of the test results for different batches of concrete specimens.

## B.2 THREE POINT BENDING TEST RESULTS OF THE SFRC BEAMS

The load – CMOD relationship curves and the corresponding CMOD load are displayed in from Table B.1 to Table B.6.

a)

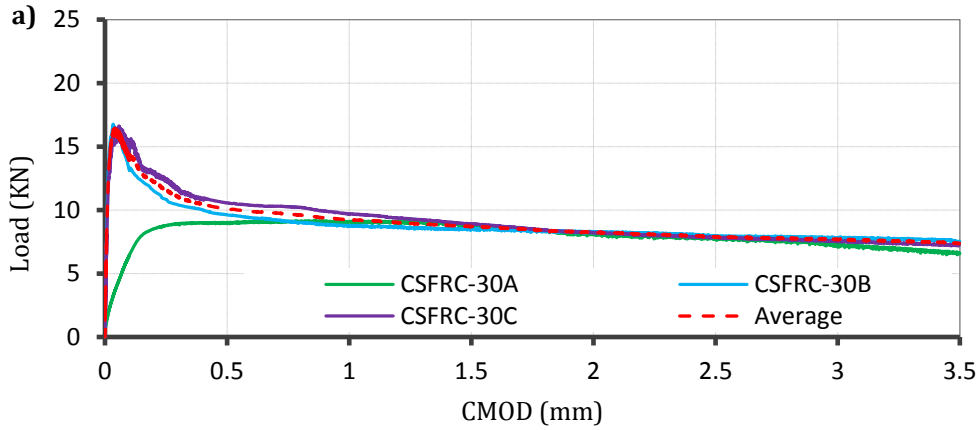


b)

| Load | CSFRC-30A | CSFRC-30B | CSFRC-30A | Average | C.V (%) |
|---|---|---|---|---|---|
| $F_{0.5}$ | 9.02 | 9.64 | 10.57 | 9.74 | 7.98 |
| $F_{1.5}$ | 8.68 | 8.51 | 8.92 | 8.71 | 2.35 |
| $F_{2.5}$ | 7.72 | 7.97 | 7.84 | 7.84 | 1.62 |
| $F_{3.5}$ | 6.61 | 7.52 | 7.24 | 7.12 | 6.51 |

*Figure B. 1 Three point bending test results of the CSFRC-30 beams a) Load – CMOD relationship; and b) the detail of the load correspond to COMD*

a)

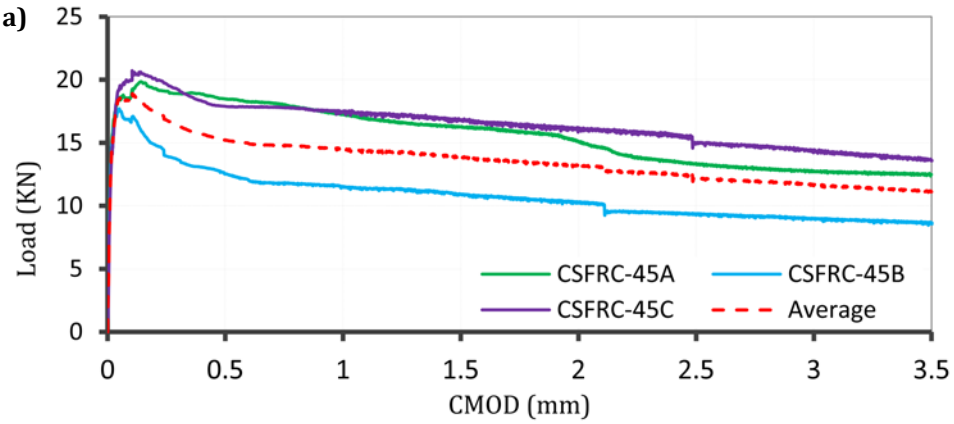


b)

| Load | CSFRC-45A | CSFRC-45B | CSFRC-45A | Average | CV (%) |
|---|---|---|---|---|---|
| $F_{0.5}$ | 18.49 | 12.52 | 17.90 | 16.30 | 20.19 |
| $F_{1.5}$ | 16.26 | 10.89 | 16.84 | 14.66 | 22.36 |
| $F_{2.5}$ | 13.38 | 9.26 | 14.96 | 12.53 | 23.50 |
| $F_{3.5}$ | 12.49 | 8.65 | 13.58 | 11.57 | 22.34 |

*Figure B. 2 Three point bending test results of the CSFRC-45 beams a) Load – CMOD relationship; and b) the detail of the load correspond to COMD*

a)

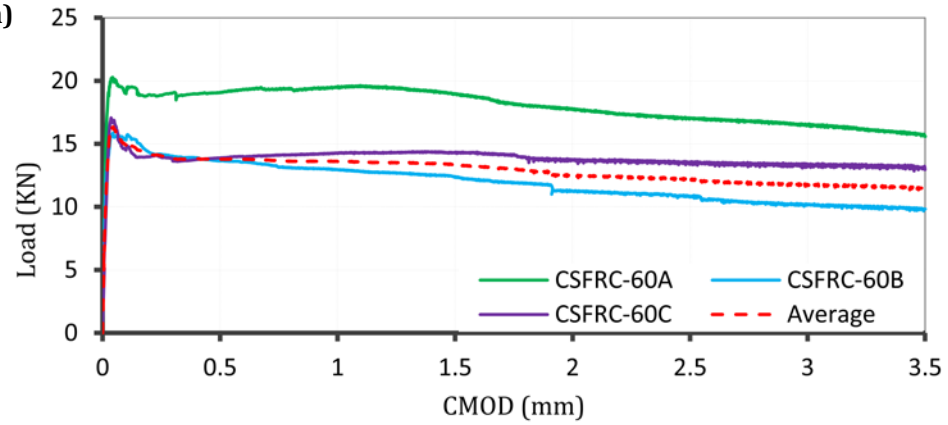


b)

| Load | CSFRC-60A | CSFRC-60B | CSFRC-60A | Average | CV (%) |
|---|---|---|---|---|---|
| $F_{0.5}$ | 19.09 | 13.66 | 13.88 | 15.55 | 19.75 |
| $F_{1.5}$ | 18.96 | 12.37 | 14.34 | 15.22 | 22.22 |
| $F_{2.5}$ | 17.01 | 10.86 | 13.37 | 13.75 | 22.48 |
| $F_{3.5}$ | 15.76 | 9.81 | 12.95 | 12.84 | 23.18 |

*Figure B. 3 Three point bending test results of the CSFRC-60 beams a) Load – CMOD relationship; and b) the detail of the load correspond to COMD*

a)

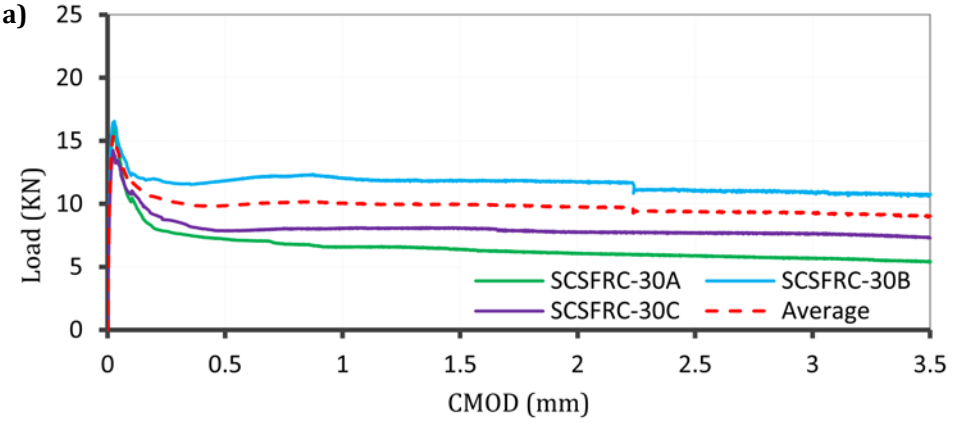


b)

| Load | SCSFRC-30A | SCSFRC-30B | SCSFRC-30A | Average | CV (%) |
|---|---|---|---|---|---|
| $F_{0.5}$ | 7.21 | 11.84 | 7.88 | 8.98 | 27.89 |
| $F_{1.5}$ | 6.40 | 11.85 | 8.10 | 8.78 | 31.74 |
| $F_{2.5}$ | 5.87 | 10.99 | 7.71 | 8.19 | 31.67 |
| $F_{3.5}$ | 5.37 | 10.72 | 7.29 | 7.79 | 34.78 |

*Figure B. 4 Three point bending test results of the SCSFRC-30 beams a) Load – CMOD relationship; and b) the detail of the load correspond to COMD*

a)

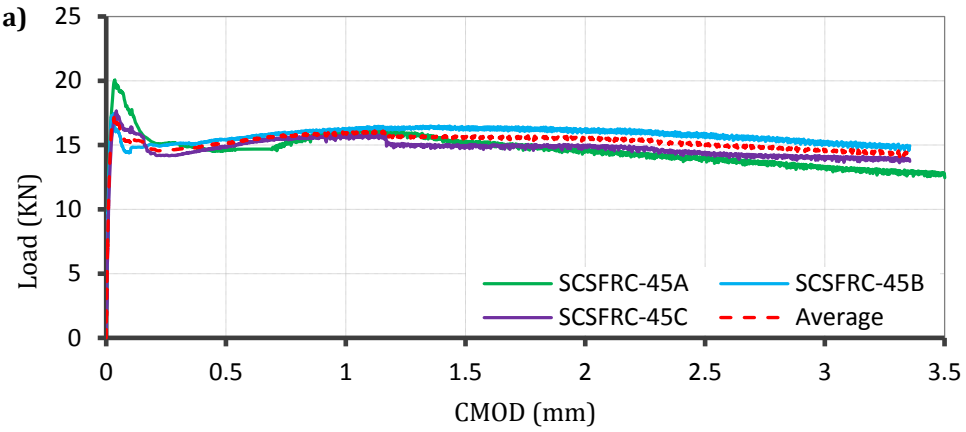


b)

| Load | SCSFRC-45A | SCSFRC-45B | SCSFRC-45A | Average | CV (%) |
|---|---|---|---|---|---|
| $F_{0.5}$ | 14.65 | 15.44 | 14.90 | 14.99 | 2.70 |
| $F_{1.5}$ | 15.11 | 16.18 | 14.92 | 15.40 | 4.43 |
| $F_{2.5}$ | 14.04 | 15.93 | 14.45 | 14.81 | 6.70 |
| $F_{3.5}$ | 12.79 | 14.79 | 13.63 | 13.74 | 7.33 |

*Figure B. 5 Three point bending test results of the SCSFRC-45 beams a) Load – CMOD relationship; and b) the detail of the load correspond to COMD*

a)

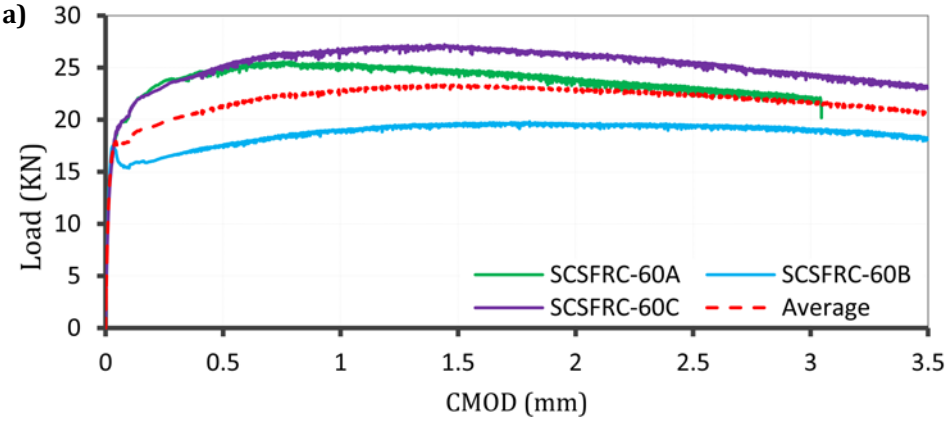


b)

| Load | SCSFRC-60A | SCSFRC-60B | SCSFRC-60A | Average | CV (%) |
|---|---|---|---|---|---|
| $F_{0.5}$ | 24.67 | 17.57 | 25.10 | 22.45 | 18.83 |
| $F_{1.5}$ | 24.47 | 19.43 | 26.80 | 23.57 | 15.99 |
| $F_{2.5}$ | 22.26 | 19.46 | 25.27 | 22.33 | 13.01 |
| $F_{3.5}$ | 20.19 | 18.09 | 23.03 | 20.44 | 12.12 |

*Figure B. 6 Three point bending test results of the SCSFRC-60 beams a) Load – CMOD relationship; and b) the detail of the load correspond to COMD*

# ANNEX C: RESULTS OF THE ANISOTROPY OF SFRC SEGMENTS

## C.1 INTRODUCTION

The contribution of fibres to the mechanical properties of concrete depends on the fibre distribution within the concrete element. Generally, a hypothesis of uniform distribution of fibres within SFRC is assumed. However, the homogeneous property could not always be guaranteed due to the influence of the varied procedures of casting. In addition that, several studies indicated that the preferential orientation of the steel fibres might be more helpful in controlling cracks and propagation in some specific concrete elements than uniform distribution. Therefore, it is significant to understand the fibre distribution within concrete elements.

In light of the significance of studying the distribution of fibres in FRC becomes evident, methodologies used to assess the fibre distribution such as magnetic method, scans as well as inductive methods have been invented. Especially the inductive test could be used to assess the amount and the distribution/orientation of fibres in SFRC presents a high accuracy and robustness. Moreover, by the combination of Barcelona test and inductive test results, it might be more precise to predict the fibre distribution within the concrete.

In the section 5.4, Chapter 5 of this doctoral thesis, different parameters related to the the anisotropy of concrete were discussed. This Annex would present the test results of cylindrical cores from different segments by means of Inductive test and Barcelona test.

## C.2 RESULTS OF THE ANISOTROPY OF SFRC SEGMENTS

The values isotropic number, fibre content, orientation number in three axes of cores and the load correspond to different vertical displacement of Barcelona test are presented from the Table C.1 to Table C.4.

*Table C. 1 The analysis of test results of C*

| Number | Ω | $C_f$ (Kg/m³) | $\eta_R$ | $\eta_T$ | $\eta_Y$ | Fmax (KN) | $F_{0.5}$ (KN) | $F_{2.5}$ (KN) |
|---|---|---|---|---|---|---|---|---|
| C_1A | 0.76 | 46.94 | 0.40 | 0.49 | 0.62 | 147.41 | 100.73 | 52.91 |
| C_1B | 0.73 | 58.59 | 0.30 | 0.66 | 0.51 | 154.13 | 128.79 | 87.73 |
| C_2A | 0.71 | 36.46 | 0.29 | 0.49 | 0.68 | 131.52 | 91.64 | 53.26 |
| C_2B | 0.70 | 62.52 | 0.27 | 0.69 | 0.49 | 153.13 | 127.54 | 80.47 |
| C_3A | 0.65 | 42.73 | 0.46 | 0.62 | 0.43 | 132.71 | 82.87 | 34.57 |
| C_3B | 0.64 | 55.91 | 0.35 | 0.69 | 0.44 | 144.90 | 116.11 | 63.98 |
| C_4A | 0.66 | 48.12 | 0.50 | 0.57 | 0.45 | 119.55 | 90.87 | 50.31 |
| C_4B | 0.88 | 57.39 | 0.37 | 0.60 | 0.53 | 160.66 | 133.25 | 76.85 |
| C_5A | 0.95 | 52.82 | 0.49 | 0.53 | 0.50 | 148.26 | 102.34 | 48.18 |
| C_5B | 0.69 | 60.25 | 0.42 | 0.63 | 0.46 | 152.39 | 106.35 | 56.08 |
| C_6A | 0.63 | 41.26 | 0.28 | 0.67 | 0.51 | 156.53 | 107.42 | 58.93 |
| C_6B | 0.53 | 53.18 | 0.39 | 0.71 | 0.37 | 164.00 | 122.70 | 70.23 |
| C_7A | 0.77 | 43.16 | 0.27 | 0.66 | 0.53 | 159.19 | 110.42 | 70.27 |
| C_7B | 0.58 | 56.56 | 0.42 | 0.61 | 0.48 | 145.93 | 101.27 | 38.87 |
| C_8A | 0.64 | 53.75 | 0.49 | 0.45 | 0.58 | 149.42 | 101.51 | 47.51 |
| C_8B | 0.85 | 56.46 | 0.42 | 0.59 | 0.51 | 173.38 | 130.73 | 78.84 |
| C_9A | 0.86 | 42.06 | 0.49 | 0.48 | 0.55 | 160.78 | 106.04 | 50.36 |
| C_9B | 0.72 | 55.82 | 0.53 | 0.57 | 0.42 | 176.74 | 122.20 | 66.74 |
| C_10A | 0.83 | 50.73 | 0.58 | 0.43 | 0.51 | 167.08 | 102.19 | 41.10 |
| C_10B | 0.88 | 52.95 | 0.42 | 0.58 | 0.52 | 169.40 | 119.21 | 66.72 |
| C_11A | 0.54 | 49.12 | 0.38 | 0.59 | 0.54 | 157.87 | 113.35 | 68.14 |
| C_11B | 0.52 | 39.47 | 0.44 | 0.68 | 0.37 | 165.37 | 99.94 | 45.35 |
| C_12A | 0.76 | 48.68 | 0.38 | 0.61 | 0.51 | 165.36 | 165.36 | 45.55 |
| C_12B | 0.49 | 48.36 | 0.49 | 0.39 | 0.62 | 171.36 | 171.36 | 37.31 |
| C_13A | 0.85 | 62.88 | 0.32 | 0.54 | 0.63 | 161.34 | 113.43 | 73.86 |
| C_13B | 0.64 | 57.30 | 0.43 | 0.60 | 0.49 | 161.11 | 110.54 | 73.49 |
| C_14A | 0.78 | 46.04 | 0.39 | 0.59 | 0.53 | 155.83 | 111.37 | 66.29 |
| C_14B | 0.84 | 45.46 | 0.63 | 0.44 | 0.44 | 162.40 | 162.40 | 41.97 |
| C_15A | 0.79 | 49.29 | 0.37 | 0.57 | 0.57 | 117.88 | 92.12 | 54.53 |
| C_15B | 0.86 | 56.49 | 0.54 | 0.47 | 0.52 | 146.40 | 91.74 | 59.57 |
| C_16A | 0.72 | 48.35 | 0.36 | 0.61 | 0.53 | 174.50 | 129.89 | 70.78 |
| C_16B | 0.61 | 49.72 | 0.64 | 0.34 | 0.52 | 158.24 | 158.24 | 33.88 |
| C_17A | 0.80 | 48.05 | 0.31 | 0.65 | 0.52 | 159.69 | 111.95 | 69.49 |
| C_17B | 0.60 | 66.96 | 0.54 | 0.42 | 0.56 | 169.84 | 119.43 | 67.37 |
| C_18A | 0.75 | 55.82 | 0.49 | 0.54 | 0.50 | 109.50 | 92.93 | 51.05 |
| C_18B | 0.68 | 48.90 | 0.56 | 0.54 | 0.42 | 174.70 | 115.92 | 60.97 |
| C_19A | 0.72 | 58.30 | 0.67 | 0.34 | 0.46 | 111.92 | 90.10 | 45.84 |
| C_19B | 0.90 | 52.97 | 0.58 | 0.45 | 0.50 | 145.25 | 103.37 | 59.49 |
| C_20A | 0.68 | 60.06 | 0.49 | 0.43 | 0.60 | 134.25 | 96.85 | 54.47 |
| C_20B | 0.96 | 58.84 | 0.56 | 0.47 | 0.49 | 150.25 | 119.39 | 59.09 |
| C_21A | 0.53 | 59.66 | 0.51 | 0.34 | 0.64 | 148.72 | 107.08 | 50.36 |
| C_21B | 0.70 | 47.26 | 0.55 | 0.51 | 0.46 | 155.36 | 106.04 | 51.44 |
| C_22A | 0.64 | 73.39 | 0.49 | 0.41 | 0.61 | 162.57 | 131.18 | 93.78 |
| C_22B | 0.77 | 49.83 | 0.48 | 0.57 | 0.47 | 151.10 | 101.02 | 55.98 |
| C_23A | 0.59 | 51.80 | 0.41 | 0.47 | 0.63 | 130.72 | 96.59 | 51.32 |
| C_23B | 0.55 | 47.12 | 0.68 | 0.31 | 0.48 | 168.73 | 65.00 | 22.14 |
| C_24A | 0.77 | 51.35 | 0.44 | 0.50 | 0.57 | 152.77 | 101.66 | 47.46 |
| C_24B | 0.54 | 49.88 | 0.64 | 0.31 | 0.53 | 162.80 | 80.27 | 33.36 |
| C_25A | 0.67 | 61.62 | 0.49 | 0.44 | 0.59 | 139.24 | 101.76 | 66.35 |

| | | | | | | | | |
|---|---|---|---|---|---|---|---|---|
| C_25B | 0.58 | 44.54 | 0.71 | 0.28 | 0.46 | 144.08 | 76.25 | 37.92 |
| C_26A | 0.74 | 67.24 | 0.49 | 0.50 | 0.54 | 136.50 | 115.13 | 66.54 |
| C_26B | 0.42 | 52.32 | 0.65 | 0.27 | 0.54 | 153.80 | 92.72 | 41.72 |
| C_27A | 0.84 | 50.18 | 0.49 | 0.50 | 0.54 | 168.71 | 104.78 | 43.82 |
| C_27B | 0.53 | 43.39 | 0.71 | 0.25 | 0.47 | 148.30 | 72.80 | 43.82 |
| C_28A | 0.37 | 56.12 | 0.45 | 0.27 | 0.72 | 162.42 | 77.06 | 25.52 |
| C_28B | 0.46 | 46.01 | 0.66 | 0.26 | 0.53 | 153.06 | 67.60 | 25.04 |
| C_29A | 0.93 | 53.28 | 0.54 | 0.50 | 0.48 | 164.67 | 89.14 | 36.38 |
| C_29B | 0.58 | 39.08 | 0.76 | 0.24 | 0.41 | 156.76 | 36.10 | 31.60 |
| C_30A | 0.78 | 53.98 | 0.43 | 0.59 | 0.50 | 149.21 | 97.88 | 55.38 |
| C_30B | 0.75 | 46.69 | 0.57 | 0.40 | 0.54 | 152.75 | 84.98 | 37.97 |
| C_31A | 0.76 | 56.83 | 0.55 | 0.46 | 0.51 | 154.31 | 88.68 | 42.60 |
| C_31B | 0.66 | 45.48 | 0.60 | 0.53 | 0.37 | 152.33 | 66.94 | 37.69 |
| C_32A | 0.91 | 59.02 | 0.56 | 0.46 | 0.50 | 162.44 | 100.05 | 57.80 |
| C_32B | 0.87 | 46.22 | 0.64 | 0.46 | 0.40 | 155.97 | 86.67 | 35.90 |
| C_33A | 0.65 | 46.94 | 0.49 | 0.44 | 0.59 | 159.59 | 93.88 | 50.70 |
| C_33B | 0.84 | 54.56 | 0.49 | 0.54 | 0.50 | 161.21 | 47.72 | 32.82 |
| C_34A | 0.74 | 49.50 | 0.58 | 0.44 | 0.50 | 154.76 | 78.76 | 48.43 |
| C_34B | 0.77 | 52.58 | 0.48 | 0.59 | 0.45 | 162.63 | 111.72 | 57.13 |
| C_35A | 0.72 | 52.88 | 0.38 | 0.61 | 0.51 | 163.70 | 105.84 | 71.32 |
| C_35B | 0.88 | 52.56 | 0.51 | 0.54 | 0.48 | 148.14 | 78.59 | 51.85 |
| C_36A | 0.71 | 52.05 | 0.34 | 0.48 | 0.66 | 160.90 | 112.21 | 58.50 |
| C_36B | 0.67 | 48.75 | 0.37 | 0.66 | 0.46 | 163.05 | 163.05 | 57.87 |
| C_37A | 0.83 | 43.81 | 0.47 | 0.56 | 0.50 | 161.36 | 96.25 | 52.38 |
| C_37B | 0.63 | 60.73 | 0.54 | 0.59 | 0.39 | 160.46 | 92.42 | 50.72 |
| C_38A | 0.68 | 40.54 | 0.43 | 0.61 | 0.47 | 160.05 | 131.41 | 46.39 |
| C_38B | 0.60 | 44.95 | 0.56 | 0.59 | 0.35 | 152.76 | 101.51 | 48.43 |
| C_39A | 0.55 | 41.06 | 0.40 | 0.49 | 0.62 | 157.46 | 109.98 | 53.12 |
| C_39B | 0.78 | 46.53 | 0.36 | 0.56 | 0.58 | 157.56 | 111.48 | 67.61 |
| C_40A | 0.55 | 47.22 | 0.32 | 0.58 | 0.59 | 164.11 | 98.87 | 52.26 |
| C_40B | 0.84 | 50.28 | 0.41 | 0.59 | 0.52 | 161.72 | 108.50 | 49.41 |
| Average | 0.71 | 51.45 | 0.48 | 0.51 | 0.51 | 154.46 | 104.54 | 53.41 |

*Table C. 2 The analysis of test results of S_A*

| **Number** | **Ω** | **$C_f$ (Kg/m$^3$)** | **$\eta_R$** | **$\eta_T$** | **$\eta_V$** | **Fmax (KN)** | **$F_{0.5}$ (KN)** | **$F_{2.5}$ (KN)** |
|---|---|---|---|---|---|---|---|---|
| S_A_1A | 0.69 | 47.12 | 0.43 | 0.62 | 0.47 | 132.79 | 70.10 | 34.89 |
| S_A_1B | 0.40 | 48.95 | 0.35 | 0.76 | 0.32 | 124.88 | 77.89 | 40.65 |
| S_A_2A | 0.68 | 49.21 | 0.24 | 0.71 | 0.48 | 130.18 | 94.58 | 65.93 |
| S_A_2B | 0.74 | 42.87 | 0.24 | 0.69 | 0.51 | 129.31 | 91.00 | 60.44 |
| S_A_3A | 0.70 | 55.68 | 0.31 | 0.59 | 0.59 | 124.06 | 70.87 | 46.13 |
| S_A_3B | 0.68 | 45.04 | 0.29 | 0.69 | 0.49 | 131.27 | 93.19 | 52.40 |
| S_A_4A | 0.49 | 46.70 | 0.47 | 0.64 | 0.38 | 121.79 | 72.52 | 37.79 |
| S_A_4B | 0.28 | 51.51 | 0.37 | 0.75 | 0.32 | 121.68 | 47.88 | 24.20 |
| S_A_5A | 0.54 | 57.90 | 0.60 | 0.41 | 0.50 | 130.74 | 78.77 | 33.04 |
| S_A_5B | 0.62 | 56.24 | 0.39 | 0.57 | 0.55 | 119.63 | 81.75 | 51.89 |
| S_A_6A | 0.71 | 47.70 | 0.48 | 0.49 | 0.56 | 123.72 | 88.41 | 43.35 |
| S_A_6B | 0.86 | 56.97 | 0.34 | 0.55 | 0.61 | 113.07 | 93.79 | 58.80 |
| S_A_7A | 0.57 | 49.69 | 0.55 | 0.52 | 0.46 | 107.94 | 77.21 | 33.60 |
| S_A_7B | 0.50 | 48.40 | 0.42 | 0.65 | 0.44 | 114.09 | 64.43 | 22.95 |
| S_A_8A | 0.47 | 50.09 | 0.40 | 0.47 | 0.63 | 131.54 | 87.71 | 39.67 |

| | | | | | | | | |
|---|---|---|---|---|---|---|---|---|
| S_A_8B | 0.36 | 44.53 | 0.43 | 0.67 | 0.39 | 119.72 | 62.15 | 24.86 |
| S_A_9A | 0.36 | 44.38 | 0.42 | 0.58 | 0.51 | 108.74 | 52.52 | 27.37 |
| S_A_9B | 0.45 | 53.01 | 0.38 | 0.53 | 0.60 | 121.82 | 66.41 | 28.33 |
| S_A_10A | 0.29 | 43.56 | 0.55 | 0.41 | 0.56 | 121.32 | 62.48 | 18.40 |
| S_A_10B | 0.33 | 46.10 | 0.48 | 0.59 | 0.45 | 131.73 | 57.40 | 30.59 |
| S_A_11A | 0.77 | 49.83 | 0.52 | 0.53 | 0.47 | 115.05 | 78.02 | 34.90 |
| S_A_11B | 0.62 | 57.27 | 0.34 | 0.49 | 0.66 | 128.73 | 80.70 | 49.75 |
| S_A_12A | 0.31 | 46.98 | 0.50 | 0.41 | 0.60 | 118.72 | 50.84 | 20.24 |
| S_A_12B | 0.37 | 57.35 | 0.46 | 0.54 | 0.52 | 137.00 | 77.73 | 33.62 |
| S_A_13A | 0.51 | 53.88 | 0.48 | 0.34 | 0.66 | 111.84 | 65.91 | 35.42 |
| S_A_13B | 0.57 | 60.26 | 0.42 | 0.39 | 0.68 | 133.82 | 90.26 | 49.95 |
| S_A_14A | 0.43 | 59.60 | 0.54 | 0.45 | 0.54 | 123.28 | 79.24 | 50.38 |
| S_A_14B | 0.65 | 63.81 | 0.37 | 0.56 | 0.58 | 136.88 | 92.50 | 45.75 |
| S_A_15A | 0.30 | 50.67 | 0.65 | 0.44 | 0.42 | 127.53 | 93.77 | 23.56 |
| S_A_15B | 0.45 | 50.74 | 0.60 | 0.51 | 0.40 | 132.05 | 64.40 | 30.47 |
| S_A_16A | 0.71 | 50.25 | 0.58 | 0.42 | 0.51 | 136.20 | 77.96 | 43.74 |
| S_A_16B | 0.71 | 52.40 | 0.67 | 0.43 | 0.38 | 145.64 | 63.89 | 37.95 |
| S_A_17A | 0.51 | 55.27 | 0.57 | 0.32 | 0.60 | 135.99 | 72.20 | 32.71 |
| S_A_17B | 0.45 | 54.12 | 0.50 | 0.37 | 0.63 | 137.35 | 82.57 | 38.79 |
| S_A_18A | 0.80 | 53.98 | 0.49 | 0.57 | 0.46 | 139.11 | 93.96 | 50.03 |
| S_A_18B | 0.55 | 52.89 | 0.55 | 0.41 | 0.56 | 140.13 | 89.19 | 43.64 |
| S_A_19A | 0.49 | 54.70 | 0.53 | 0.51 | 0.49 | 119.10 | 80.57 | 45.57 |
| S_A_19B | 0.46 | 51.31 | 0.59 | 0.48 | 0.45 | 135.52 | 76.70 | 41.13 |
| S_A_20A | 0.57 | 56.18 | 0.41 | 0.42 | 0.67 | 139.96 | 81.11 | 53.27 |
| S_A_20B | 0.39 | 46.00 | 0.71 | 0.38 | 0.37 | 153.44 | 45.21 | 27.34 |
| S_A_21A | 0.50 | 56.59 | 0.40 | 0.35 | 0.71 | 132.24 | 81.96 | 43.15 |
| S_A_21B | 0.41 | 58.03 | 0.55 | 0.33 | 0.61 | 148.23 | 61.14 | 33.58 |
| S_A_22A | 0.55 | 54.18 | 0.43 | 0.38 | 0.67 | 130.90 | 75.78 | 40.83 |
| S_A_22B | 0.41 | 50.80 | 0.60 | 0.25 | 0.61 | 129.14 | 25.28 | 11.57 |
| S_A_23A | 0.38 | 51.67 | 0.61 | 0.49 | 0.41 | 151.72 | 84.66 | 42.18 |
| S_A_23B | 0.61 | 43.08 | 0.66 | 0.45 | 0.38 | 153.02 | 88.83 | 36.20 |
| S_A_24A | 0.63 | 64.02 | 0.52 | 0.60 | 0.39 | 154.17 | 90.74 | 43.06 |
| S_A_24B | 0.82 | 57.28 | 0.60 | 0.50 | 0.41 | 135.62 | 85.40 | 43.88 |
| S_A_25A | 0.82 | 53.80 | 0.62 | 0.48 | 0.42 | 131.54 | 87.71 | 39.67 |
| S_A_25B | 0.83 | 44.80 | 0.71 | 0.39 | 0.37 | 159.81 | 72.99 | 31.70 |
| S_A_26A | 0.58 | 51.74 | 0.45 | 0.42 | 0.64 | 138.02 | 97.44 | 51.67 |
| S_A_26B | 0.46 | 42.71 | 0.62 | 0.47 | 0.42 | 143.93 | 78.70 | 36.74 |
| S_A_27A | 0.61 | 48.05 | 0.56 | 0.36 | 0.59 | 133.88 | 68.97 | 31.78 |
| S_A_27B | 0.61 | 53.78 | 0.71 | 0.28 | 0.45 | 139.59 | 72.37 | 32.58 |
| S_A_28A | 0.77 | 54.17 | 0.52 | 0.49 | 0.52 | 133.52 | 81.43 | 43.19 |
| S_A_28B | 0.63 | 64.14 | 0.74 | 0.36 | 0.34 | 151.94 | 69.24 | 28.51 |
| S_A_29A | 0.61 | 51.72 | 0.59 | 0.46 | 0.47 | 141.06 | 77.60 | 43.73 |
| S_A_29B | 0.44 | 42.18 | 0.70 | 0.51 | 0.23 | 142.47 | 52.76 | 27.68 |
| S_A_30A | 0.89 | 51.35 | 0.54 | 0.51 | 0.48 | 169.76 | 106.85 | 63.07 |
| S_A_30B | 0.73 | 53.05 | 0.34 | 0.66 | 0.48 | 156.33 | 93.68 | 43.70 |
| S_A_31A | 0.85 | 56.37 | 0.48 | 0.48 | 0.56 | 167.05 | 111.78 | 57.51 |
| S_A_31B | 0.77 | 49.26 | 0.43 | 0.56 | 0.54 | 155.91 | 93.23 | 60.40 |
| S_A_32A | 0.47 | 53.25 | 0.40 | 0.70 | 0.37 | 135.59 | 77.10 | 35.34 |
| S_A_32B | 0.40 | 52.61 | 0.46 | 0.70 | 0.31 | 131.65 | 78.76 | 34.55 |
| S_A_33A | 0.39 | 41.79 | 0.47 | 0.55 | 0.51 | 137.70 | 85.84 | 28.29 |
| S_A_33B | 0.57 | 45.20 | 0.35 | 0.60 | 0.55 | 139.71 | 84.11 | 35.78 |

| | | | | | | | | |
|---|---|---|---|---|---|---|---|---|
| S_A_34A | 0.54 | 46.48 | 0.57 | 0.37 | 0.57 | 135.56 | 135.56 | 27.10 |
| S_A_34B | 0.72 | 50.28 | 0.40 | 0.62 | 0.49 | 135.80 | 135.71 | 39.57 |
| S_A_35A | 0.38 | 45.23 | 0.43 | 0.68 | 0.37 | 141.81 | 141.81 | 22.18 |
| S_A_35B | 0.36 | 43.86 | 0.29 | 0.77 | 0.34 | 140.08 | 80.24 | 36.56 |
| S_A_36A | 0.43 | 49.41 | 0.51 | 0.49 | 0.52 | 137.71 | 65.64 | 20.78 |
| S_A_36B | 0.39 | 48.24 | 0.52 | 0.64 | 0.32 | 141.60 | 141.60 | 26.82 |
| S_A_37A | 0.55 | 54.63 | 0.61 | 0.37 | 0.52 | 125.45 | 80.96 | 31.95 |
| S_A_37B | 0.54 | 50.68 | 0.52 | 0.51 | 0.50 | 114.18 | 73.12 | 31.60 |
| S_A_38A | 0.66 | 38.55 | 0.54 | 0.51 | 0.47 | 134.28 | 66.01 | 34.16 |
| S_A_38B | 0.50 | 55.05 | 0.60 | 0.55 | 0.35 | 136.49 | 79.90 | 34.32 |
| S_A_39A | 0.37 | 53.10 | 0.67 | 0.34 | 0.48 | 153.05 | 153.05 | 40.46 |
| S_A_39B | 0.43 | 55.83 | 0.65 | 0.44 | 0.41 | 149.49 | 149.49 | 36.15 |
| S_A_40A | 0.54 | 43.68 | 0.56 | 0.42 | 0.54 | 130.60 | 67.75 | 40.64 |
| S_A_40B | 0.73 | 60.09 | 0.49 | 0.49 | 0.55 | 145.25 | 97.08 | 48.10 |
| S_A_41A | 0.62 | 40.84 | 0.50 | 0.40 | 0.61 | 143.55 | 85.27 | 40.70 |
| S_A_41B | 0.72 | 52.58 | 0.56 | 0.41 | 0.55 | 133.83 | 86.13 | 31.43 |
| S_A_42A | 0.86 | 44.07 | 0.44 | 0.51 | 0.57 | 153.87 | 89.51 | 51.17 |
| S_A_42B | 0.76 | 50.28 | 0.55 | 0.51 | 0.48 | 153.91 | 91.91 | 40.48 |
| S_A_43A | 0.59 | 48.26 | 0.56 | 0.41 | 0.55 | 145.48 | 82.01 | 40.89 |
| S_A_43B | 0.43 | 51.79 | 0.66 | 0.29 | 0.52 | 139.95 | 119.82 | 25.37 |
| S_A_44A | 0.65 | 52.27 | 0.46 | 0.50 | 0.57 | 141.57 | 138.95 | 44.85 |
| S_A_44B | 0.54 | 52.18 | 0.61 | 0.44 | 0.46 | 136.35 | 50.51 | 21.33 |
| S_A_45A | 0.77 | 44.31 | 0.56 | 0.43 | 0.53 | 143.46 | 99.59 | 51.80 |
| S_A_45B | 0.67 | 51.88 | 0.66 | 0.46 | 0.37 | 146.94 | 146.64 | 39.06 |
| S_A_46A | 0.75 | 53.58 | 0.42 | 0.48 | 0.61 | 151.97 | 78.61 | 34.03 |
| S_A_46B | 0.59 | 51.43 | 0.56 | 0.47 | 0.50 | 143.52 | 74.27 | 31.52 |
| S_A_47A | 0.36 | 42.74 | 0.51 | 0.64 | 0.35 | 156.32 | 156.32 | 28.40 |
| S_A_47B | 0.45 | 44.03 | 0.71 | 0.39 | 0.37 | 137.56 | 78.25 | 24.73 |
| S_A_48A | 0.45 | 48.37 | 0.58 | 0.47 | 0.48 | 175.33 | 175.33 | 37.96 |
| S_A_48B | 0.51 | 46.59 | 0.76 | 0.36 | 0.29 | 166.72 | 31.87 | 26.79 |
| S_A_49A | 0.55 | 54.71 | 0.53 | 0.44 | 0.56 | 155.12 | 91.52 | 43.53 |
| S_A_49B | 0.52 | 54.17 | 0.63 | 0.39 | 0.49 | 160.37 | 160.37 | 47.42 |
| S_A_50A | 0.82 | 51.61 | 0.56 | 0.45 | 0.51 | 157.88 | 157.88 | 57.26 |
| S_A_50B | 0.84 | 52.51 | 0.53 | 0.52 | 0.48 | 167.42 | 96.64 | 64.44 |
| S_A_51A | 0.51 | 49.64 | 0.61 | 0.44 | 0.47 | 162.21 | 162.21 | 23.79 |
| S_A_51B | 0.60 | 50.13 | 0.66 | 0.46 | 0.37 | 147.22 | 147.22 | 27.11 |
| S_A_52A | 0.70 | 47.42 | 0.58 | 0.45 | 0.48 | 162.53 | 102.48 | 56.52 |
| S_A_52B | 0.57 | 50.28 | 0.66 | 0.49 | 0.33 | 158.68 | 76.92 | 28.18 |
| S_A_53A | 0.71 | 59.05 | 0.49 | 0.57 | 0.46 | 173.20 | 125.63 | 68.62 |
| S_A_53B | 0.78 | 54.21 | 0.65 | 0.41 | 0.44 | 159.90 | 101.22 | 47.25 |
| S_A_54A | 0.75 | 51.17 | 0.45 | 0.55 | 0.52 | 180.80 | 107.62 | 63.34 |
| S_A_54B | 0.59 | 64.98 | 0.57 | 0.43 | 0.52 | 176.37 | 113.75 | 57.95 |
| S_A_55A | 0.64 | 49.86 | 0.60 | 0.35 | 0.55 | 156.83 | 156.83 | 30.26 |
| S_A_55B | 0.80 | 47.33 | 0.68 | 0.37 | 0.44 | 153.78 | 153.72 | 30.16 |
| Average | 0.58 | 51.06 | 0.52 | 0.49 | 0.49 | 140.14 | 90.17 | 38.82 |

*Table C. 3 The analysis of test results of S_B*

| Number | Ω | $C_f$ (Kg/m³) | $\eta_R$ | $\eta_T$ | $\eta_Y$ | Fmax (KN) | $F_{0.5}$ (KN) | $F_{2.5}$ (KN) |
|---|---|---|---|---|---|---|---|---|
| S_B_1A | 0.68 | 48.90 | 0.64 | 0.48 | 0.38 | 164.98 | 114.50 | 51.12 |
| S_B_1B | 0.85 | 48.62 | 0.63 | 0.45 | 0.42 | 160.51 | 90.79 | 32.59 |
| S_B_2A | 0.67 | 53.63 | 0.63 | 0.49 | 0.38 | 169.71 | 118.68 | 52.01 |
| S_B_2B | 0.40 | 48.60 | 0.42 | 0.73 | 0.30 | 164.58 | 81.63 | 29.83 |
| S_B_3A | 0.66 | 43.31 | 0.69 | 0.31 | 0.47 | 163.65 | 63.94 | 25.74 |
| S_B_3B | 0.90 | 39.90 | 0.65 | 0.44 | 0.41 | 186.72 | 90.39 | 37.30 |
| S_B_4A | 0.48 | 54.23 | 0.57 | 0.30 | 0.61 | 165.31 | 139.29 | 61.05 |
| S_B_4B | 0.51 | 48.16 | 0.70 | 0.29 | 0.46 | 162.67 | 53.42 | 26.94 |
| S_B_5A | 0.83 | 59.10 | 0.63 | 0.42 | 0.45 | 168.42 | 91.68 | 41.17 |
| S_B_5B | 0.58 | 49.54 | 0.71 | 0.31 | 0.43 | 154.80 | 90.03 | 39.94 |
| S_B_6A | 0.55 | 52.16 | 0.62 | 0.33 | 0.55 | 174.37 | 89.23 | 46.17 |
| S_B_6B | 0.63 | 53.85 | 0.64 | 0.33 | 0.52 | 171.86 | 83.04 | 36.09 |
| S_B_7A | 0.65 | 52.67 | 0.61 | 0.35 | 0.53 | 176.69 | 159.24 | 73.16 |
| S_B_7B | 0.70 | 119.95 | 0.58 | 0.39 | 0.55 | 161.27 | 99.45 | 42.22 |
| S_B_8A | 0.63 | 46.12 | 0.63 | 0.37 | 0.50 | 168.05 | 88.49 | 37.81 |
| S_B_8B | 0.89 | 55.24 | 0.65 | 0.43 | 0.42 | 168.28 | 100.15 | 45.61 |
| S_B_9A | 0.34 | 51.27 | 0.55 | 0.33 | 0.61 | 164.32 | 75.66 | 27.80 |
| S_B_9B | 0.55 | 79.22 | 0.53 | 0.51 | 0.49 | 169.43 | 106.98 | 48.85 |
| S_B_10A | 0.40 | 51.14 | 0.53 | 0.37 | 0.61 | 154.89 | 119.83 | 57.31 |
| S_B_10B | 0.57 | 54.88 | 0.48 | 0.46 | 0.58 | 154.28 | 88.23 | 37.43 |
| S_B_11A | 0.75 | 41.70 | 0.57 | 0.44 | 0.51 | 150.70 | 58.05 | 23.31 |
| S_B_11B | 0.41 | 43.54 | 0.41 | 0.69 | 0.39 | 162.64 | 90.84 | 39.42 |
| S_B_12A | 0.27 | 48.40 | 0.45 | 0.22 | 0.74 | 147.08 | 70.40 | 24.52 |
| S_B_12B | 0.45 | 56.96 | 0.58 | 0.43 | 0.51 | 161.74 | 59.64 | 20.44 |
| Average | 0.60 | 54.21 | 0.59 | 0.41 | 0.49 | 164.46 | 92.65 | 39.91 |

*Table C. 4 The analysis of test results of S_D*

| Number | Ω | $C_f$ (Kg/m3) | $\eta_R$ | $\eta_T$ | $\eta_Y$ | Fmax (KN) | $F_{0.5}$ (KN) | $F_{2.5}$ (KN) |
|---|---|---|---|---|---|---|---|---|
| S_C_1A | 0.79 | 50.34 | 0.55 | 0.53 | 0.44 | 205.53 | 125.30 | 56.52 |
| S_C_1B | 0.84 | 49.29 | 0.61 | 0.49 | 0.42 | 177.01 | 108.29 | 45.89 |
| S_C_2A | 0.87 | 55.39 | 0.56 | 0.51 | 0.45 | 182.79 | 52.70 | 23.34 |
| S_C_2B | 0.65 | 52.54 | 0.55 | 0.58 | 0.38 | 172.36 | 82.36 | 34.19 |
| S_C_3A | 0.69 | 50.69 | 0.66 | 0.35 | 0.48 | 172.18 | 45.43 | 18.20 |
| S_C_3B | 0.78 | 44.63 | 0.67 | 0.37 | 0.46 | 174.18 | 65.52 | 26.65 |
| S_C_4A | 0.63 | 36.19 | 0.44 | 0.48 | 0.60 | 177.03 | 128.94 | 57.51 |
| S_C_4B | 0.56 | 46.19 | 0.59 | 0.35 | 0.56 | 168.34 | 104.89 | 47.48 |
| S_C_5A | 0.71 | 19.63 | 0.55 | 0.40 | 0.56 | 181.86 | 68.23 | 31.40 |
| S_C_5B | 0.82 | 42.76 | 0.65 | 0.38 | 0.46 | 168.36 | 81.78 | 36.82 |
| S_C_6A | 0.55 | 51.38 | 0.74 | 0.37 | 0.34 | 163.23 | 86.40 | 39.00 |
| S_C_6B | 0.72 | 52.46 | 0.67 | 0.34 | 0.48 | 169.82 | 84.73 | 39.65 |
| S_C_7A | 0.29 | 70.94 | 0.36 | 0.24 | 0.79 | 178.65 | 132.47 | 61.94 |
| S_C_7B | 0.55 | 81.19 | 0.53 | 0.34 | 0.62 | 172.20 | 127.73 | 57.89 |
| S_C_8A | 0.21 | 78.44 | 0.46 | 0.33 | 0.68 | 162.85 | 35.39 | 13.80 |
| S_C_8B | 0.51 | 59.93 | 0.57 | 0.37 | 0.57 | 166.39 | 73.20 | 31.78 |
| S_C_9A | 0.37 | 60.67 | 0.35 | 0.43 | 0.70 | 149.97 | 110.82 | 51.88 |
| S_C_9B | 0.73 | 63.72 | 0.49 | 0.44 | 0.59 | 161.24 | 96.56 | 42.38 |
| S_C_10A | 0.39 | 55.27 | 0.47 | 0.59 | 0.47 | 163.73 | 110.12 | 57.03 |

| | | | | | | | | |
|---|---|---|---|---|---|---|---|---|
| S_C_10B | 0.86 | 53.77 | 0.49 | 0.48 | 0.55 | 157.63 | 104.06 | 49.63 |
| S_C_11A | 0.54 | 55.67 | 0.57 | 0.35 | 0.59 | 134.48 | 159.82 | 57.47 |
| S_C_11B | 0.69 | 46.97 | 0.52 | 0.50 | 0.51 | 149.27 | 101.94 | 39.68 |
| S_C_12A | 0.36 | 46.59 | 0.46 | 0.65 | 0.39 | 134.78 | 73.94 | 27.00 |
| S_C_12B | 0.80 | 50.65 | 0.50 | 0.46 | 0.56 | 147.87 | 66.82 | 23.58 |
| Average | 0.62 | 53.14 | 0.54 | 0.43 | 0.53 | 166.32 | 92.81 | 40.4 |

# PUBLICATIONS

## PAPERS

Liao, L., de la Fuente, A., Cavalaro, S. and Aguado, A., Carbonari, G. Experimental and analytical study of concrete blocks subjected to concentrated loads with an application to TBM-constructed tunnels，Tunnelling and Underground Space Technology. Vol 49, June 01, 2015 pp.: 295-306. DOI: 10.1016/j.tust.2015.04.020

Liao, L., de la Fuente, A., Cavalaro, S. and Aguado, A. Design of FRC tunnel segments considering the ductility requirements of the MC 2010，Tunnelling and Underground Space Technology. Vol 47, Issue 3. pp.: 200-210. March 2015. DOI: 10.1016/j.tust.2015.01.006

Liao, L., Cavalaro, S., de la Fuente, A., and Aguado, A. Complementary Use of Inductive Test and Bending Test for the Characterization of SFRC. Applied Mechanics and Materials. Vol. 580-583 (2014) doi:10.4028/www.scientific.net/AMM.580-583. 2213

Liao, L., de la Fuente, A., Cavalaro, S. and Aguado, A. Design procedure and experimental study on FRC segmental rings for vertical shafts. Materials and Design. ***(Under review).***

## CONFERENCES

de la Fuente, A., Liao, L., Cavalaro, S. and Aguado, A. Fibre reinforced precast concrete segments: design and applications，World Tunnel Congress 2014 & 40th ITA-AITES General Assembly, 9-15 May, 2014, Iguassu Falls, Brazil.

de la Fuente, A., Liao, L., Cavalaro, S. and Aguado, A. Design of FRC tunnel segments considering the ductility requirements of the MC-2010 – Application to the Barcelona Metro Line 9, FRC 2014 Joint ACI-fib International Workshop. 24-25 July 2014, Montreal, Canada.

Liao, L., de la Fuente, A., Cavalaro, S. and Aguado, A. Analysis of Differences in the Behaviour of Traditional and Self-Compacting Steel Fibre Reinforced Concrete，7th International Conference, FIBRE CONCRETE 2013, 12-13 September, 2013, Prague, Czech Republic.

de la Fuente, A., Cavalaro, S., Liao, L., and Aguado, A., Steel fibre reinforced concrete precast segments for vertical shafts. 7th International Conference, FIBRE CONCRETE 2013, 12-13 September, 2013, Prague, Czech Republic.